

Optimum Retrieval Techniques in Remote Sensing of
Atmospheric Temperature, Liquid Water,
and Water Vapor

by

William Henry Ledsham

B.E., Stevens Institute of Technology
(1970)

S.M., Massachusetts Institute of Technology
(1972)

E.E., Massachusetts Institute of Technology
(1974)

SUBMITTED IN PARTIAL FULFILLMENT
OF THE REQUIREMENTS FOR THE
DEGREE OF

DOCTOR OF PHILOSOPHY

at the

MASSACHUSETTS INSTITUTE OF TECHNOLOGY

(DATE: May, 1978)

Copyright, 1978, M.I.T.

Signature of Author..... Signature redacted
Department of Electrical Engineering and Computer Science,
May 16, 1978

Certified by..... Signature redacted
Thesis Supervisor

Accepted by..... Signature redacted
Chairman, Department Committee

ARCHIVES
MASSACHUSETTS INSTITUTE
OF TECHNOLOGY

JUL 28 1978

LIBRARIES

Optimum Retrieval Techniques in Remote Sensing of
Atmospheric Temperature, Liquid Water,
and Water Vapor

by

William Henry Ledsham

Submitted to the Department of Electrical Engineering
and Computer Science
on May 16, 1978 in partial fulfillment of the requirements
for the degree of Doctor of Philosophy

ABSTRACT

In recent years a number of satellite platform remote sensors have been launched for the purpose of inferring atmospheric temperature, liquid water, and water vapor. One problem in the area of remote sensing of these parameters is the method of parameter retrieval because of the non-linear effects of the physics involved and the non-stationary nature of the data fields. This thesis applies the techniques of modern recursive estimation theory (Kalman-Bucy filtering) to the problem of estimating these parameters from data produced by the SCanning Microwave Spectrometer (SCAMS) carried on the NIMBUS 6 satellite. Two primary experiments were conducted in this thesis. The first was the design and implementation of an extended Kalman-Bucy filter for estimation of vertical temperature profiles. The filter of this experiment was operated in three modes: a causal mode, a non-causal mode and a precomputed parameter mode. The second experiment was the design and implementation of an extended Kalman-Bucy filter for estimation of liquid water and water vapor columns in the atmosphere.

The conclusions reached from the results of these experiments are: The Kalman-Bucy filter is a valuable method for estimation of the state of the earth's atmosphere based on passive remote observations. The estimates of temperature profiles obtained with a causal filter show an improvement in accuracy over those obtained with a regression inversion technique. This improvement is greater with a non-causal filter. The use of either precomputed gain or error covariance matrices in the Kalman filter produces little degradation in the accuracy of the retrieved

profiles, but produces a substantial reduction in the computational burden of the filter. The use of an extended Kalman filter in retrievals of liquid water and water vapor shows a factor of three improvement over a regression inversion in a simulation of the data observed by SCAMS.

Thesis supervisor: Dr. D. H. Staelin

Title: Professor of Electrical Engineering

To

Leslie and my Parents

ACKNOWLEDGEMENTS

The work represented by this thesis would have not been possible without the selfless assistance of a large number of people. Because of limited space, I can not thank all of these people individually. It is hoped that my personal thanks in the past will take the place of any omission in these acknowledgements. Certain people or groups have contributed so heavily to this work that their omission would be unforgivable.

My deepest thanks to Dr. D. H. Staelin for his many years of guidance in remote sensing theory and this thesis, and for his faith in the results. A great many insights into modern recursive estimation theory were provided by Dr. D. Gustafson of Scientific Systems Inc, Cambridge, Ma. Mary Grace Fowler of Environmental Research and Technology Inc. provided the raw datasets that have formed the basis for Appendix A. I also wish to thank Dr. S. Mitter and Dr. J. Shapiro who are my readers for this thesis. Many members of the NEMS/SCAMS group have provided very valuable assistance during the process of problem formulation and solution. Of this group, I would like to thank Dr. P. W. Rosenkranz in particular. The oxygen absorption model used in this thesis (Rosenkranz, 1976) and several other routines are of his

authorship. He also produced the Statistical D method results used in this thesis.

I would like to thank the staff of Information Processing Services at the Massachusetts Institute of Technology in general, and the staff of Operations in particular for their patience and assistance.

Finally, I wish to thank my wife, Leslie, for her valuable programming assistance and both her and my parents for their infinite patience.

The work represented by this thesis was supported in whole or in part by contract NAS5-21980. The resources provided by the Macsyma Consortium are also gratefully acknowledged.

Table of Contents

List of Figures	13
List of Tables	15
Chapter I - Introduction	23
Chapter II - The Radiative Transfer Basis of Passive Remote Sensing	
A - The equations of radiative transfer	29
B - Absorption by the atmosphere	31
C - Surface effects	36
D - The concept of a temperature weighting function	38
Chapter III - Theory of the Discrete Kalman-Bucy Filter	
A - A Heuristic derivation	45
B - A structured derivation	49
C - The innovations process	55
D - The Square Root Algorithm	62
E - The Extended Kalman Filter	69
F - The non-causal filter	75

Chapter IV - The Temperature Experiment

A - General description	81
B - The SCAMS instrument	85
C - The temperature system identification	86
D - Observation matrices	93
E - The filter program	100
F - Tuning and problems	105
G - The causal experiment	109
H - The non-causal experiment	155
I - The precomputed sub-optimal filter experiment	170

Chapter V - The Water Vapor and Liquid Water Experiment

A - General description	211
B - System identification	212
C - Observations and observation matrices	214
D - The simulation	221
E - Results	223

Chapter VI - Summary and Recommendations for Future Research	247
Appendix A - Comparisons Between Point and Area Sounders	249
Appendix B - Sensitivity of Oxygen Absorption and Weighting Functions to Temperature	273
Appendix C - Program Descriptions	285
References	305
Biographical Note	313

Table of Figures

1 - SCAMS Continuous Weighting Functions	42
2 - SCAMS Verification Areas	84
3 - Causal Filter Error Performance August 7 - 9, 1975 (Extreme Scan)	112
4 - Causal Filter Error Performance August 7 - 9, 1975 (Nadir Scan)	113
5 - Causal Filter Error Performance February 3 - 6, 1976 (Extreme Scan)	114
6 - Causal Filter Error Performance February 3 - 6, 1976 (Nadir Scan)	115
7 - Causal versus Non-causal Filter Error Performance One Spot Filter, October 22 - 25, 1975	156
8 - Causal Versus Non-causal Filter Error Performance Three Spot Filter, October 22 - 25, 1975	157
9 - Typical 850 mb Error Covariance History	172

10 - Typical 850 mb Kalman Gain History	173
11 - Typical 850 mb Error History	174
12 - Brightness Temperature at 31.65 GHz. versus Liquid Water Column	229
13 - Water Vapor Error Response to a Liquid Water Impulse	231
14 - Liquid Water Error Response to a Liquid Water Impulse	232
15 - 500 mb Correlation Coefficient versus Distance Region 2	254
16 - 300 mb Correlation Model	255
17 - 850 mb Correlation Model	256

List of Tables

1 - SCAMS Discrete Weighting Functions	43
2 - Heights of Various Pressure Surfaces in the Supplemental Atmospheres	98
3 - Periods of Data Used in the Temperature Experiment	110
4 - 21 One Spot Causal Filter Performance	
4 - Scan Angle 0, August 7 - 9, 1975	116
5 - Scan Angle 3, August 7 - 9, 1975	117
6 - Scan Angle 6, August 7 - 9, 1975	118
7 - Scan Angle 0, October 3 - 5, 1975	119
8 - Scan Angle 3, October 3 - 5, 1975	120
9 - Scan Angle 6, October 3 - 5, 1975	121
10 - Scan Angle 0, October 22 - 25, 1975	122
11 - Scan Angle 3, October 22 - 25, 1975	123
12 - Scan Angle 6, October 22 - 25, 1975	124
13 - Scan Angle 0, December 5 - 8, 1975	125
14 - Scan Angle 3, December 5 - 8, 1975	126
15 - Scan Angle 6, December 5 - 8, 1975	127
16 - Scan Angle 0, January 24 - 25, 1976	128
17 - Scan Angle 3, January 24 - 25, 1976	129

18 - Scan Angle 6, January 24 - 25, 1976	130
19 - Scan Angle 0, February 3 - 6, 1976	131
20 - Scan Angle 3, February 3 - 6, 1976	132
21 - Scan Angle 6, February 3 - 6, 1976	133
22 - 27 Two Spot Causal Filter Performance	
22 - August 7 - 9, 1975	134
23 - October 3 - 5, 1975	135
24 - October 22 - 25, 1975	136
25 - December 5 - 8, 1975	137
26 - January 24 - 25, 1976	138
27 - February 3 - 6, 1976	139
28 - 39 Three Spot Causal Filter Performance	
28 - Extreme Scan, August 7 - 9, 1975	140
29 - Close Scan, August 7 - 9, 1975	141
30 - Extreme Scan, October 3 - 5, 1975	142
31 - Close Scan, October 3 - 5, 1975	143
32 - Extreme Scan, October 22 - 25, 1975	144
33 - Close Scan, October 22 - 25, 1975	145
34 - Extreme Scan, December 5 - 8, 1975	146
35 - Close Scan, December 5 - 8, 1975	147
36 - Extreme Scan, January 24 - 25, 1976	148
37 - Close Scan, January 24 - 25, 1976	149
38 - Extreme Scan, February 3 - 6, 1976	150

39 - Close Scan, February 3 - 6, 1976	151
40 - 42 One Spot Non-causal Filter Performance	
40 - August 7 - 9, 1975	158
41 - October 22 - 25, 1975	159
42 - January 24 - 25, 1976	160
43 - 45 Two Spot Non-causal Filter Performance	
43 - August 7 - 9, 1975	161
44 - October 22 - 25, 1975	162
45 - January 24 - 25, 1976	163
46 - 51 Three Spot Non-causal Filter Performance	
46 - Extreme Scan, August 7 - 9, 1975	164
47 - Close Scan, August 7 - 9, 1975	165
48 - Extreme Scan, October 22 - 25, 1975	166
49 - Close Scan, October 22 - 25, 1975	167
50 - Extreme Scan, January 24 - 25, 1976	168
51 - Close Scan, January 24 - 25, 1976	169
52 - 59 One Spot Precomputed Sub-optimal Filter Performance	
52 - Precomputed Covariance, August 7 - 9, 1975	176
53 - Precomputed Gain, August 7 - 9, 1975	177
54 - Precomputed Covariance, October 3 - 5, 1975	178
55 - Precomputed Gain, October 3 - 5, 1975	179

56 - Precomputed Covariance, December 5 - 8, 1975	180
57 - Precomputed Gain, December 5 - 8, 1975	181
58 - Precomputed Covariance, February 3 - 6, 1976	182
59 - Precomputed Gain, February 3 - 6, 1976	183
60 - 67 Two Spot Precomputed Sub-optimal Filter Performance	
60 - Precomputed Covariance, August 7 - 9, 1975	184
61 - Precomputed Gain, August 7 - 9, 1975	185
62 - Precomputed Covariance, October 3 - 5, 1975	186
63 - Precomputed Gain, October 3 - 5, 1975	187
64 - Precomputed Covariance, December 5 - 8, 1975	188
65 - Precomputed Gain, December 5 - 8, 1975	189
66 - Precomputed Covariance, February 3 - 6, 1976	190
67 - Precomputed Gain, February 3 - 6, 1976	191
68 - 79 Three Spot Precomputed Sub-optimal Filter Performance	
68 - Precomputed Covariance, Extreme Scan, August 7 - 9, 1975	192
69 - Precomputed Covariance, Close Scan, August 7 - 9, 1975	193
70 - Precomputed Gain, Extreme Scan, August 7 - 9, 1975	194
71 - Precomputed Gain, Close Scan, August 7 - 9, 1975	195
72 - Precomputed Covariance, Extreme Scan, October 3 - 5, 1975	196

73 - Precomputed Covariance, Close Scan, October 3 - 5, 1975	197
74 - Precomputed Gain, Extreme Scan, October 3 - 5, 1975	198
75 - Precomputed Gain, Close Scan, October 3 - 5, 1975	199
76 - Precomputed Covariance, Extreme Scan, December 5 - 8, 1975	200
77 - Precomputed Covariance, Close Scan, December 5 - 8, 1975	201
78 - Precomputed Gain, Extreme Scan, December 5 - 8, 1975	202
79 - Precomputed Gain, Close Scan, December 5 - 8, 1975	203
80 - Precomputed Covariance, Extreme Scan, February 3 - 6, 1976	204
81 - Precomputed Covariance, Close Scan, February 3 - 6, 1976	205
82 - Precomputed Gain, Extreme Scan, February 3 - 6, 1976	206
83 - Precomputed Gain, Close Scan, February 3 - 6, 1976	207
84 - Comparative Timings of Various Filters	208
85 - Water Vapor Retrieval Error	224
86 - Liquid Water Retrieval Error	225
87 - Water Vapor Retrieval Error (High Liquid Water Experiment)	226

88 - Liquid Water Retrieval Error	
(High Liquid Water Experiment)	227
89 - Water Vapor Retrieval Error	
(No Temperature Knowledge Experiment)	233
90 - Liquid Water Retrieval Error	
(No Temperature Knowledge Experiment)	234
91 - Water Vapor Retrieval Error	
(No Atmospheric Temperature Knowledge)	235
92 - Liquid Water Retrieval Error	
(No Atmospheric Temperature Knowledge)	236
93 - Water Vapor Retrieval Error	
(No Surface Temperature Knowledge)	237
94 - Liquid Water Retrieval Error	
(No Surface Temperature Knowledge)	238
95 - Water Vapor Retrieval Error	
(3 km Water Vapor Scale Height)	240

96 - Liquid Water Retrieval Error	
(3 km Water Vapor Scale Height)	241
97 - Water Vapor Retrieval Error	
(1 km Water Vapor Scale Height)	242
98 - Liquid Water Retrieval Error	
(1 km Water Vapor Scale Height)	243
99 - Water Vapor Retrieval Error	
(Mixed Water Vapor Scale Heights)	244
100 - Liquid Water Retrieval Error	
(Mixed Water Vapor Scale Heights)	245
101 - Region 1 Correlation Regression Coefficients	258
102 - Region 2 Correlation Regression Coefficients	259
103 - Region 3 Correlation Regression Coefficients	260
104 - Region 4 Correlation Regression Coefficients	261
105 - Near Field Correlation Lengths	263

106 - Values of the Integrals I_1 and I_2	266
107 - Variances of Temperatures In the Atmosphere	268
108 - Apparent Radiosonde Error Performance	270
109 - 117 Computed Sensitivity of Oxygen Absorbtion to Temperature From 10 - 150 GHz.	
109 - 720 Torr, 300° K	276
110 - 360 Torr, 300° K	277
111 - 180 Torr, 300° K	278
112 - 720 Torr, 250° K	279
113 - 360 Torr, 250° K	280
114 - 180 Torr, 250° K	281
115 - 720 Torr, 200° K	282
116 - 360 Torr, 200° K	283
117 - 180 Torr, 200° K	284

Chapter I

Introduction

Remote sensing of the environment is becoming an area of increasing importance in both application and research. The ability to determine accurately the state of the environment on both a global and timely basis is expected to have profound human and economic impact. As a specific example, weather predictions are produced with large numerical models which solve the differential equations that describe heat, mass and momentum transfer in the earth's atmosphere. For these models to perform adequately, it is important that the boundary conditions at the initiation of the algorithm be as accurate as possible. Historically, these boundary conditions have been provided by a network of observing stations that provide information about the earth's upper atmosphere through the release of radiosondes or the launch of rocketsondes. For logistic and economic reasons, most of these stations are situated in economically developed and densely populated land regions. As a result, the ability to perform accurate long range prognosis has been severely limited in the past, because of the lack of

data over a large percentage of the earth's surface. Fortunately, this situation is changing.

As suggested by Kaplan (1959) in the infrared spectrum and by Meeks and Lilley (1963) in the microwave, many of the variables needed for the initialization of weather prediction models may be inferred by observing the thermal emission from the earth's atmosphere. If the frequency of observation is chosen to be in a region of absorption or emission of a uniformly mixed gas such as carbon dioxide or oxygen, the thermal radiation may be interpreted in terms of temperature in the atmosphere. If the observed wavelength lies near a region of absorption by a species whose concentration in the atmosphere varies, such as water or ozone, the observation may be related to concentration. Finally, instruments may infer characteristics of the terrestrial surface by observing it in regions where the atmosphere has little absorptive effect. Satellites and ground-based radiometers that observe in one or more of these spectral regions have been used either experimentally or operationally for a number of years. It is hoped that the inclusion of data from these instruments will improve the skill of numerical forecast models in the future.

The design and implementation of a passive microwave sounding system is a multi-discipline effort. The desired products are in the area of meteorology, the fundamental

processes are in the realm of physics, the instrument design and implementation lie with the electrical engineer, and the interpretation and handling of the resulting data with the computer scientist and estimation theorist. The contribution of this thesis is in that final area.

A large body of techniques, both statistical and non-statistical, have been proposed for processing data from remote sounders to produce estimates of the state of the earth's atmosphere. These methods have included the regression or statistical D method (Rosenkranz et al., 1972, Waters et al., 1975), the minimum information technique (Fleming and Smith 1971, Fritz et al. 1972), the empirical eigenfunction technique (Smith and Woolf, 1976), and various numerical relaxation techniques such as those due to Chahine. The purpose of this thesis is to introduce into this field the methods of modern recursive estimation theory, specifically, the Kalman-Bucy filter.

While it has been recognized for a period of time now that the Kalman-Bucy filter is an optimum estimation technique and should produce superior estimates based on radiometer data, no such filter has been successfully implemented. This thesis represents the first successful implementation of that technique on remote sensing data in the area of estimation of meteorological processes. As such, it does not claim to be an advance in either Kalman

filtering theory or in fundamental remote sensing theory. It is an advance in the art of the analysis of data from such remote sensors.

The body of this thesis is divided into a number of chapters. In Chapter II, the theory of radiative transfer in the atmosphere is presented. Special emphasis is placed on those aspects that allow inference of meteorological parameters. Chapter III discusses Kalman-Bucy filtering theory in its various aspects. Chapter IV presents the summary of the results of a temperature profile inverting Kalman-Bucy filter that operated on data from the SCanning Microwave Spectrometer (SCAMS) carried on the Nimbus 6 satellite (Staelin et al., 1975). Chapter V presents the results of an extended Kalman-Bucy filter for estimation of water vapor and liquid water columns operating on simulated SCAMS data.

Appendix A contains the results obtained from the analysis of the synoptic radiosonde observations of North America during January and February 1973. The results contained in Appendix A are interpreted primarily in terms of the difference between a point sensor (such as a radiosonde) and an area sensor (such as a radiometer) temperature profile retrieval in a random temperature field. The results, however, should be useful in system identification of plant matrices and the Gandin (1964)

weighting in synoptic analysis. Appendix B considers the sensitivity of the oxygen temperature weighting function and microwave absorption coefficient to changes in the temperature profile. Appendix C is an extensive verbal description of the Kalman filter algorithm implemented in this thesis.

Chapter II

The Radiative Transfer Basis of Passive Remote Sensing

Section A. The equations of radiative transfer

The ability to perform remote sensing derives from the fact that, by proper selection of observation wavelengths, the thermal emission radiating from the surface of the earth and its atmosphere may be measured. The equations that describe the production and propagation of this energy are generally called the equations of radiative transfer.

The particular equation of radiative transfer that is of greatest interest for this thesis is that for the received flux seen by an observer looking downward through a non-scattering absorbing medium toward a partially reflecting surface. For this case, the flux seen is:

$$I(\nu) = \int_{H_s}^H B(\nu, T(h)) K(\nu, h) [\tau(h, H) + R(\nu) \tau(H_s, h) \tau(H_s, H)] dh$$
$$+ (1 - R(\nu)) \tau(H_s, H) B(\nu, T_s)$$
$$+ R(\nu) \tau^2(H_s, H) I_{sky}(\nu)$$

2.1

where

$B(\nu, T)$ is the Plank function at frequency ν and temperature T ,

H and H_s describe the relative positions of the observer and the surface,

h traces a ray from the observer to the surface,

$I(\nu)$ is the received flux at frequency ν ,

$I_{SKY}(\nu)$ is the background flux from behind the surface directed at the surface,

$K(\nu, h)$ is the absorption coefficient of the medium at frequency ν and position h ,

$R(\nu)$ is the reflectivity of the surface boundary,

$T(h)$ is the temperature of the medium at h ,

T_s is the temperature of the surface boundary, and

$\mathcal{T}(h_1, h_2)$ is the extinction of the medium from h_1 to h_2 equal to:

$$\mathcal{T}(h_1, h_2) = \text{EXP} \left\{ - \int_{h_1}^{h_2} K(\nu, h) dh \right\} \quad 2.2$$

For microwave frequencies, it is permissible to invoke the Raleigh-Jeans approximation to simplify 2.1 (e.g.

Staelin, 1969, Rosenkranz, 1972) to obtain:

$$\begin{aligned}
 T(\nu) = & \int_{H_s}^H T(h) K(\nu, h) [\tau(h, H) + R(\nu) \tau(H_s, h) \tau(H_s, H)] dh \\
 & + (1 - R(\nu)) \tau(H_s, H) T_s \\
 & + R(\nu) \tau^2(H_s, H) T_{sky}
 \end{aligned} \tag{2.3}$$

where $T_B(\nu)$ is called the brightness temperature and is equal to the temperature of a black body that will produce a flux equal to the one observed. Likewise, T_{sky} is the equivalent black body temperature of the background and is often called the sky temperature.

Section B. Absorption by the atmosphere

In the context of passive remote sensing from satellites, the equations of radiative transfer 2.1 and 2.3 describe the interaction of the atmosphere, the earth's surface and cold space with the energy observed by the down-looking radiometer. In this case, the absorbing medium is the atmosphere, the surface boundary is the earth's surface, and the background is the cosmic background. This section will primarily consider the nature of absorption by the atmosphere in the microwave region of the spectrum. The

theory of how this absorption occurs will not be discussed in any detail, but rather, a qualitative feeling will be sought.

There are two major microwave absorbers of meteorological interest in the lower microwave region. They are oxygen and water in both liquid and vapor form. Oxygen, which is used primarily for temperature profile sensing, has a series of lines due to magnetic moment transitions. These transitions form a complex of resonant lines from approximately 50 Ghz. to 70 GHz. and an isolated line at 118.75 GHz. The line centers for these transitions have been calculated by a number of experimenters (Wilheit and Barrett, 1970, Wilheit, 1970, Liebe and Welch, 1977). The shapes of the individual lines and their interaction are determined by collisional broadening. Numerous expressions accounting for this effect have been derived over the years. Some of these have included those derived by Van Vleck and Weisskopf (1945), Meeks and Lilley (1963), Lenoir (1965), and Rosenkranz (1975). While it will be noted here that one of the later oxygen lineshape models derived by Rosenkranz was used in the experiments of this thesis, a discussion of the physics of oxygen lineshape is outside its scope.

The prime consideration in developing a qualitative feeling for the lineshape is that the broadening of the

oxygen is affected by two quantities; temperature and pressure. As the pressure increases, the absorption increases. Over the range of temperatures encountered in the terrestrial atmosphere, an increase in temperature implies a decrease in absorption. empirical fit by Poon (1976) to several lineshapes gives the form of this relation for a given frequency relating the absorption K to the pressure P and temperature T as:

$$K = a P^x T^y \quad 2.4$$

where a and x are positive constants and y is a negative constant over a given pressure temperature domain.

Another important microwave absorber in the earth's atmosphere is water in both its liquid and vapor forms. Water vapor in the atmosphere absorbs by means of rotational energy transitions of an electric dipole contained in an asymmetric top. These energy transitions produce a series of resonant lines in the microwave region. The first two lines (22.235 GHz. and 183.310 GHz.) are of present practical interest in passive remote sensing.

The line shape of the water vapor resonances are affected by collisional broadening (Staelin, 1966, Gaut, 1968, Reifenstein and Gaut, 1971). Its spectrum is thus comprised of a series of broadened lines combined with a non-resonant

component. There is however, an anomalous absorption in its spectrum that has yet to be adequately explained. It has been suggested that this is caused by the action of water vapor dimers, but studies by Poon (1974) have found this explanation to be inadequate. The one item of importance in the absorption by water vapor besides the usual collisional broadening behaviour, is that the expression for the absorption coefficient contains a quadratic term due to the higher effectiveness of $H_2O - H_2O$ collisions when compared to $H_2O - O_2$ and $H_2O - N_2$ collisions in broadening the line.

The last absorber that will be discussed in this section is liquid water. Liquid water exists in the atmosphere in the form of clouds and rain. As such it is in the form of dielectric spheres and the theory of Mie may be applied. This theory has been extensively discussed in the literature (e.g. Van DeHulst, 1957) and so will not be covered here.

For the cases of interest in this thesis, the wavelengths of the radiation are much larger than the drop sizes. In this case, it is customary to use the Raleigh limit to evaluate the absorption. In this limit the absorption efficiency of a droplet is given by the

expression:

$$Q_n(r, \lambda, T) = 4\alpha \operatorname{IM} \left\{ -\tilde{K}(\lambda, T) \right\} \quad 2.5$$

where

$$\tilde{K}(\lambda, T) = \frac{\tilde{n}^2(\lambda, T) - 1}{\tilde{n}^2(\lambda, T) + 2} \quad 2.6$$

and \tilde{n} is the complex dielectric coefficient of the sphere which is a function of wavelength and temperature. α is the dropsize parameter given by the expression:

$$\alpha = 2\pi r / \lambda \quad 2.7$$

where r is the drop radius and λ is the wavelength of interest. To obtain the absorption by a unit volume we may integrate the expression:

$$K(\lambda, T) = \int_0^{\infty} N(r) Q_n(r, \lambda, T) \pi r^2 dr \quad 2.8$$

where $N(r)$ is the number of drops with radius r per unit volume. Substituting for $Q_n(r, \lambda, T)$ we obtain:

$$K(\lambda, T) = \int_0^{\infty} N(r) \frac{8\pi r^3}{\lambda} \operatorname{IM} \left\{ -\tilde{K}(\lambda, T) \right\} \quad 2.9$$

Using the fact that the mass density of the drops in the volume is:

$$m = \frac{4\pi\rho}{3} \int_0^{\infty} N(r) r^3 dr \quad 2.10$$

we obtain:

$$K(\lambda, T) = \frac{6\pi m}{\rho\lambda} \operatorname{IM} \left\{ -\tilde{K}(\lambda, T) \right\} \quad 2.11$$

This function has been empirically evaluated by Staelin (1966), with the result that the absorption due to clouds is approximately:

$$K(\lambda, T) = 1.71 m f^2 10^{-0.0122 T} \text{ db/km} \quad 2.12$$

where f is the frequency in GHz., T is the temperature in degrees Kelvin, and m is the density of the cloud in gm/m^3 .

Section C. Surface effects

The discussion of Section A of this chapter has

indicated that the observed brightness temperature is primarily a function of three variables: the temperature of the earth's atmosphere and surface, the absorption of the earth's atmosphere along the path and finally, the reflectivity of the earth's surface. This section will discuss the behaviour of this last variable.

A radiometer viewing the earth sees three major classes of surfaces: land, ice and snow, and lakes or ocean. Each of these has its own behaviour with respect to reflectivity. Land areas act for the most part as nearly black bodies in the microwave region unless there is appreciable soil moisture or standing water. Statistics compiled by Rosenkranz (1971) during flights of a prototype of the Nimbus E Microwave Spectrometer give a range of average land emissivity from 0.9 to 0.95. These emissivities are basically independent of surface temperature.

The second major surface type seen by a radiometer is ice and snow. The passive remote sensing of this surface is an area of research in its own right. Emissivity signatures of different types of snow and ice allow the type of cover to be inferred. For the purposes of this thesis, it will suffice to note that the range of emissivities for snow and ice is from 0.6 to 0.9 and that the emissivity is again basically insensitive to temperature change.

The final major surface type is open water. The horizontal and vertical components of the reflectivity from a calm sea may be determined analytically from the angle of incidence and the complex dielectric coefficient of seawater. Since the dielectric constant varies with temperature, the reflectivity does also. The basic form of this variation is for the emissivity to decrease with increasing temperature. Over some ranges of frequencies, the product of the emissivity and the surface temperature may have a negative slope. However, since a decrease in the emissivity implies an increase in reflectivity, the percentage of the sky component of the brightness temperature (radiation from the atmosphere directed at the earth) that is reflected back to the radiometer increases. For frequencies of interest in this thesis, the two effects nearly cancel each other and the sensitivity of the observed brightness temperature to the sea surface temperature is small.

Section D. The concept of a temperature weighting function

In this section, concepts of the continuous and

discrete temperature weighting functions will be developed. As these functions are commonly assumed to be independent of temperature in the case of oxygen, an examination will be made of this assumption.

To derive the concept of the temperature weighting function, it will be convenient to rewrite 2.3 as:

$$T_B(\nu) = \int T(h) W(h, \nu, R) dh + T_s W_s(\nu, R) + T_{sky} W_{sky}(\nu, R) \quad 2.13$$

where:

$$W(h, \nu, R) = K(\nu, h) [\tau(h, H) + R(\nu) \tau(H_s, h) \tau(H_s, H)] \quad 2.14$$

$$W_s(\nu, R) = [1 - R(\nu)] \tau(H_s, H) \quad 2.15$$

$$W_{sky}(\nu, R) = R(\nu) \tau^2(H, H) \quad 2.16$$

If the absorption coefficient of the atmosphere at frequency ν does not change with concentration or temperature, but solely with height or pressure, these three functions will be a function only of ν and the surface reflectivity $R(\nu)$. In this case, the functions are called the continuous temperature weighting functions since they

describe the relative weight given to the temperature $T(h)$, the surface temperature T_s and the sky temperature T_{sky} in the observed brightness temperature.

It is often convenient to model the atmosphere as composed of a number of slabs. The vertical temperature within such a slab i is assumed to be determined by the temperature at some altitude h_i and a function such as a lapse rate. Under these assumptions, 2.13 assumes the form:

$$T_B(\nu) = \sum_{i=1}^N T(h_i) W_i(\nu, R) \quad 2.17$$

$$+ T_s W_s(\nu, R) + T_{SKY} W_{SKY}(\nu, R)$$

where $W_i(\nu, R)$ is called the discrete weighting function for level i and equals:

$$W_i(\nu, R) = \int_{L_i}^{U_i} F_i(T(h), T(h_i)) W(h, \nu, R) dh \quad 2.18$$

where:

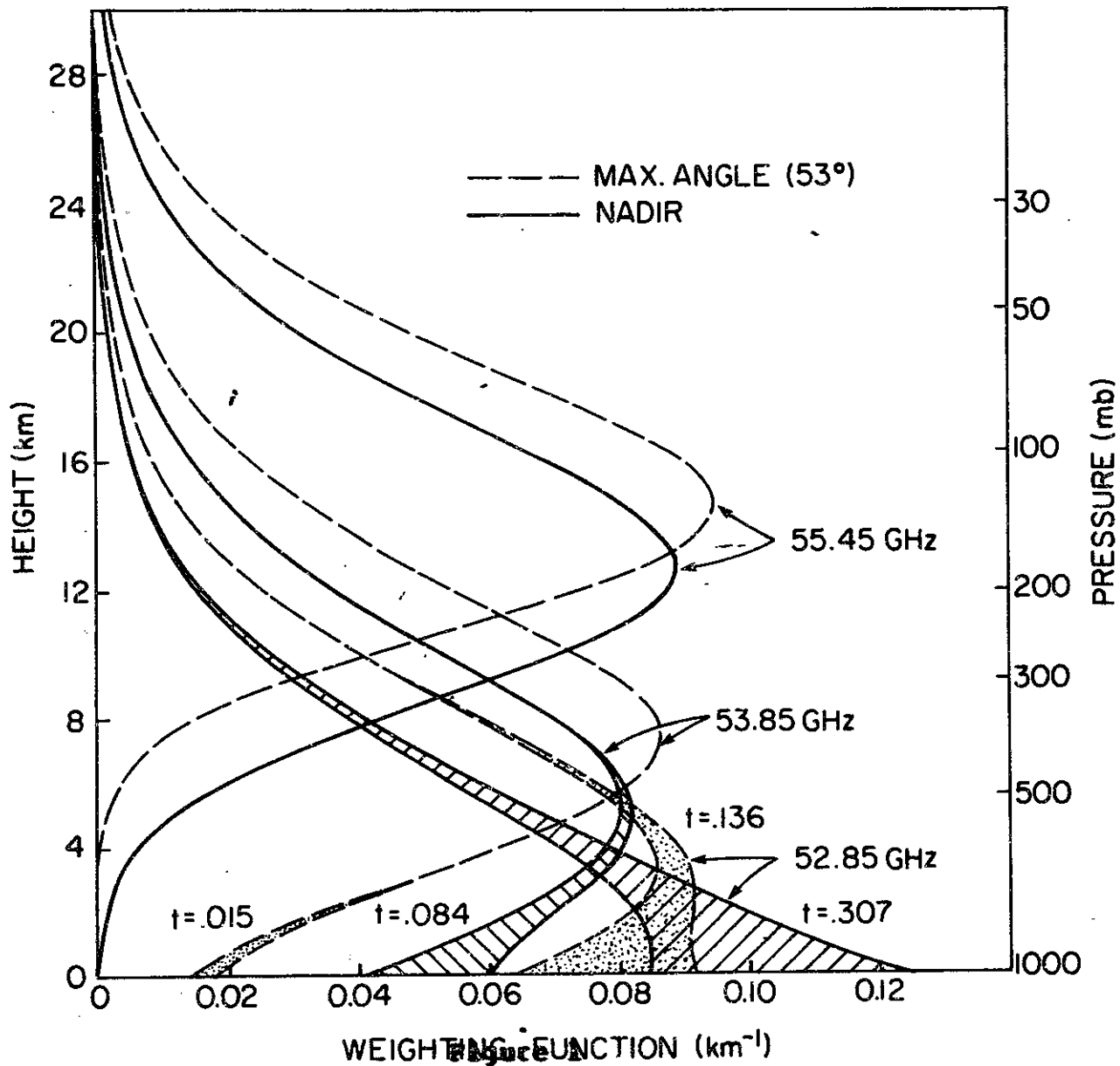
L_i, U_i are the lower and upper boundaries of an atmospheric slab whose temperature structure is described by $T(h_i)$ and

$F_i(T(h), T(h_i))$ is the function relating $T(h)$ to $T(h_i)$

within slab i . By defining a vector of temperatures T that include the $T(h_i)$, T_s and T_{sky} and a similar vector W of discrete weighting functions, 2.17 may be expressed as the matrix equation:

$$T_B(\nu) = W T \quad 2.19$$

The continuous weighting functions for the passive microwave sounder SCAMS (after Staelin et al., 1975) are shown in Figure 1. These weighting functions have been computed under the assumption that the atmosphere is represented by the U. S. Standard Atmosphere. A number of curves are given in this figure. The solid lines correspond to the weighting functions at the nadir look angle. The dashed curves correspond to the weighting functions at the extreme scan angle. The outermost curve for a given frequency and look angle is the weighting function over ocean, while the inner curve is the weighting function over land. The area between these two curves is hatched or dotted. The value of t in this figure is the extinction through the atmosphere. A similar set of discrete weighting functions for this instrument are contained in Table 1. In this case, the table contains the weighting functions computed for a 60 N latitude winter average atmosphere and the difference between these



SCAMS Continuous Weighting Functions
Outer line over ocean, inner line over land.
 t = transmission from surface.

Table 1

Pressure (mb)	Channel 3 (52.85 GHz)		Channel 4 (53.85 GHz)		Channel 5 (55.45 GHz)		Slab Definition (mb)
	60° Winter	Difference 60° Winter 15° Annual	60° Winter	Difference 60° Winter 15° Annual	60° Winter	Difference 60° Winter 15° Annual	
Surface	.285	.032	.078	.010	.000	.000	Surface
1000	.058	-.006	.030	-.001	.000	.000	1013 - 925
850	.135	.011	.076	-.003	.001	.000	925 - 775
700	.151	-.011	.139	+.006	.007	.000	775 - 600
500	.138	-.004	.173	-.003	.028	-.001	600 - 450
400	.086	-.002	.135	-.004	.058	-.002	450 - 350
300	.059	-.001	.106	-.004	.094	-.002	350 - 275
250	.035	.001	.069	-.001	.103	-.001	275 - 225
200	.030	.000	.065	.000	.145	-.001	227 - 175
150	.025	.000	.059	.004	.189	.002	175 - 125
100	.015	.000	.038	.003	.167	-.003	125 - 85
70	.006	.000	.015	.002	.077	.004	85 - 60
50	.006	.000	.014	.001	.080	.002	60 - 40
30	.003	.000	.007	.001	.042	.002	40 - 20
10	.001	.000	.002	.000	.013	.001	20 - 7.5

weighting functions and those computed for a 15°N latitude average annual atmosphere. The manner in which these weighting functions were calculated is described in Chapter IV.

Referring to Table 1, it may be seen that the assumption of invariance of the weighting functions is a fairly good one in the middle and upper atmosphere. In the lower atmosphere, the variability of the absorption coefficient with water vapor concentration introduces a noticeable effect. However, it should be noted that the difference in the water vapor concentrations between the two atmospheres in Table 1 was a factor of twenty, and that both atmospheres represent extreme conditions. The insensitivity of the temperature weighting function with regard to the sensitivity of oxygen absorption to temperature is further considered in Appendix B.

Chapter III

Theory of the Discrete Kalman-Bucy Filter

Section A. A heuristic derivation

The theory of the discrete and continuous Kalman-Bucy filter has been widely discussed (Kalman, 1960, Jazwinski, 1970, Leondes, 1970, Schweppe, 1973, Gelb, 1974). Thus the purpose of this section and those that follow is to provide a basic understanding of the discrete Kalman-Bucy filter. This will be done in order to facilitate an understanding of the temperature filter experiment and liquid water and water vapor experiment which comprise the bulk of the experimental work of this thesis. Only those aspects of the filtering theory which relate to these experiments will be covered in this chapter. This section provides a heuristic derivation of the Kalman filter from a Bayesian estimation viewpoint, while Section B provides a derivation from a structured viewpoint that assumes a form for the estimator. Section C discusses the properties of the innovations sequence of the filter and covers the topic of testing the filter using the innovations sequence. Section D investigates the square

root algorithm for a covariance filter. Section E describes the extended Kalman-Bucy filter. Finally, Section F presents the forward-backward algorithm for non-causal Kalman filtering.

The notation used in this chapter and those that follow is that of Gelb (1974). In this notation, quantities are often followed by a minus or plus sign and are subscripted. The discrete time coordinate of the quantity is determined by the subscript. The parenthesised minus or plus signs refer to the values at time i before and after the processing of data received at time i . As is customary, the optimum estimate is denoted by a caret ($\hat{}$). Thus, the optimum estimate of A before the processing of data received at time i is $\hat{A}_i(-)$. The value of a parameter B after the processing of data received at time j is $B_j(+)$. It should be noted that although the coordinate of the data reception is referred to as "time", it is an arbitrary running coordinate. For remote profile sensing this coordinate is both spatial and temporal.

In order to develop the theory of the Kalman-Bucy filter, we will make the following assumptions: The process to be estimated is an n vector X_i . This vector is assumed to have an expectation or mean conditioned on the time of the start of processing equal to $\hat{X}_i(-)$. The error covariance of this conditional mean is assumed to be known

and is a n by n matrix $P_i(-)$. The observed process is represented by a m vector Z_i which is related to X_i by the linear relation:

$$Z_i = H_i X_i + N_i \quad 3.1$$

where H_i is a m by n dimensional observation matrix and N_i is a zero mean white Gaussian process with covariance matrix R_i .

Then, given that data has been observed at time 1, the optimum estimate of X_1 using a simple Bayesian approach is:

$$\hat{X}_1(+) = \hat{X}_1(-) + [K_1 Z_1 - \hat{Z}_1(-)] \quad 3.2$$

where:

$$\hat{Z}_1(-) = H_1 \hat{X}_1(-) \quad 3.3$$

and

$$K_1 = P_1(-) H_1^T [H_1 P_1(-) H_1^T + R_1]^{-1} \quad 3.4$$

The a posteriori error covariance of the estimate will be

given by:

$$P_i(+)= [I - K_i H_i] P_i(-) \quad 3.5$$

where I is the n by n identity matrix. Being a Bayesian estimate, the estimate $\hat{X}_i(+)$ will have the property that it is a conditional mean of X_i , where the conditioning is now additionally on the fact that Z_i was observed.

The crucial point in the development of the filter now occurs if the process X_i is constrained to be a first order Gauss-Markov process. In the discrete case at hand this implies that:

$$X_{i+1} = \Phi_{i,i+1} X_i + V_i \quad 3.6$$

where $\Phi_{i,i+1}$ is called the state transition matrix from time i to $i+1$ and represents the deterministic transition of X_i . V_i is a zero mean white Gaussian process, independent of X_i , with covariance matrix Q_i . It represents the truly random factors in the transition and is often called the plant noise. If a process is a first order Gauss-Markov process, the conditional mean at time i may be propagated to time $i+1$ by:

$$\hat{X}_{i+1}(-) = \Phi_{i,i+1} \hat{X}_i(+) \quad 3.7$$

and the error covariance of the mean by:

$$P_{i+1} (-) = \Phi_{i,i+1} P_i (+) \Phi_{i,i+1}^T + Q_i \quad 3.8$$

These two equations then provide a means of obtaining the a priori conditional mean and its error covariance at time 2 from the a posteriori conditional mean (the estimate) and its error covariance at time 1. These quantities provide the necessary conditions to perform a Bayesian estimate at time 2. A recursive filter is thus obtained in which the estimate and its error covariance are fed forward and used in the next step.

It should be noted that nowhere in the development of the filter are any assumptions made concerning the stationarity of the processes. The matrices Q_i , H_i , R_i and $\Phi_{i,i+1}$ may be time space varying and so non-stationary processes may be estimated using the Kalman-Bucy filter.

Section B. A structured derivation

One of the many possible approaches of mathematically

deriving the discrete Kalman-Bucy filter is a structured derivation. In this approach the linear of the estimator is assumed a priori. The desired lack of bias and minimum quadratic cost properties of the estimate combined with the fact that the process being estimated is a first order Gauss-Markov process then yield the discrete Kalman-Bucy filter.

To begin the structured derivation, it will be assumed that the observation vector Z_i is a noisy linear function of the vector of state:

$$Z_i = H_i X_i + N_i \quad \begin{array}{l} 3.1 \\ \text{(REPEATED)} \end{array}$$

and that the desired estimator is of the form:

$$\hat{X}_i(+)= K_i' \hat{X}_i(-) + K_i Z_i \quad 3.9$$

where K_i' and K_i are two gains to be determined.

The errors associated with the estimates $\hat{X}_i(+)$ and $\hat{X}_i(-)$ are:

$$\tilde{X}_i(+)= \hat{X}_i(+)- X_i \quad 3.10$$

and

$$\tilde{X}_i(-) = \hat{X}_i(-) - X_i \quad 3.11$$

Substituting 3.1, 3.10, and 3.11 into 3.9 yields:

$$\tilde{X}_i(+) = [K_i' + K_i H_i - 1] X_i + K_i' \tilde{X}_i(-) + K_i N_i \quad 3.12$$

Taking the expectation over N_i and $\tilde{X}_i(-)$ on both sides of 3.12 and assuming that $\hat{X}_i(-)$ is an unbiased estimate, we note that $\hat{X}_i(+)$ will be an unbiased estimate only if:

$$[K_i' + K_i H_i - 1] = 0 \quad 3.13$$

Thus it is required that:

$$K_i' = 1 - K_i H_i \quad 3.14$$

Substituting 3.14 into 3.12 and 3.9 yields:

$$\tilde{X}_i(+) = [1 - K_i H_i] \tilde{X}_i(-) + K_i N_i \quad 3.15$$

and

$$\hat{X}_i(+)=\hat{X}_i(-)+K_i[Z_i-H_i\hat{X}_i(-)] \quad 3.16$$

The error covariance of 3.16 will be given by the expectation of 3.15 times its transpose or:

$$\begin{aligned} P_i(+)= & [I-K_iH_i]P_i(-)[I-K_iH_i]^T \\ & + [I-K_iH_i]E\{\tilde{X}_i(-)N_i^TK_i^T\} \\ & + K_iE\{N_i\tilde{X}_i^T(-)\}[I-K_iH_i]^T \\ & + K_iR_iK_i^T \end{aligned} \quad 3.17$$

Since N_i is assumed to be statistically independent of $\tilde{X}_i(-)$ this simplifies to:

$$P_i(+)= [I-K_iH_i]P_i(-)[I-K_iH_i]^T + K_iR_iK_i^T \quad 3.18$$

To choose the optimum value for the gain K we will desire to minimize the quadratic cost function:

$$J = E\{\tilde{X}_i(+)^T S \tilde{X}_i(+)\} \quad 3.19$$

for any positive definite error weighting matrix S . As this

may be shown to be equivalent to minimizing the trace of $P_i(+)$, we will choose to optimize the gain to minimize this function instead.

Using the relation that:

$$\frac{\partial}{\partial A} \text{tr} \{A B A^T\} = 2 A B \quad 3.20$$

for a symmetric matrix B, we differentiate $\text{tr}\{P_i(+)\}$ with respect to K_i in 3.18 to yield:

$$\frac{\partial}{\partial K} \text{tr} \{P_i(+)\} = 2 [I - K_i H_i] P_i(-) H_i^T + 2 K_i R_i \quad 3.21$$

For the extrema of $\text{tr}\{P_i(+)\}$, we require this to be zero.

Thus:

$$K_i = P_i(-) H_i^T [H_i P_i(-) H_i^T + R_i]^{-1} \quad 3.22$$

The second derivative of $\text{tr}\{P_i(+)\}$ with respect to K is:

$$\frac{\partial^2}{\partial K^2} \text{tr} \{P_i(+)\} = 2 [H_i P_i(-) H_i^T + R_i] \quad 3.23$$

This matrix is positive semi-definite for all H_i . Thus the

gain of 3.22 gives a minimum for the $\text{tr}\{P_i(+)\}$.

As before, we will now invoke the first order Gauss-Markov assumption on the process X_i . This produces the relation:

$$X_{i+1} = \Phi_{i,i+1} X_i + V_i \quad \begin{array}{l} \text{3.6} \\ \text{(REPEATED)} \end{array}$$

Taking the expectation of both sides conditioned on the observation of data through time i yields:

$$\hat{X}_{i+1}(-) = \Phi_{i,i+1} \hat{X}_i(+) \quad \begin{array}{l} \text{3.7} \\ \text{(REPEATED)} \end{array}$$

Again this describes the propagation of the estimate at one time to the prior at the next. Subtracting 3.6 from 3.7 yields:

$$\tilde{X}_{i+1}(-) = \Phi_{i,i+1} \tilde{X}_i(+) - V_i \quad \text{3.24}$$

Multiplying 3.24 by its transpose and taking expectations yields:

$$P_{i+1}(-) = \Phi_{i,i+1} P_i(+) \Phi_{i,i+1} + Q_i \quad \text{3.8}$$

since V_i is assumed to be independent of $\tilde{X}_i(+)$. As before, this describes the propagation of the error covariance of

the estimate between measurements.

Section C. The innovations process

The quantity:

$$\nu_i = Z_i - H_i \hat{X}_i(-) \quad 3.25$$

is defined in the literature of Kalman-Bucy filtering as the innovations process of the observations. Heuristically, it represents the new information brought into the system by the measurement Z_i . If ν_i is zero, this information is that the propagation of $\hat{X}_{i-1}(+)$ to $\hat{X}_i(-)$ was adequate and that our prior was most likely the correct state. If ν_i is not zero, it means that the value of $\hat{X}_i(-)$ must be modified to "explain" the observation. The innovations sequence of the optimal filter has several valuable properties which may be used to test the filter and the data. These properties are that the innovations sequence is a white Gaussian zero mean process with a known covariance.

It is easily shown that any unbiased prior $\hat{X}_i(-)$ produces innovations with a zero mean provided that the observation matrix assumed by the filter corresponds with

reality. Substituting 3.1 and 3.11 into 3.25 we get:

$$V_i = N_i - H_i \tilde{X}_i(-) \quad 3.26$$

Taking expectations, this will be zero since we have assumed that the observation noise N_i is zero mean as is the error of the prior.

It is interesting to note what happens when the observation model that is assumed by the estimation scheme is not correct. Let us say that the estimation scheme assumes that the observation matrix is H_i' while in reality it is H_i . The innovation is then:

$$V_i = (H_i - H_i') X_i + N_i - H_i' \tilde{X}_i(-) \quad 3.27$$

Still assuming that $\hat{X}_i(-)$ is an unbiased prior such as a mean, we find that the mean of the innovations will be zero if and only if X_i is zero mean.

Unfortunately, a non-zero mean serves only as a warning flag that something is not right. It does not unequivocally point to an incorrect observation model. Many practical instruments will contain an unknown bias dependent on the observation matrix H_i . The actual observation then becomes:

$$Z_i = H_i X_i + b(H_i) + N_i \quad 3.28$$

where b is a bias. The innovation here is:

$$v_i = b(H_i) + (H_i - H_i') X_i + N_i - H_i' \tilde{X}_i(-) \quad 3.29$$

If we examine only the mean of the innovation we have

$$E\{v_i\} = b(H_i) + (H_i - H_i') E\{X_i\} \quad 3.30$$

and cannot in general discriminate between the two sources.

To determine the covariance of the innovations, we multiply 3.26 by its transpose and take expectations to yield:

$$E\{v_i v_i^T\} = H_i P_i(-) H_i^T + R_i \quad 3.31$$

To verify the Gaussian nature of the innovations we will assume that the error of the prior at step $i-1$ is a Gaussian random variable. Then

$$\tilde{X}_{i-1}(+) = [1 - K_{i-1} H_{i-1}] \tilde{X}_{i-1}(-) + K_{i-1} N_{i-1} \quad 3.15$$

is a Gaussian random variable since it is the sum of rotated Gaussian random variables. The one step prediction gives us:

$$\tilde{X}_i(-) = \Phi_{i-1,i} \tilde{X}_{i-1}(+) - V_{i-1} \quad 3.24 \quad (\text{REPEATED})$$

Again, this is a Gaussian random variable for the same reasons. Substituting this into 3.26 demonstrates the Gaussian nature of the innovations.

It may be shown that the innovations process must be a white process in the optimal filter. To do this we first will multiply 3.26 taken at time i by the transpose of 3.26 taken at time j and take expectations to find:

$$\begin{aligned} E\{V_i V_j^T\} &= E\{N_i N_j^T\} - E\{N_i \tilde{X}_j^T(-)\} H_j^T \\ &\quad - H_i E\{\tilde{X}_i(-) N_j^T\} + H_i E\{\tilde{X}_i(-) \tilde{X}_j^T(-)\} H_j \end{aligned} \quad 3.32$$

As N_i is a white process the $E\{N_i N_j\}$ is 0 for $i \neq j$, and since our interest here is exactly $i \neq j$, we will drop it from further formulae. Restricting our interest to the case of $i > j$ we note that:

$$E\{N_i \tilde{X}_j^T(-)\} = 0 \quad 3.33$$

since the observation noise is independent of all processes

at earlier times. We will now seek a relation for $\tilde{X}(-)$ in terms of $\tilde{X}(-)$. Substituting 3.15 into 3.24 we get:

$$\tilde{X}_{i+1}(-) = \Phi_{i,i+1} \left\{ [I - K_i H_i] \tilde{X}_i(-) + K_i N_i \right\} - V_i \quad 3.34$$

This gives a recursive relation for $\tilde{X}_{i+1}(-)$ in terms of $\tilde{X}_i(-)$. We may expand this recursion to show that:

$$\begin{aligned} \tilde{X}_i(-) &= \left\{ \prod_{n=j}^{i-1} \Phi_{n,n+1} [I - K_n H_n] \right\} \tilde{X}_j(-) \\ &+ \sum_{k=j}^{i-1} \left\{ \prod_{n=k+1}^{i-1} \Phi_{n,n+1} [I - K_n H_n] \right\} \Phi_{k,k+1} K_k N_k \quad 3.35 \\ &+ \sum_{k=j}^{i-1} \left\{ \prod_{n=k+1}^{i-1} \Phi_{n,n+1} [I - K_n H_n] \right\} V_k \end{aligned}$$

The products here are left matrix multiplications and if the lower limit exceeds the upper limit, the product is the appropriate identity matrix. We now substitute this into 3.32 and using the statistical independence of the plant noise and observation noise, both with respect to each other and to errors and noises at earlier times we may simplify 3.32 to:

$$\begin{aligned} E\{V_i V_j\} &= H_i \left(\prod_{n=j+1}^{i-1} \Phi_{n,n+1} [I - K_n H_n] \right) * \\ &\Phi_{j,j+1} \left\{ -K_j R_j + [I - K_j H_j] P_j(-) H_j^T \right\} \quad 3.36 \end{aligned}$$

The quantity in braces may be rearranged as:

$$P_j(-) H_j^T - K_j [H_j P_j(-) H_j^T + R_j] \quad 3.37$$

If the gain K is the optimal Kalman gain, this reduces 3.37 to

$$\begin{aligned} P_j(-) H_j^T - P_j(-) H_j^T [H_j P_j(-) H_j^T + R_j]^{-1} [H_j P_j(-) H_j^T + R_j] \\ = P_j(-) H_j^T - P_j(-) H_j^T \\ = 0 \end{aligned} \quad 3.38$$

Thus, $E\{v_i v_j^T\}$ is zero for all $i > j$ providing that the optimum gain is used at time j .

It is possible to perform a number of tests on both the data stream and the models assumed in the estimation scheme using the innovations sequence. As indicated earlier, one is a simple mean test. If the sample mean of the innovations is not zero within the confidence indicated by the variance of v and the number of samples, it indicates that there are unresolved problems in either the observation matrices, state propagation, or instrument bias. Likewise it is possible to test the sample variance of the innovations to reveal other problems. Finally, it is possible to examine the whiteness of the innovations to

determine if the estimation scheme is suboptimum.

Given that the estimation scheme does not pass these various tests, it is potentially possible to modify the estimation scheme by a procedure known as "Adaptive Kalman Filtering". Some methods for doing this are indicated by Jazwinski (1970) and Mehra (1970, 1971).

Another set of possible tests that are possible using the innovations are often called "data reasonableness tests". The basis of these tests lies in the fact that not all instruments are well behaved and obey the assumptions made about them all the time. As a specific example of interest, consider a sporadically malfunctioning radiometer observing a dynamic process operating over a digital transmission link. If everything is operating correctly, the data link does not produce errors and the observation noise is determined by the front end noise of the instrument. The innovations sequence will then be well behaved and will have the statistical behaviour that we have derived in this section. If the digital transmission link produces an error, this fact should be observable from the fact that such an error is usually as likely to appear on the most significant bit as the least significant bit. An error of this sort will usually lead to the rejection of the hypothesis that the innovation was drawn from a $N(0, H_i P_i (-) H_i^T + R_i)$ population. Transmission errors

may then be detected by innovations testing.

A similar test should identify sporadic malfunctions in the instrument. In such cases it will be assumed that H_i is known if the instrument is functioning properly, but that when it malfunctions, it switches into an observation mode H_i^j . As an example, such a switch may be caused by a malfunctioning automatic gain control. Again we can test the innovations to see if they are drawn from the population we expect. If the modes of malfunction are known, another possibility is to perform what is sometimes termed "alternative hypothesis testing". That is, under the hypothesis that the instrument is observing with one of several observation matrices H_i^j , it is possible to test the innovations to determine which H_i^j was the most likely to produce the innovation. This observation matrix may be then used to process the data. Alternatively, a number of Kalman filters may be run in parallel and their outputs combined through a weighting on the probability that their observation matrices correspond to reality (Athans, 1975).

Section D. The Square Root Algorithm

The numerical characteristics of the Kalman-Bucy filter

are of vital importance in its implementation. A simplistic implementation of the formulas given earlier in this chapter will often lead to a problem known as true divergence when applied to some systems. This problem is evidenced by the fact that $P_i(+)$ ceases to be positive definite at some time in its history, a requirement of any covariance matrix. After this point, the errors of the filter may grow without limit. The basic cause of this problem is the fact that finite length word lengths are used in the computation of the matrices used by the filter. The problems attendant to finite word length arithmetic thus occur. This is especially true in the inversion of the matrix $[H_i P_i (-)H_i^T + R_i]$, which may be ill conditioned in practice. Since the filter is recursive, numerical errors in earlier computations may propagate forward with disastrous results.

One possible "fix" to the problem of numerical divergence is simply to increase the precision of the computations by use of multiple precision arithmetic. This "fix" should be avoided for three reasons: First, the speed of the algorithm may be seriously degraded. Secondly, the implementor may still find that the filter continues to diverge, a now doubly expensive lesson. Finally, the use of the Square Root Algorithm guarantees that these problems will never occur.

The Square Root Algorithm was developed specifically to circumvent the problems of numerical divergence in Kalman filters. It is algorithmically equivalent to the so called "batch" algorithm presented earlier in this chapter, but offers effectively double precision results using single precision arithmetic. Most importantly, it guarantees that the error covariance, $P_i (+)$, is positive semi-definite at any step in the algorithm. Finally, it easily mechanizes the use of innovations for data reasonableness tests.

The square root formulation presented in this section follows that of an excellent review paper on the subject by Kaminski et al. (1971). The reader interested in implementing a Kalman filter is highly urged to read this paper and that of Schmidt (1970).

The square root filter has its foundation in two facts: The first is that any vector of measurements may be included into the estimation scheme one at a time provided that their measurement noises are independent. If the measurement noises are not independent, the measurement space may be rotated to yield such independence. The algorithm processes the first measurement as if it were the only measurement that it was ever going to receive. It then processes the second measurement as if it were the only additional measurement, etc. The second fact is that since $P_i (\bullet)$ is a positive semi-definite matrix, it may be factored into a

matrix times its transpose. This matrix is often called the square root of $P_i(\bullet)$ and is not a unique matrix. For the purposes of this section, it will be assumed that the square root is a Cholesky decomposition at the beginning of the algorithm. We will denote this decomposition by:

$$P_i(\bullet) = S_i(\bullet) S_i^T(\bullet) \quad 3.39$$

To derive the square root formulation, we will begin with the covariance update equation 3.5 on the assumption that we are updating for only a single measurement.

Equation 3.5 then becomes:

$$P_{i,j}(+) = P_{i,j}(-) - K_{i,j} H_{i,j} P_{i,j}(-) \quad 3.40$$

where $H_{i,j}$ is the j th row of H_i and $K_{i,j}$ is the gain for including measurement j equal to:

$$K_{i,j} = P_{i,j}(-) H_{i,j}^T / (H_{i,j} P_{i,j}(-) H_{i,j}^T + R_{i,j}) \quad 3.41$$

where $R_{i,j}$ is the measurement noise for channel j . We note that $H_{i,j} P_{i,j}(-) H_{i,j}^T + R_{i,j}$ is a scalar for a single measurement and that it is the variance of the innovation

for the jth channel. Defining:

$$1/\alpha = H_{ij} P_{ij}(-) H_{ij}^T + R_{ij} \quad 3.42$$

we will then substitute 3.42 and 3.39 into 3.40 to yield:

$$P_{ij}(+) = S_{ij}(-) S_{ij}^T(-) - \alpha S_{ij}(-) S_{ij}^T(-) H_{ij}^T H_{ij} S_{ij}(-) S_{ij}^T(-) \quad 3.43$$

Defining

$$F_{ij} = S_{ij}^T(-) H_{ij}^T \quad 3.44$$

and substituting into 3.43 now gives us:

$$S_{ij}(+) S_{ij}^T(+) = S_{ij}(-) [I - \alpha F_{ij} F_{ij}^T] S_{ij}^T(-) \quad 3.45$$

It may be shown that $[I - \alpha F F^T]$ may be factored as:

$$[I - \alpha F_{ij} F_{ij}^T] = [I - \alpha \gamma F_{ij} F_{ij}^T] [I - \alpha \gamma F_{ij} F_{ij}^T] \quad 3.46$$

where:

$$\gamma = 1 / (1 + \sqrt{\alpha R_{ij}}) \quad 3.48$$

Thus 3.45 may be factored as:

$$S_{ij}(+) = S_{ij}(-) [I - \alpha \gamma F_{ij} F_{ij}^T] \quad 3.48$$

Using 3.39 and 3.42 in 3.41, the gain for measurement j is:

$$K_{ij} = \alpha S_{ij}(-) F_{ij} \quad 3.49$$

The error covariance after the jth measurement is:

$$P_{ij}(+) = S_{ij}(+) S_{ij}^T(+) \quad 3.39 \text{ (REPEATED)}$$

Since this is a product of a matrix times its transpose, $P_{ij}(+)$ is guaranteed to be a positive semi-definite matrix.

Operationally, several items should be noted; First, while it is possible to carry the square root of $P_{ij}(\bullet)$ rather than $P_{ij}(\bullet)$ throughout the entire life of the filter, it is often more convenient to propagate $P_i(+)$ to $P_{i+1}(-)$ by use of the usual covariance propagation equation 3.8, decompose it to $S_{i+1}(-)$ in order to produce the gains and covariance update, and then reform it to produce $P_{i+1}(+)$ for the next propagation. This is due to two factors, the first is that the procedures necessary to do the decomposition and reformation of $P_i(\bullet)$ to and from its square root are

readily available as library subroutines, while the procedures necessary to perform the propagation of S_i (+) between measurements are not. More importantly, it is easier to monitor the predicted performance of the filter by observing the diagonal elements of P_i (•). The equivalent information is contained in S_i (•) of course, but it is not so readily available.

A second operational note is that the square root filter facilitates data reasonableness test of the individual measurements. As has been noted earlier in this section, the quantity $1/a$ represents the variance of the innovation for the measurement being processed. The hypothesis that the data from that measurement is "reasonable" is thus easily tested. If the measurement is unreasonable, the gain computation may be aborted, the gain for that measurement set to zero and S_{ij} (-) returned as S_{ij} (+). If the data is accepted, the gain may then be computed and S_{ij} (-) updated for the measurement inclusion. The gain from the measurement may then be used to update the state estimate and compute new innovations for the measurements yet to be processed.

Finally, it should be noted that the operation counts such as those of Kaminski et al. (1971) are somewhat misleading. In actual fact, a Square Root Covariance I filter (the form described in this section) may actually run

faster than a Conventional Covariance filter despite the apparent increase in operation count. This is due to the fact that the conventional filter performs all of its arithmetic using matrices while the square root filter performs many of its operations using vectors. The access to any element of a matrix from a higher level language usually implies a multiply and an add, while a vector reference does not. As an example, adding two matrix elements requires 2 multiply and 3 add instructions. A similar operation with vectors requires a single add. These hidden operations in the covariance filter may actually make it more computationally complex than a square root filter.

Section E. The Extended Kalman Filter

In a great many cases of practical interest, the observed measurements are non-linear functions of the variables to be estimated. That is, the observations are of the form:

$$Z_i = h_i(X_i) + N_i \quad 3.50$$

where $h_i(\bullet)$ is a non-linear, deterministic function of its

argument and N_i is a white Gaussian noise. To derive one possible estimator for this case, we will follow a structured development such as given in Section B of this chapter.

The estimator that we will desire to produce is a linear function of the observation:

$$\hat{X}_i(+)=A_i+K_i Z_i \quad 3.51$$

where A_i and K_i are to be determined. Since we will require the estimator to be unbiased, we substitute for $\hat{X}_i(+)$, X_i , and Z_i to yield:

$$\tilde{X}_i(+)+X_i=A_i+K_i[h_i(X_i)+N_i] \quad 3.52$$

$$\tilde{X}_i(+)-\tilde{X}_i(-)=A_i+K_i[h_i(X_i)+N_i] \quad 3.53$$

Taking expectations over X_i and requiring that the prior is unbiased we find that:

$$A_i=\hat{X}_i(-)-K_i\hat{h}_i(X_i) \quad 3.54$$

Thus the estimator is of the form:

$$\hat{X}_i(+)=\hat{X}_i(-)+K_i[Z_i-\hat{h}_i(X_i)] \quad 3.55$$

The error of the estimate is:

$$\tilde{X}_i(+)=\tilde{X}_i(-)+K_i[h_i(X_i)-\hat{h}_i(X_i)]+K_i N_i \quad 3.56$$

Desiring a minimum variance estimator, we multiply 3.56 times its transpose and take expectations over X_i :

$$\begin{aligned} P_i(+)=P_i(-)+K_i E\{[h_i(X_i)-\hat{h}_i(X_i)][h_i(X_i)-\hat{h}_i(X_i)]^T\}K_i^T+K_i R_i K_i \\ +E\{\tilde{X}_i(-)[h_i(X_i)-\hat{h}_i(X_i)]^T\}K_i^T \\ +K_i E\{[h_i(X_i)-\hat{h}_i(X_i)]\tilde{X}_i^T(-)\} \end{aligned} \quad 3.57$$

The derivative of the trace of $P_i(+)$ with respect to K_i is:

$$\begin{aligned} \frac{\partial}{\partial K_i} \text{tr } P_i(+)=2 K_i E\{[h_i(X_i)-\hat{h}_i(X_i)] \\ [h_i(X_i)-\hat{h}_i(X_i)]^T\} \\ +2 E\{\tilde{X}_i(-)[h_i(X_i)-\hat{h}_i(X_i)]^T\} \\ +2 K_i R_i \end{aligned} \quad 3.58$$

Setting this to zero gives K_i as:

$$K_i = -E\left\{\tilde{X}_i(-) [h_i(X_i) - \hat{h}_i(X_i)]^T\right\} \quad 3.59$$

$$\left[E\left\{[h_i(X_i) - \hat{h}_i(X_i)][h_i(X_i) - \hat{h}_i(X_i)]^T\right\} + R_i\right]^{-1}$$

Again, the second derivative of $\text{tr}\{P_i(+)\}$ is a positive semi-definite matrix, thus this is a solution for the minimum.

Unfortunately, 3.59 is not very useful in determining a numerical value for the gain due to its dependence on the probability density of X_i . One way to help overcome this is the approach of expanding a function in terms of its Taylor series. Choosing to expand $h_i(X_i)$ and $\hat{h}_i(X_i)$ around the prior, we get the expressions:

$$h_i(X_i) = h_i(\hat{X}_i(-)) + \sum_{j=1}^{\infty} \frac{\partial^j}{\partial X_i^j} h_i(X) \bigg|_{X = \hat{X}_i(-)} \tilde{X}_i^j(-) \quad 3.60$$

$$\hat{h}_i(X) = h_i(\hat{X}_i(-)) + \sum_{j=1}^{\infty} \frac{\partial^j}{\partial X_i^j} h_i(X) \bigg|_{X = \hat{X}_i(-)} E\{\tilde{X}_i^j(-)\} \quad 3.61$$

Defining

$$H_i(\hat{X}_i(-)) = \frac{\partial}{\partial X} h_i(X) \bigg|_{X = \hat{X}_i(-)} \quad 3.62$$

we then truncate both series after the first derivative and substitute into 3.59 to get an approximation to the gain as:

$$K_i = P_i(-) H_i^T(\hat{X}_i(-)) \left[H_i(\hat{X}_i(-)) P_i(-) H_i^T(\hat{X}_i(-)) + R_i \right]^{-1} \quad 3.63$$

The form of the estimator using this approximation is then:

$$\hat{X}_i(+) = \hat{X}_i(-) + K_i [Z_i - h_i(\hat{X}_i(-))] \quad 3.64$$

with the covariance update equation:

$$P_i(+) = [I - K_i H_i(\hat{X}_i(-))] P_i(-) \quad 3.65$$

It should be noted that the covariance update equation of 3.63 yields only an approximation to the actual error covariance. It will be valid only to the extent that the truncation of the Taylor series was valid.

The validity of the truncation is determined by the bandwidth of the process when compared to the higher order derivatives of $h_i(X_i)$. If the product of the bandwidth, or higher order moments of $X_i(-)$, and the higher order derivatives are relatively large, the approximation will be invalid. In these cases, it is possible to retain more

terms in the Taylor series to get Second Order, Third Order, etc. Kalman filters. Another approach is to iterate the extended filter to get what is termed the Iterated-Extended Kalman filter. A discussion of these types of filters is given by Gelb (1974).

One significant difference between the Extended Kalman filter and the standard Kalman filter is the dependence of the gain K_i on the prior \hat{X}_i (-). In the standard filter, this dependence does not occur. Thus, the gain sequence K_i may be precomputed in the standard filter, but not in the extended filter. To allow precomputation in the case of the extended filter, one must make a further level of approximation. This approximation is that the future values of the process X_i will lie "close" to a nominal trajectory. If this approximation is used, several variants of approximate precomputation are possible. The first is to precompute the covariance of the prior, P_i (-), leaving the actual gain calculation to depend on the observed priors \hat{X}_i (-). The second is to totally precompute K_i along the nominal trajectory. The third is to operate the full extended Kalman filter for some period of time and then switch to either of the above strategies. In all cases, one is hoping to ease the computational burden without a large

degradation in performance.

Section F. The non-causal filter

For a number of cases, there is no requirement that estimates be produced in real time. One of the primary uses (at least potentially) for remotely sensed temperature profiles is in the production of synoptic analyses. These analyses are normally produced for 0000Z and 1200Z. For this use, there is no requirement that the estimate be produced in real time. The only requirement is that the collection of data for input to an analysis scheme cease by some cutoff time and the results reported. In view of this requirement, it is then permissible to produce an estimate at a point based on the totality of data collected through this cutoff. Since temperature profiles are correlated in time and space, the use of "future" observations will add information and reduce the error in the estimate. The purpose of this section is to discuss one form of the non-causal Kalman filter that allows such processing, the forward-backward smoother.

As a preparation for defining the non-causal filter, it will be assumed that there exist two unbiased estimates of

X_i , (\hat{X}_i' and \hat{X}_i'') having statistically independent errors. It is then desired to combine these two estimates to obtain a minimum variance estimate of X_i by using the linear scheme:

$$\hat{X}_i = A_i \hat{X}_i' + B_i \hat{X}_i'' \quad 3.66$$

where A and B are two weighting matrices to be determined. This scheme will be optimum if the errors \tilde{X}_i' and \tilde{X}_i'' are Gaussian random variables. To determine the relation of A to B we will demand that \hat{X}_i be an unbiased estimator. This condition yields:

$$E\{X_i\} = E\{A_i(X_i + X_i') + B_i(X_i + X_i'') - X_i\} = 0 \quad 3.67$$

Since the estimators \hat{X}_i' and \hat{X}_i'' are unbiased this gives an expression relating A to B:

$$A_i = I - B_i \quad 3.68$$

Substituting 3.68 into 3.66 obtains the expression for the error of the estimate \hat{X}_i as:

$$\tilde{X}_i = A_i \tilde{X}_i' + (I - A_i) \tilde{X}_i'' \quad 3.69$$

Multiplying this by its transpose and taking expectations gives the equation for the error covariance of the estimate as:

$$P_i = A_i P_i' A_i^T + (1 - A_i) P_i'' (1 - A_i)^T \quad 3.70$$

since we have assumed that the errors \tilde{X}_i' and \tilde{X}_i'' are independent. Minimizing the trace of P_i by differentiating the trace of P_i with respect to A_i and setting the results to zero gives:

$$A_i P_i' - (1 - A_i) P_i'' = 0 \quad 3.71$$

and so:

$$A_i = P_i'' [P_i' + P_i'']^{-1} \quad 3.72$$

$$B_i = P_i' [P_i' + P_i'']^{-1} \quad 3.73$$

$$P_i^{-1} = P_i'^{-1} + P_i''^{-1} \quad 3.74$$

This defines the optimum variance combination of two

estimators with independent errors. Note that 3.74 guarantees that such a combination will always be at least as good as either of the estimators considered separately.

One very simple method of generating two estimates of X_i that meet the requirement of independent errors under certain conditions is as follows: First partition the data into two segments. One will consist of all the data through the point i whose value we wish to estimate. The second will consist of all the data from time $i+1$ through the cutoff time n . Next, run a standard Kalman filter on the data through time i . This will be the first estimate \hat{X}_i' . Finally, run a Kalman filter backwards in time from time n to time $i+1$ and then perform a one step "prediction" from time $i+1$ to time i . This will be the second estimate \hat{X}_i'' .

The form of the Kalman filter running backwards in time (the backwards filter) is basically the same as that of the Kalman filter running forward in time (the forward filter). The sole exception is that the forward state transition matrix $\Phi_{i,i+1}$ must be replaced by the reverse state transition matrix $\Phi_{i,i-1}$. It is easy to show that the reverse state transition matrix is given by:

$$\Phi_{i,i-1} = \Phi_{i,i+1}^{-1} \quad 3.75$$

In the general case, the estimates \hat{X}_i' and \hat{X}_i''

obtained by this method will not have independent errors and so the assumptions that lead to the weights derived earlier are violated. There are, however, cases of practical importance where the errors are either independent or asymptotically so. One case in which the errors will be independent is the case in which the errors of the priors $\hat{X}_1(-)$ and $\hat{X}_N(-)$ for the forward and backward filters are independent. Such a circumstance will occur if either of these priors is the result of a known state at X_0 or X_{N+1} .

Asymptotic independence of the errors will occur for processes that may be referred to as lossy long observation time processes (LLOT). A lossy process is one in which the state transition matrix is such that:

$$\lim_{n \rightarrow \infty} \prod_{i=1}^n \Phi_{i,i+1} = 0 \quad 3.76$$

In such processes, the initial state is eventually forgotten and the state at any point interior to the interval is determined by the plant noise sequence. Once this has occurred, the errors of the filters may be regarded as errors in estimating the plant noise sequence. Since the plant noise is a white process, we then argue that the errors of the two filters will be independent.

Other formulations of non-causal filters such as fixed lag smoothers are possible. The primary advantage of the

formulation presented in this section is the generality of the lag and the reduction in the need for new software. To produce a backward filter from a forward filter, it is only necessary to modify it to produce the priors and the covariance of the priors rather than the estimate and the covariance of the estimate. This is usually a simple programming change. To combine the two estimates and produce the smoothed estimate, it is only necessary to write a short program to read the results of the two filters and perform the necessary manipulations. We may guarantee a long observation time for the process by simply halting processing using the forward filter at the cutoff time n and then restarting it as more data becomes available.

Chapter IV

The Temperature Experiment

Section A. General description

The temperature experiment was concerned with the design and implementation of a practical Kalman-Bucy filter for estimating temperatures in the atmosphere from data produced by the SCanned Microwave Spectrometer (SCAMS) carried on the NIMBUS 6 satellite. The experiment was divided into three major phases: The first was the design and implementation of an extended filter for the estimation of the temperature of the surface and the atmosphere at what are called the 14 mandatory pressure levels at one or more SCAMS scan angles. These mandatory pressure levels are located at 1000, 850, 700, 500, 400, 300, 250, 200, 150, 100, 70, 50, 30, and 10 mb of atmospheric pressure. They are the standard temperature and height fields produced by the synoptic analysis schemes and are used by numerical forecast models. The vector of state for a single spot inversion may be thus described as $[T_s, T_{1000}, T_{850},$

$T_{700}, \dots, T_{30}, T_{10}$. For a multi-spot inversion, the state vector is a concatenation of such single spot vectors. The second part of this experiment was the implementation of the forward-backward smoother for noncausal estimation of these temperature fields. The final experiment consisted of the implementation of a sub-optimal filter in which either the covariance or gain history of the filter was precomputed along a nominal satellite track.

The data used in the experiment were several periods of actual SCAMS brightness temperatures. These periods of data spanned an interval from August, 1975 to February, 1976. The standard of comparison used for verification in the experiments was the National Meteorological Center (NMC) K27 synoptic analysis grid interpolated to the satellite position in space and time. This grid consists of an octagonally shaped mesh covering the northern hemisphere. The individual cells in the grid are roughly 400 km wide. This and several other special purpose analyses are produced for 0Z and 12Z each day from all available operational observations (primarily radiosondes) and represent one of the best analysis efforts available on an operational basis. The accuracy of the grid is thought to be better than 1° K in areas where reporting stations are spatially dense. These areas have been historically considered to be Japan, the United States and Canada, and western Europe

(Waters et al., 1975). These regions are diagrammed in Figure 2. In order to attempt to guarantee validity of comparisons between the estimates of the Kalman filter and the verification data, comparisons were restricted to these areas.

A number of topics will be discussed in this chapter. Section B will give a brief description of the SCAMS instrument. Section C will discuss the system identification aspects of the implementation of an extended Kalman-Bucy filter for temperature retrieval. Section D will discuss the synthesis of the observation matrices. A general description of the filter program and its capabilities will be given in Section E. A much more complete description of the program with design philosophies and descriptions of the flow in each module is given in Appendix C. Section F will cover the tuning procedures that were used in the filter and problems that occurred in its implementation. A summary of the results that were obtained with the causal filter are given in Section G. Section H will present the results of the non-causal experiment. Finally, Section I will explore the sub-optimal but fast precomputed parameter filter.

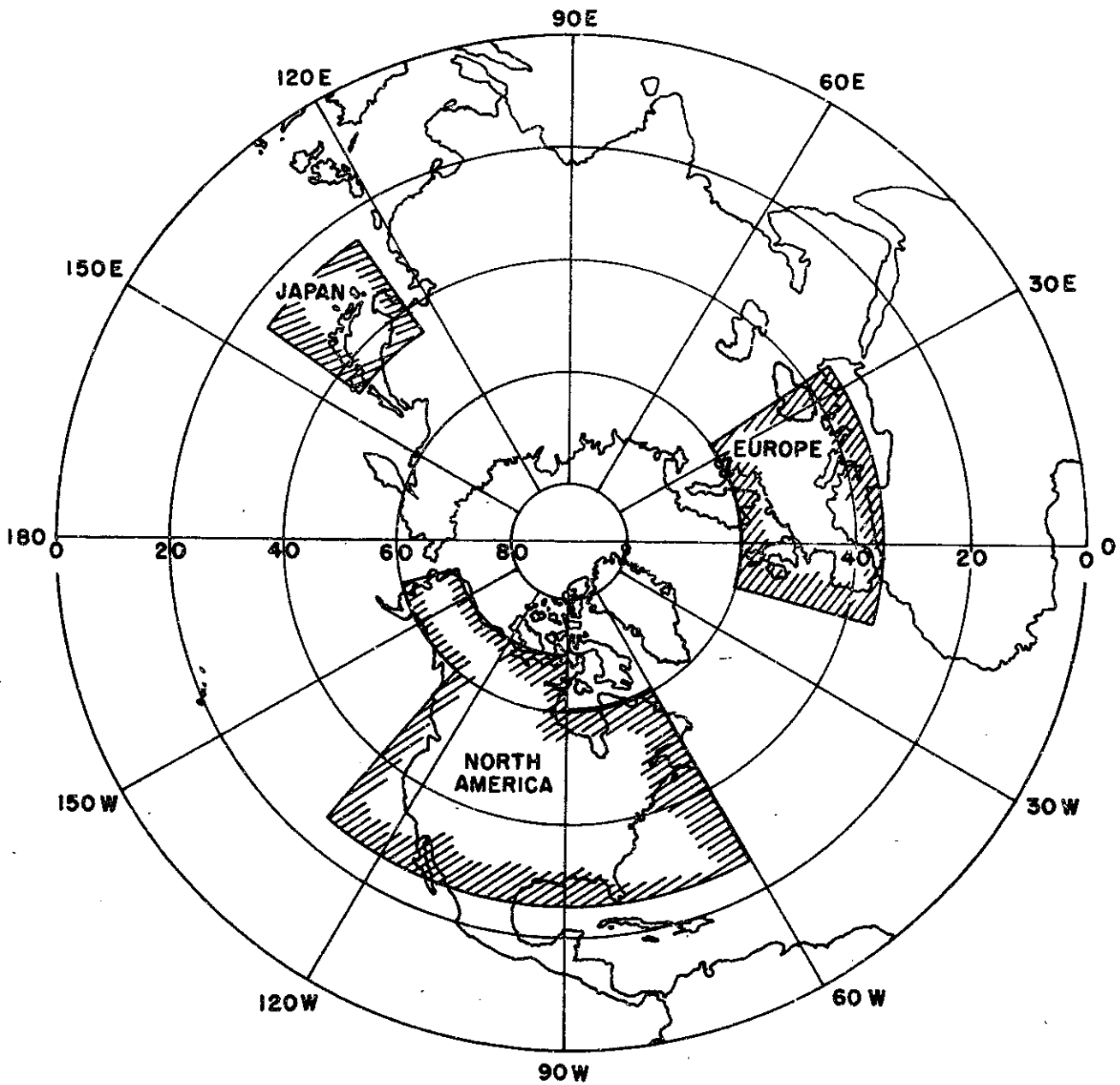


Figure 2
- 84 -
SCANS Verification Areas

Section B. The SCAMS instrument

The SCAMS instrument is a scanning microwave spectrometer that observed the upwelling radiation from the earth at five frequencies (Staelin et al., 1975, 1977). Three of these frequencies (52.85 Ghz., 53.85 GHz., and 55.45 Ghz.) are in an oxygen absorption complex and respond primarily to the temperature in the earth's atmosphere. The frequencies have been chosen to produce weighting functions that peak in the lower, middle and upper atmosphere. The remaining two channels (22.235 GHz. and 31.65 GHz.) are situated on a water vapor resonance and in an atmospheric window respectively. These two channels are used primarily to produce estimates of liquid water and water vapor over ocean and surface characteristics of ice pack or land (Grody and Pelligrino, 1977, Staelin et al., 1977, Ledsham and Staelin, 1978).

Electrically, the SCAMS instrument uses a separate Dicke-switched radiometer for each channel. These radiometers have a noise of about 0.5° K rms for a one second integration time. The three oxygen band channels share a common antenna, while the two lower frequencies have separate antennas. These antennas are positioned in front of reflectors that are rotated by means of stepping motors.

These motors drive the reflectors to give thirteen earth views of roughly one second each in angular increments of 7.2° . They then rotate to provide a view of an ambient temperature target and cold space for instrumental calibration purposes. The total scan takes a period of sixteen seconds which will be called a major frame or frame in this thesis. All antennas have 7.5° beamwidths at their half power points.

The total antenna geometry and satellite orbit produce a set of linear scans of the earth roughly 2400 km long with a 100 km separation between the centers of the scans. The size of the earth view (often called a spot, footprint or pixel) varies from an approximate 144 km circle at the nadir view to a 221 km downtrack by 361 km crosstrack ellipse at the extreme scan angles.

Section C. The temperature system identification

As discussed in the chapter on the discrete Kalman-Bucy filter, several a priori matrices are necessary for the operation of the filter. Specifically, these matrices are the state transition matrix $\Phi_{i,i+1}$, the plant noise covariance Q_i , associated with the message generation process, the

observation matrices H_i , the observation noise R_i that describe the message reception. In addition, the mean of the process at the initiation of processing, $\hat{X}_1(-)$, and its error covariance matrix $P_1(-)$ must also be specified. This section will deal with the determination of $\Phi_{i,i+1}$, Q_i , $\hat{X}_1(-)$, and $P_1(-)$. The discussion of H_i and R_i will be left to Sections D and F respectively.

Of the two tasks addressed by this section, the determination of $\hat{X}_1(-)$ and its covariance matrix was the easiest to accomplish. A large body of meteorological experience have led to the specification of what are called the supplemental standard atmospheres (Valley, 1966). Determined for 15 degree intervals in latitude from 15 degrees to 75 degrees for both summer and winter conditions, these atmospheres are typical of global means. The 15 degree atmosphere is actually defined for only a single season reflecting the conditions occurring in the tropics, and the 75 degree winter atmosphere is only defined through an altitude of 30 km after which it bifurcates into one of two atmospheres. The prior was taken to be an interpolation of these atmospheres in latitude.

While the values of the supplemental atmospheres are specified, their covariance matrix is not. To generate this matrix, the covariance matrix of the NMC K27 grid was examined. The analysis along a satellite track for a period

of two days was retrieved from a merged SCAMS tape. The covariance around the means derived from the interpolated supplemental standard atmospheres for the five central SCAMS spots was then computed. This analysis was performed on data from January 26-27, 1976, to represent the winter statistics and from August 7-9, 1975, to represent the summer statistics. These statistics were computed for 22.5 degree latitude bands.

While this procedure yielded what is felt to be a reasonable estimate of the covariance of the prior for the atmosphere, the covariance of the surface temperature had yet to be determined since the NMC K27 grid contains no information on this quantity. The solution adopted for this problem was to insert the variance of the surface as twice that of the 1000 mb temperature along the diagonal of the covariance matrix and equal to the 1000 mb covariances on the off diagonal elements. This was felt to be justified by the rationale that the 1000 mb temperature and the surface temperature are coupled through convection. However, because of the variation in ground cover and the fact that the earth's oceans act as a thermal source/sink, it was decided to increase the variance of the prior. The manner in which this was done was consistent with the assumption that the surface temperature is equal to the 1000 mb temperature plus an independent noise component.

The identification of the state transition matrix and the plant noise Q , should, in theory, be derivable from the primitive equations that describe the transfer of heat, mass, and momentum in the earth's atmosphere. These equations are unfortunately quite complicated in practice. The problem of system identification using these equations is not unlike the problem of construction of a large scale computer starting with Maxwell's equations.

The problem of identification was thus first approached in a statistical manner similar to that used to derive the covariance matrix of the prior. A stepwise regression of each NMC K27 levels at a SCAMS spot was performed with the entire NMC K27 grid at the previous scan acting as the predictors. The mean of the predictors was taken to be the interpolated supplemental atmospheres. As with the covariance of the prior, the northern hemisphere was divided into four latitude bands of 22.5 degrees and a separate regression was performed in each band. Since weather systems and phenomena vary on a latitudinal basis, this segmentation is a natural one. The choice of four bands was arbitrary, but was designed to yield one tropical, one arctic, one sub-tropical, and one sub-arctic plant. The regression coefficients were interpreted as the elements of the state transition matrix and the covariance of the residuals as the plant noise. The elements of the plant

noise for the surface were inserted in the same manner as the covariance of the prior, and the elements of the state transition matrix for the surface were taken to be the same as those of 1000 mb. Early experiments using these choices of $\Phi_{i,i+1}$ and Q_i disclosed that this approach was unsatisfactory. Examination of the diagonal elements of the predicted error covariance matrix, $P_i (+)$, versus the actual error performance disclosed that the filter was performing much worse than it "thought" it was, especially in the vicinity of tropopause.

A re-examination of the system identification disclosed the most probable cause. Remembering that the scans of SCAMS are separated by about 100 km and that the grid cell is approximately 400 km wide yields the conclusion that it takes about four scans to cross a grid point. The approach described above is thus roughly equivalent to the problem of a grid point predicting itself. This it can do with little error.

The next approach attempted was used in the actual filter. An identity state transition matrix was initially assumed and the resulting error of the prediction five frames later was then computed. If the choice of an identity transition was correct, this quantity is five times the plant noise. Again, the surface elements were assumed and inserted. While the identity matrix state transition

was assumed in this plant noise construction and tested in the filter due to its advantages in the state and error covariance propagation, it is a physically impossible matrix in practice. Adjacent temperature layers transfer energy between themselves in the real atmosphere. Doing so, they attempt to restore the overall temperature profile to one consistent with the ideal gas law, solar flux, geostrophic wind, etc. Thus, it was decided to allow the elements of the state transition matrix to be adjustable at run time even though the plant noise was computed using an identity matrix for $\Phi_{i,i+1}$. For reasons of practicality, the run time transition matrix allowed only interaction with nearest neighbors in pressure. The form of interaction was constrained to be a weighted average of the deviation of the temperatures from the climatology as represented by the interpolated supplemental atmospheres. For most levels at the center spot of a three spot filter, this interaction is described by the expression:

$$T_{i,j} = \sum_{k=i-1}^{i+1} \sum_{n=j-1}^{j+1} W_{kn} (T'_{kn} - \bar{T}'_{kn}) + \bar{T}_{kn} \quad 4.1$$

where $T_{i,j}$ is the temperature at spot i , pressure level j to be predicted, $T'_{k|n}$ is the estimate at spot k , pressure level n from the previous scan, W_{kn} is the weight given to T'_{kn} and \bar{T}_{kn} is the appropriate interpolated

supplemental atmosphere. For the two edge profiles of the three spot filter, the interaction is:

$$T_{ij} = \sum_{k=i}^m \sum_{n=j-l}^{j+l} W_{kn} (T'_{kn} - \bar{T}'_{kn}) + \bar{T}_{kn} \quad 4.2$$

where m is either $i+1$ or $i-1$, dependent on the edge being predicted. A two spot prediction was considered to be a case of two such edges. A single spot prediction simply used the second summation of 4.2.

In all cases, the prediction algorithm must take into account the fact that the altitude of the surface is a variable. As an example, an altitude of roughly 1 km places the surface at a pressure altitude of 925 mb. In this case, the 1000 mb slab no longer exists, except as perhaps a "virtual" one. For these cases, the surface should interact with the slab above it and not with any "virtual" ones. For temperatures in the atmosphere, interaction between "virtual" and real slabs should be permitted to prevent these "virtual" slabs from being propagated in a pure prediction mode for long periods of time.

The determination of the weights used in the implementation of the filter are discussed in the section on filter tuning. However, it will be mentioned at this time that the best performance seemed to be obtained with $W_{i+1,j}$ and $W_{i-1,j} = 0.0$, $W_{i,i} = 0.5$ and $W_{i,i+1}$ and $W_{i,i-1} = 0.25$.

Other possibilities exist for the state identification process. One would have been through the use of the previous SCAMS temperature estimates produced by the Statistical D inversion method. The second would have involved the use of an ensemble of radiosondes such as described in Appendix A. The first was not used in order to divorce the filter from the present inversion method. The second was rejected because of the lack of a summer dataset and the magnitude of effort required.

Section D. Observation matrices

Following the discussion of Chapters II and III, it may be seen that the discrete weighting functions correspond to the Kalman-Bucy filter observation matrices. That is, a noiseless brightness temperature may be computed through the equation:

$$T = H(R(\nu), H_s) T \quad 4.3$$

where the matrix H is a function only of the reflectivity $R(\nu)$ and the surface elevation H_s . For estimation over land areas, it is reasonable to assume that both $R(\nu)$ and

H_s were known to the filter from independent sources. For temperature estimation over water areas, $R(\nu)$ is a deterministic function of T_s in the absence of ocean roughness. It is thus still possible to use 4.1 to obtain the predicted brightness temperature, $h(\hat{X}_i(-))$, by using the predicted surface temperature to evaluate $R(\nu)$. However, since the problem is now nonlinear, we require an extended Kalman-Bucy filter. For this filter we will also require the matrix:

$$H_i(\hat{X}_i(-)) = \left. \frac{\partial}{\partial X} h_i(X) \right|_{X = \hat{X}_i(-)} \quad \begin{array}{l} 3.62 \\ \text{(REPEATED)} \end{array}$$

This section will be concerned with the determination of both matrices.

The computation of the observation matrices of equation 4.1 is a straight forward matter. For a given atmospheric state, it is possible to evaluate the equation:

$$W_i(\nu, R) = \int_L^{U_i} F_i(T(h), T(h_i)) W(h, \nu, R) dh \quad \begin{array}{l} 2.18 \\ \text{(REPEATED)} \end{array}$$

which relates the discrete weighting function to the continuous weighting function. The matters of judgment in

this process are: For which atmospheres and reflectivities should the function be evaluated? What is the form of the function $F_i(\bullet)$ for the slab i , and what are the upper and lower boundaries of the slab? Finally there is the question of how surface elevation effects will be handled.

The issue of reflectivities is the easiest to handle. If we examine the form of the continuous weighting function we find:

$$W(h, \nu, R) = K(\nu, h) \tau(h, H) + R(\nu) K(\nu, h) \tau(H_s, h) \tau(H_s, H) \quad 4.4$$

We note that this is a linear function in reflectivity. It is thus possible to obtain a weighting function for any reflectivity by a simple interpolation between a weighting function computed for $R(\nu) = 0$ and $R(\nu) = 1$.

The choice of the atmospheres over which to evaluate the weighting functions was also an easy one. As noted in Chapter II, the weighting functions are relatively insensitive to temperature. However, as a matter of principle, the atmospheres should be close to the atmospheric conditions that are expected to be observed. Given the ready availability of the supplemental standard atmospheres, it was decided to use them as models for which the weighting functions were computed. The winter

atmospheres would provide the weighting functions for the months of November through April in the northern hemisphere, and the summer atmospheres would provide the weighting functions for the other months. The weighting function whose model was closest in latitude to the observation would be used with the exception of the region above 60 degrees in latitude. Here, the 60° latitude atmospheres were used because of the bifurcation of the 75° winter atmosphere.

In the choice of variables used to characterize the atmosphere and observations (the vector of state), it was decided to use the temperatures at the 14 mandatory pressure levels and the surface temperature. The sky temperature ($\sim 2.5^\circ$ K) is well known a priori and so appears as a bias. After a round trip through the atmosphere, its impact on the most transparent oxygen channel is a maximum of roughly 0.1° K. The choice of the slab definition to describe the weighting functions for these variables was somewhat arbitrary. It was chosen to split the pressure levels in pressure altitude. The 1000 mb temperature thus characterized a slab from the surface (1013 mb) to 925 mb, the 850 mb temperature characterizes a slab from 925 mb to 775 mb, etc. There is undoubtedly a more enlightened slab definition possible.

The various supplemental atmospheres were then examined to determine the heights of the various mandatory pressure

levels and slab definition pressures. These heights are given in Table 2 and form the L_i and U_i altitudes for the integration of the continuous weighting functions. The above choices give the form of $F_i(T(h), T(h_i))$ as a simple ratio of $T(h)$ to $T(h_i)$.

The final problem that was addressed for the determination of the discrete weighting functions over land was the problem of surface elevation. Since the weighting function for a level is defined in terms of the extinction from the surface to that level and from the surface to the radiometer, the surface elevation has an effect on the continuous (and hence discrete) weighting function. While it would have been possible to have constructed an elaborate scheme to interpolate weighting functions to account for elevation effects, a simple linear interpolation was used in the filter. This was not because of the linearity of the weighting functions with surface altitude, but rather the fact that the elevation information available to the filter was rather coarse spatially. It was felt that the use of an elaborate scheme in these circumstances was unjustified. The choice of elevations for which the weighting functions were evaluated was 0, 0.5, 1.0, 1.5, 2.0, and 3.0 km.

Having made these engineering decisions, the discrete weighting functions were evaluated over all possible permutations of of the two reflectivities, two seasons, four

Table 2

Heights of Various Pressure Surfaces
in the Supplemental Atmospheres

Pres. (mb)	60S height (km)	45S height (km)	30S height (km)	15A height (km)	30W height (km)	45W height (km)	60W height (km)
1013	0.000	0.000	0.000	0.000	0.000	0.000	0.000
1000	0.084	0.115	0.118	0.115	0.175	0.142	0.101
925	0.734	0.782	0.797	0.793	0.826	0.759	0.690
850	1.430	1.497	1.533	1.517	1.528	1.424	1.330
775	2.180	2.281	2.313	2.302	2.299	2.143	2.024
700	2.994	3.118	3.160	3.173	3.123	2.927	2.783
600	4.202	4.357	4.416	4.428	4.341	4.098	3.910
500	5.601	5.781	5.862	5.865	5.736	5.438	5.219
450	6.382	6.594	6.703	6.672	6.521	6.192	5.950
400	7.235	7.471	7.593	7.555	7.380	7.020	6.749
350	8.178	8.442	8.577	8.531	8.330	7.938	7.632
300	9.234	9.534	9.679	9.628	9.398	8.971	8.652
275	9.816	10.136	10.286	10.232	9.986	9.542	9.180
250	10.452	10.784	10.938	10.882	10.622	10.173	9.786
225	11.145	11.486	11.645	11.586	11.310	10.850	10.456
200	11.921	12.256	12.417	12.357	12.099	11.606	11.204
175	12.803	13.128	13.270	13.209	12.939	12.461	12.053
150	13.816	14.101	14.226	14.166	13.899	13.446	13.033
125	15.019	15.253	15.366	15.260	15.020	14.607	14.191
100	16.490	16.662	16.702	16.676	16.370	16.025	15.624
85	17.561	17.705	17.681	17.559	17.367	17.055	16.654
70	18.841	18.939	18.863	18.692	18.530	18.281	17.881
60	19.329	19.413	19.318	19.132	18.974	18.749	18.348
50	21.060	21.099	20.947	20.719	20.568	20.439	19.996
40	22.529	22.545	22.387	22.147	21.947	21.846	21.392
30	24.481	24.426	24.227	23.978	23.783	23.658	23.184
20	27.203	27.178	26.873	26.617	26.382	26.211	25.746
10	31.968	31.899	31.543	31.292	30.969	30.656	30.089
7.5	34.069	33.968	33.654	33.295	33.034	32.545	31.917

XXS implies the summer atmospheres at latitude XX.
XXW implies the winter atmospheres at latitude XX.

latitudes, and six surface elevations for each of the seven different SCAMS scan angles.

The problem of determining the matrix $H_i(\hat{X}_i(-))$ was easily mechanized by the above approach to determining the discrete weighting functions. The elements $\frac{\partial}{\partial T_i} T_B$ (where T_i is a temperature in the atmosphere) are the same as those of the discrete weighting functions. The element for the surface however, must be computed separately. Writing the brightness temperature as the sum:

$$T_B(\nu) = \sum_{i=1}^{14} T_i W_i(\nu, R(\nu, T_s)) + T_s W_s(\nu, R(\nu, T_s)) \quad 4.5$$

we differentiate to yield:

$$\begin{aligned} \frac{\partial}{\partial T_s} T_B(\nu) = & \sum_{i=1}^{14} T_i \frac{\partial}{\partial R(\nu, T_s)} W_i(\nu, R(\nu, T_s)) \frac{\partial}{\partial T_s} R(\nu, T_s) \\ & + \frac{\partial}{\partial R(\nu, T_s)} W_s(\nu, R(\nu, T_s)) \frac{\partial}{\partial T_s} R(\nu, T_s) \quad 4.6 \\ & + W_s(\nu, R(\nu, T_s)) \end{aligned}$$

Because of the linear interpolation scheme used in the synthesis of the discrete weighting functions for an arbitrary reflectivity, the evaluation of the differentials of the weighting functions with respect to reflectivity is trivial. The derivative of the reflectivity with respect to

temperature is easily table-driven. For the filter implemented, this table consisted of 45 entries in one degree kelvin increments.

Section E. The filter program

The basic requirement adopted for the design and implementation of the Kalman filter program was that the overall program be as general as possible. Further, it was required that the program be constructed in a modular fashion with each module having a readily identifiable task.

To a large extent, this goal was realized. The program produced is general enough to handle a great many temperature profile estimation problems. All the results contained in this chapter have been produced using a single program. Specifically, the program is capable of:

- 1) Handling any inversion scheme from one to thirteen scan angles. However, as a practical matter, the upper limit is about five angles due to limits on storage and complexity. A five scan angle required a 75 state filter. A thirteen spot filter would have required a 195 state

filter.

- 2) Running as either a forward or backward filter.
- 3) Using precomputed gain or covariance matrices.
- 4) Being used in either a batch or interactive mode with prompting.
- 5) Producing print output, at intervals of the user's selection, of items of interest such as the diagonal of the error coavarience matrix, the innovations, etc.
- 6) Performing data reasonableness testing as an option. The rejection criteria is selectable by the user.
- 7) Being easily modified to accommodate a different instrument.
- 8) Producing timings of any of the major tasks in the estimation process such as the gain computation, prediction, etc. at the user's option.

The program consists of a number of subroutines and a dummy main routine written in an admixture of PL/I and IBM 370

assembler language. The names and purposes of the routines are:

FOO - This is the dummy main program. Its sole purpose is to determine the order of the filter to be run and compute the amount of storage needed for the program. It also configures the output files of the filter to conform to the filter order. It calls routine KALMAN.

KALMAN - This is the actual "main" program. It allocates storage for all matrices used in most of the filter, reads and unpacks the input data and accounts for missing data points. It creates the initial prior and initializes the environment by calling routine INIT. It propagates the estimates and error covariances by calling routine PREDICT and acquires the observation matrices by calling routine CMATRIX, after which innovations are computed. The gain is computed by a call to the routine GAIN and the innovations and gain are used to update the state. All the timing options and most of the printing options are implemented in this routine. The routine also collects performance statistics when run on a merged analysis tape.

INIT - This routine initializes the environment in general. It acquires an initial prior from routine TEMPS, constructs

a state transition matrix and initializes the error covariance matrix from a disk file. It also calls all initialization entry points on routines that require initialization before they themselves are called.

TEMPS - This routine returns the temperatures, lapse rates, and pressure surface altitudes for a given latitude using a cubic spline interpolation of the supplemental standard atmospheres.

PREDICT - This routine implements the state and error covariance propagation. If precomputed gain or covariance matrices are used, the error covariance propagation section is bypassed. It calls PHIEPHI and STATE.

STATE - This routine returns the plant noise matrix for a given latitude partition.

PHIEPHI - This routine computes the matrix product $\Phi P \Phi^T$ for sparse Φ . It is written in assembly language.

CMATRIX - This routine computes the necessary observation matrices for a given latitude, scan angle, elevation,

reflectivity, and predicted state vector combination.

GAIN - This is the Square Root gain computation and covariance update routine. It also performs data reasonableness testing on the innovation if this option was requested. If the routine was called with P_i (-), rather than S_i (-), it decomposes the covariance into its square root by calling **MFS**. It is also capable of reforming the matrix from its square root by calling **SSQUARE**.

MFS - This is an assembly language version of the **SL-MATH** routine of the same name. It performs a Cholesky decomposition of the covariance matrix. It has been carefully optimized to perform all operations in a manner to take full advantage of pipelining and the IBM 370 instruction set capabilities. It attempts to maintain all important variables in registers.

SSQUARE - This routine reforms the matrix P (+) from the product S_i (+) S_i^T (+). It is written in optimized assembler.

This completes a short description of the routines in the program. A more exhaustive description of the program logic is given in Appendix C.

The modularity of the filter structure has proven itself in actual usage. The water vapor/liquid water filter of Chapter V was constructed of many of the above routines. For the most part, only the observation matrix and prediction routines were changed to reflect the difference in the plant and physics of observation.

Section F. Tuning and problems

As with any filter designed to interact with reality, the filter used in this thesis went through innumerable revisions, modifications, and tunings. Some of these revisions were due to a lack of appreciation or a misunderstanding of the physical processes at work. Others were somewhat more fundamental to the nature of the process being estimated. This latter area will be covered in this section.

One of the more persistent problems in the overall filter has been the values of the state transition matrix and the plant noise. The plant noise was computed under the assumption that the state transition matrix was identity. However, when the filter was first operated with a unity state transition matrix, the lack of observability in the

system quickly manifested itself in the form of a persistent temperature inversion in the lower atmosphere of the estimated temperature profiles. A modification of the prediction procedure to allow smoothing to take place between the adjacent levels removed this problem. The amount of smoothing necessary seems to be uncritical and a rather broad region of good performance seems to exist. The performance seems to be optimum at the point where the weight given the two adjacent levels is about half of the the weight given to the level being propagated. This also appears to be invariant of season. Because of the problems mentioned in the section on system identification, the plant noise was not recomputed on this state transition matrix.

As with all practical instruments, there is some divergence between the observation matrix used by the instrument and the one used by the filter. The case under study was no exception. Numerical approximations in the computation of the observation matrices, instrument biases, and other unknown causes produced errors when the observed brightness temperatures were compared with the brightness temperatures using the observation matrices and the NMC K27 grid. Lacking knowledge of the source, it was decided to compensate the brightness temperatures by means of an empirical correction. Several days of observed brightness temperatures were matched with the brightness temperatures

produced using the observation matrices and the NMC K27 grid. As the errors had a mild latitudinal and scan angle dependent character, separate corrections were computed for each scan angle in 10° latitude bands. The first attempt to use these corrections produced "shock" in the filter at the points where the correction coefficients were changed. This problem was eliminated by interpolation of the correction coefficients.

When the filtering algorithm was first implemented, the processing order of the observations was left to right, channel 3 to channel 5. That is, the lowest number spot's channel 3 was processed first, then the lowest number spot's channel 4, etc. through the highest number spot's channel 5. Observation of the error performance and the Kalman gain indicated that this processing order was inappropriate. In the optimal linear Kalman filter, the order of processing does not affect the overall accuracy of the final estimate. The filter of this chapter, however, was neither linear nor optimal. The observation matrices were determined by the reflectivity and elevation of the surface, items that were not known exactly to the filter. As a result, errors in the predicted observations were "reflected" into the upper atmosphere and adjacent spots by correlations in the error covariance matrix. The reduction in the elements of the covariance matrix due to the processing of channel 3 at a

spot then caused the upper atmosphere channel to be given less weight, although its observation matrix elements were not subject to the same uncertainty. To reduce this problem, it was decided to reorder the processing so that channel 5 was processed first, left to right, then channel 4, left to right, etc. By processing the most linear channel first, it was hoped that the uncertainties in the surface character would be reduced. This has proved to be the case.

Finally, the filter required tuning for observation noise. The nominal performance of the three oxygen channels is roughly 0.5° K rms. While this is undoubtedly the actual performance, the approximations made in the computation of the weighting functions and surface effects produce additional errors. The filter was thus tuned by varying the observation noise on all channels and observing the error performance on two datasets, one in January, 1976, and one in August, 1975. The results in both cases were that the optimal noise for channel 3 was 1.0° K rms. The optimal noise for channels 4 and 5 was 0.7° K rms.

Section G. The causal experiment

The temperature Kalman-Bucy filter was exercised in four modes in the course of this thesis: a causal mode, a non-causal mode, a precomputed error covariance mode, and a precomputed gain mode. The data available for these experiments consisted of SCAMS data for six periods of time during which it could be merged with the NMC K27 grid. These periods are listed in Table 3 and span the expected seasonal variations in climate. January and February are considered winter months in the northern hemisphere, August is a summer month and October and December are considered transition months.

In order to produce as many useful comparisons as possible at the lowest cost, the data from the merged tapes was examined, and only those passes over the good verification regions of Figure 2 were used to exercise the filter. These segments of data began at least 10 frames before the satellite entered a verification region.

To test stability of the filter, an unmerged tape was used as a test input. The filter was run as a single spot inverter for a period of several thousand frames without exhibiting instability.

The filter was tested in three basic inversion schemes:

Table 3

Tape Number	Coverage	Approximate Number of Comparisons
1	August 7-9, 1975	240
2	October 3-5, 1975	260
3	October 22-25, 1975	420
4	December 5-8, 1975	400
5	January 24-25, 1976	250
6	February 3-6, 1976	700

a one, two and three spot inversion. In the one spot inversion, the data from a single scan angle was used to perform the inversion. In the two and three spot scheme, data from two and three adjacent scan angles were used as the observation vector. In order to investigate the effect of scan angle, both spots at the extreme scan angle and near nadir were used in the inversions.

The results of these these experiments are given in Tables 4 - 39. In the single spot portion of these tables, the performance of the Statistical D method of inversion is shown as a standard of comparison. The results for the extreme and nadir scans of the February and August datasets are shown in Figures 3 - 6. In these figures, the solid line represents the Statistical D inversion results, the long dashed line represents the one spot inversion, and the short dashed line represents a three spot inversion.

There are a number of conclusions that may be drawn from this experiment: First, the performance of the Kalman filter improves with scan angle. This is probably because of the fact that as the scan angle increases, the peak of the weighting functions increase in altitude or lift. Thus, as the scan angles increases, the observation matrices are less dependent on the character of the surface, and the components of these matrices that are in the atmosphere increase. The filter thus observes more of the atmosphere,

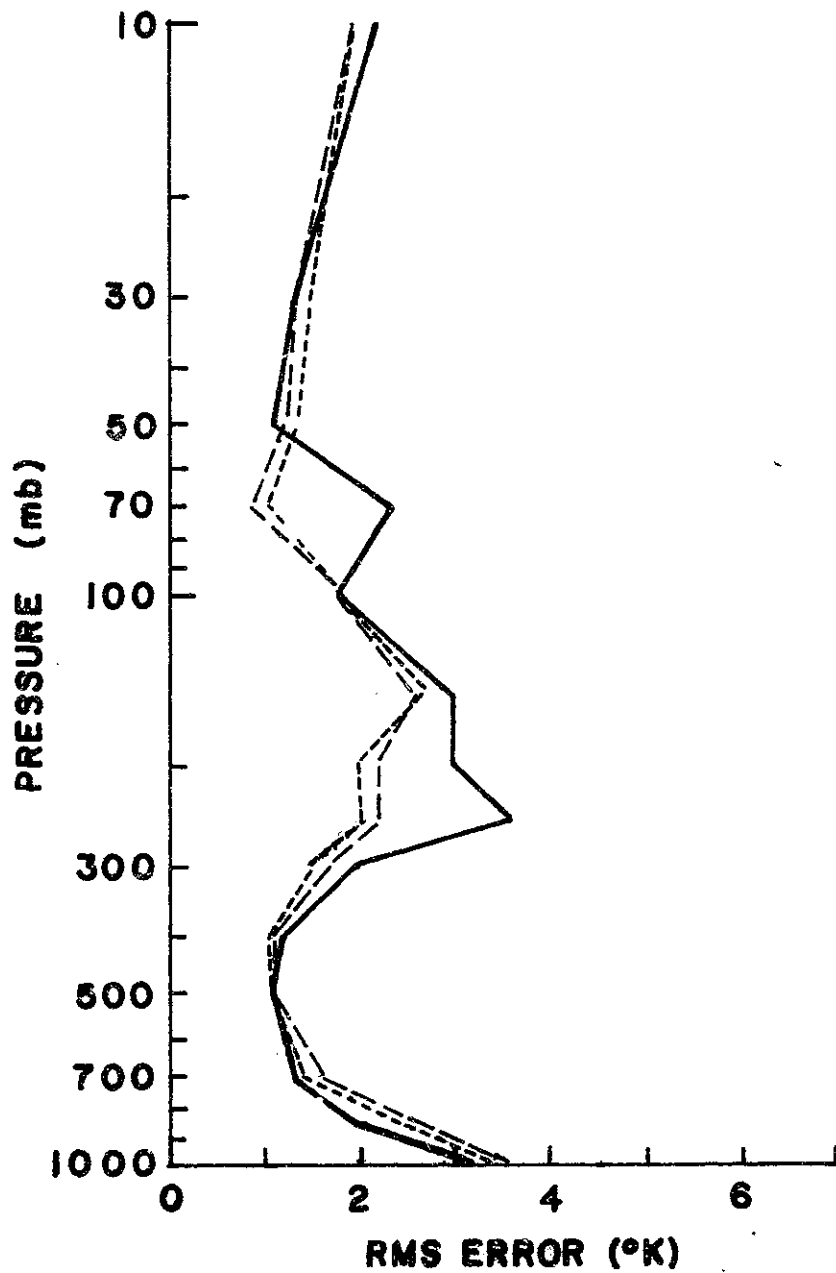


Figure 3
 Causal Filter Error Performance (Extreme Scan), August 7-9, 1975 (Solid line - Statistical D, Long dash - one spot Kalman filter, Short dash - three spot Kalman filter)

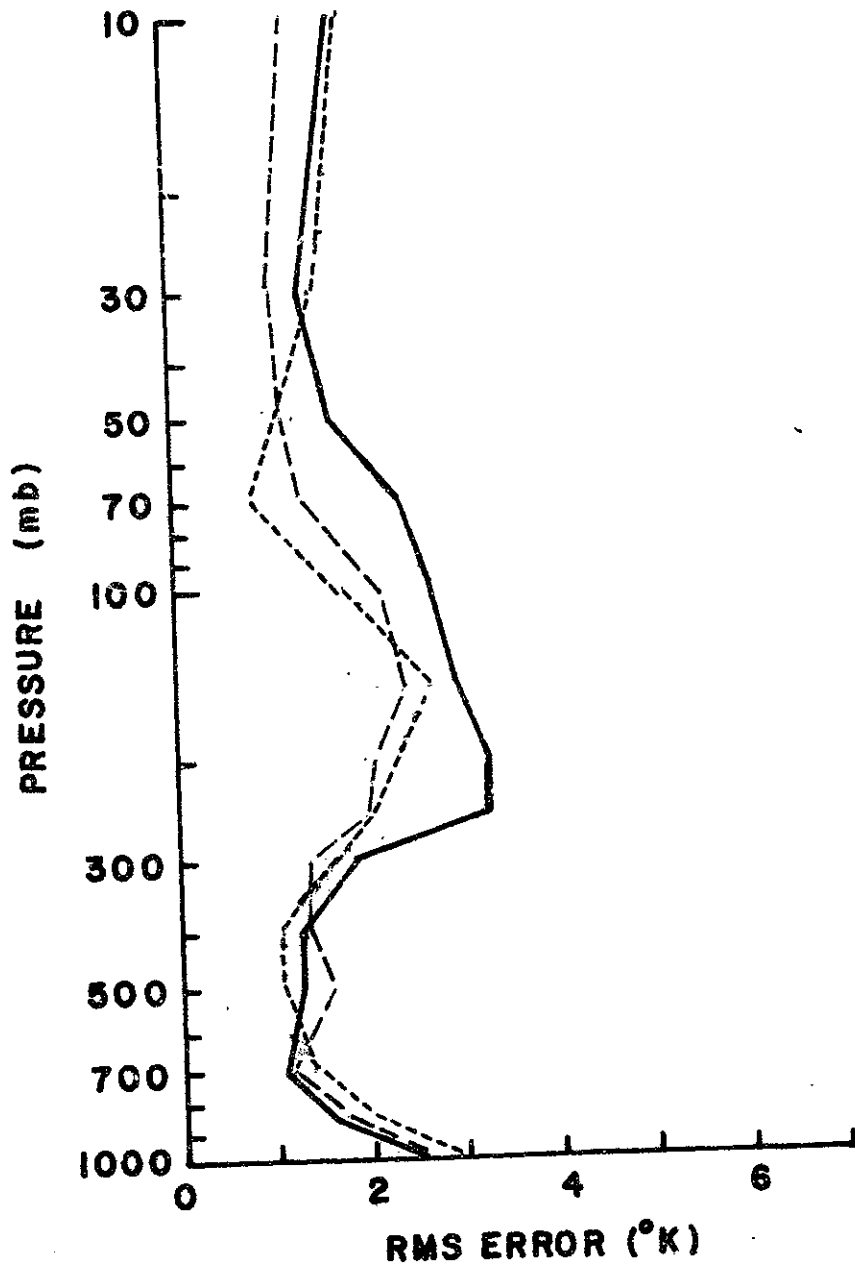


Figure 4
 Causal Filter Error Performance (Nadir Scan), August 7-9, 1975 (Solid line - Statistical D, Long dash - one spot Kalman filter, Short dash - three spot Kalman filter)

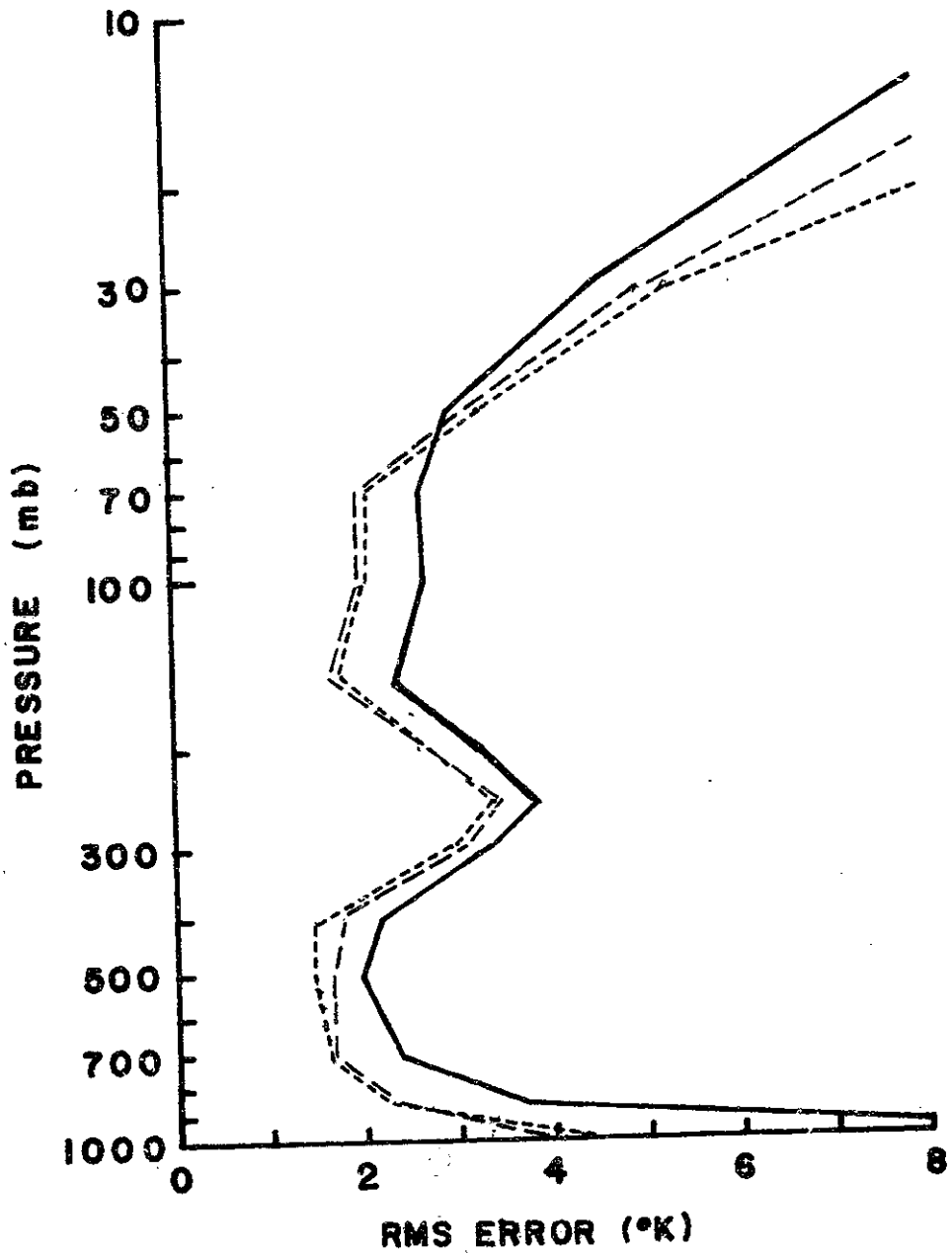


Figure 5
Causal Filter Error Performance (Extreme Scan), February 3-6, 1976 (Solid Line - Statistical, Long dash - one spot Kalman filter, Short dash - three spot Kalman filter)

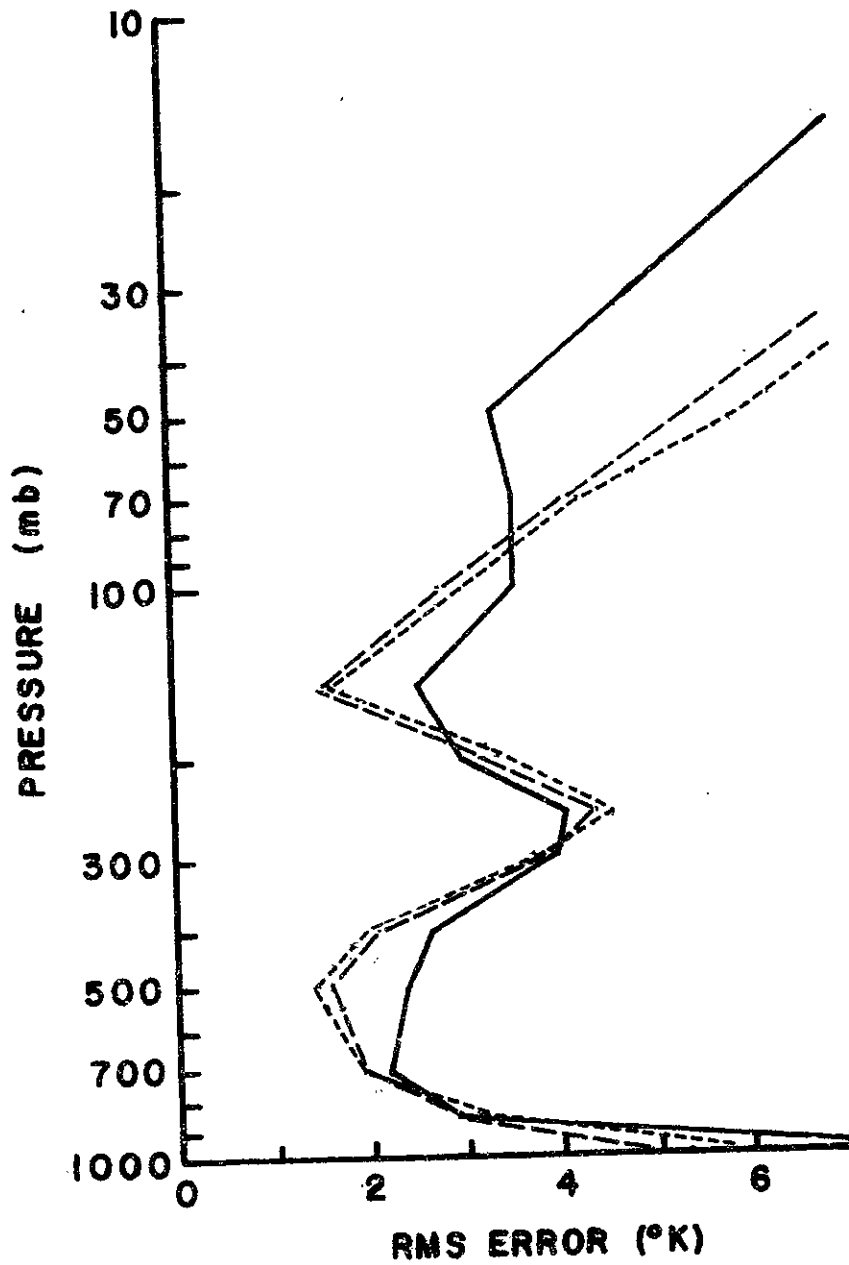


Figure 6
 Causal Filter Error Performance (Nadir Scan), February
 3-6, 1976 (Solid line - Statistical D, Long dash - one spot
 Kalman filter, Short dash - three spot Kalman filter)

Table 4

One spot filter retrieval errors, Aug. 7-9, 1975

Extreme scan
(Scan angle 0)

Pressure (mb)	Statistical D		Kalman-Bucy	
	Mean Error (K)	RMS Error (K)	Mean Error (K)	RMS Error (K)
1000	-4.8	3.2	0.2	3.4
850	-3.2	2.0	0.6	2.4
700	-1.2	1.3	0.6	1.6
500	-0.1	1.1	0.4	1.1
400	-0.1	1.2	-0.2	1.1
300	0.5	2.0	-0.2	1.7
250	2.6	3.6	0.3	2.2
200	1.8	3.0	0.5	2.2
150	1.3	3.0	0.2	2.6
100	2.3	1.8	1.3	1.8
70	1.0	2.3	-0.9	0.9
50	0.8	1.1	-0.8	1.2
30	1.2	1.3	-0.5	1.4
10	-0.4	2.2	0.3	1.9

Table 5

One spot filter retrieval errors, Aug. 7-9, 1975

Mid-scan
(Scan angle 3)

Pressure (mb)	Statistical D		Kalman-Bucy	
	Mean Error (K)	RMS Error (K)	Mean Error (K)	RMS Error (K)
1000	-4.2	3.1	-0.1	3.1
850	-2.3	2.1	0.4	2.1
700	-0.4	1.3	0.4	1.3
500	0.7	1.2	0.2	1.2
400	0.4	1.2	-0.2	1.0
300	0.0	1.8	-0.1	1.2
250	0.8	3.3	0.4	1.9
200	0.9	3.4	0.4	2.3
150	0.7	2.6	0.0	2.0
100	0.3	2.3	1.5	1.9
70	-1.6	2.3	-0.9	1.1
50	-0.7	1.4	-1.2	1.1
30	0.6	1.2	-0.8	1.0
10	0.5	2.0	0.1	1.4

Table 6

One spot filter retrieval errors, Aug. 7-9, 1975

Nadir
(Scan angle 6)

Pressure (mb)	Statistical D		Kalman-Bucy	
	Mean Error (K)	RMS Error (K)	Mean Error (K)	RMS Error (K)
1000	-3.7	2.5	0.7	2.5
850	-1.8	1.6	0.9	1.7
700	0.0	1.1	0.5	1.2
500	0.7	1.3	0.1	1.6
400	0.5	1.3	-0.3	1.4
300	-0.3	1.9	-0.1	1.4
250	0.3	3.3	0.5	2.0
200	0.4	3.3	0.3	2.1
150	0.4	3.0	-0.1	2.4
100	0.0	2.7	1.7	2.2
70	-2.1	2.4	-0.8	1.4
50	-1.0	1.7	-1.2	1.2
30	0.5	1.4	-0.9	1.1
10	-0.5	1.8	0.0	1.3

Table 7

One spot filter retrieval errors, Oct. 3-5, 1975

Extreme scan
(Scan angle 0)

Pressure (mb)	Statistical D		Kalman-Bucy	
	Mean Error (K)	RMS Error (K)	Mean Error (K)	RMS Error (K)
1000	-0.3	4.5	2.6	3.8
850	-0.5	2.8	1.6	2.3
700	0.0	1.7	0.4	1.3
500	-0.8	1.5	-0.3	1.4
400	-1.0	1.5	0.0	1.4
300	-0.8	1.9	0.9	1.8
250	0.2	3.4	1.5	2.3
200	0.6	3.1	-1.2	2.7
150	2.1	2.9	-2.8	3.0
100	2.9	2.4	0.8	2.5
70	0.7	2.4	0.7	2.0
50	1.1	1.8	1.2	2.9
30	1.8	2.2	2.6	4.1
10	0.4	3.0	7.4	5.5

Table 8

One spot filter retrieval errors, Oct. 3-5, 1975

Mid-scan
(Scan angle 3)

Pressure (mb)	Statistical D		Kalman-Bucy	
	Mean Error (K)	RMS Error (K)	Mean Error (K)	RMS Error (K)
1000	0.0	3.7	2.4	3.3
850	0.3	2.5	1.4	2.1
700	0.8	1.7	0.3	1.1
500	-0.3	1.4	-0.7	1.2
400	-0.9	1.7	-0.3	1.4
300	-1.2	2.3	0.4	2.0
250	-1.0	3.4	0.4	2.7
200	-0.4	3.2	-1.8	3.4
150	1.6	2.8	-2.1	2.9
100	2.7	3.2	1.6	2.9
70	0.5	3.1	1.1	2.7
50	0.7	2.1	1.5	3.9
30	0.7	2.0	2.7	4.9
10	-0.6	2.7	7.3	5.9

Table 9

One spot filter retrieval errors, Oct. 3-5, 1975

Nadir
(Scan angle 6)

Pressure (mb)	Statistical D		Kalman-Bucy	
	Mean Error (K)	RMS Error (K)	Mean Error (K)	RMS Error (K)
1000	0.4	3.1	2.8	2.6
850	0.8	2.4	1.8	1.8
700	1.2	2.1	0.5	1.2
500	0.0	2.3	-0.7	1.4
400	-0.5	2.5	-0.3	1.6
300	-0.9	2.7	0.3	2.5
250	-1.3	3.1	-0.3	2.9
200	-0.2	3.5	-2.0	3.6
150	1.6	2.5	-2.4	2.8
100	2.2	3.3	1.4	2.8
70	0.1	3.6	0.9	3.3
50	0.4	2.4	1.6	4.5
30	0.5	2.3	2.7	5.8
10	-1.1	3.4	7.1	6.7

Table 10

One spot filter retrieval errors, Oct. 22-25, 1975

Extreme scan
(Scan angle 0)

Pressure (mb)	Statistical D		Kalman-Bucy	
	Mean Error (K)	RMS Error (K)	Mean Error (K)	RMS Error (K)
1000	2.1	3.8	4.7	3.3
850	-1.1	3.6	1.1	2.0
700	-1.4	3.9	0.1	1.2
500	-0.4	4.3	0.3	1.6
400	-0.3	4.3	1.3	1.7
300	-1.1	4.3	1.4	1.8
250	1.8	4.8	0.1	3.0
200	-0.7	3.7	-2.7	3.3
150	0.7	2.1	-4.5	2.3
100	3.6	3.3	1.3	1.5
70	0.5	4.9	0.6	2.7
50	1.2	4.5	1.7	4.4
30	1.7	5.6	4.0	6.3
10	0.9	9.2	10.0	9.3

Table 11

One spot filter retrieval errors, Oct. 22-25, 1975

Mid-scan
(Scan angle 3)

Pressure (mb)	Statistical D		Kalman-Bucy	
	Mean Error (K)	RMS Error (K)	Mean Error (K)	RMS Error (K)
1000	2.8	2.9	5.4	3.1
850	0.1	1.8	1.5	1.9
700	0.6	1.3	0.3	1.0
500	0.3	1.3	0.1	1.7
400	0.1	1.3	0.7	1.8
300	-0.8	1.6	0.7	2.1
250	-1.5	2.6	-0.4	3.4
200	-0.8	2.3	-2.7	3.0
150	0.0	1.5	-4.4	1.9
100	2.7	2.5	1.3	1.6
70	-0.2	3.5	0.9	3.0
50	0.8	2.5	2.3	4.3
30	1.7	2.7	4.7	6.0
10	0.9	4.4	10.8	8.9

Table 12

One spot filter retrieval errors, Oct. 22-25, 1975

Nadir
(Scan angle 6)

Pressure (mb)	Statistical D		Kalman-Bucy	
	Mean Error (K)	RMS Error (K)	Mean Error (K)	RMS Error (K)
1000	2.3	2.6	5.0	3.5
850	0.0	1.8	1.2	2.2
700	0.7	1.4	0.3	1.2
500	0.4	1.3	0.1	1.6
400	0.1	1.7	0.7	1.8
300	-1.0	1.7	0.5	2.1
250	-1.9	2.7	-0.5	3.4
200	-1.3	2.4	-2.7	2.8
150	0.0	1.6	-4.3	1.9
100	2.8	2.3	1.5	1.7
70	-0.2	3.4	0.8	3.0
50	0.8	2.8	2.1	4.3
30	1.7	2.9	4.3	5.8
10	0.7	4.6	10.0	8.3

Table 13

One spot filter retrieval errors, Dec. 5-8, 1975

Extreme scan
(Scan angle 0)

Pressure (mb)	Statistical D		Kalman-Bucy	
	Mean Error (K)	RMS Error (K)	Mean Error (K)	RMS Error (K)
1000	9.7	8.2	3.2	3.7
850	2.3	3.8	1.8	2.1
700	0.8	2.1	1.4	1.6
500	-1.4	1.6	0.0	1.5
400	-1.7	1.9	0.4	1.3
300	-2.1	2.9	0.0	2.5
250	-2.1	3.5	-0.8	3.1
200	1.2	2.4	-1.1	3.2
150	2.5	2.0	-1.4	2.1
100	3.9	2.9	1.9	2.0
70	0.8	2.4	-0.2	2.4
50	1.3	2.2	-0.4	3.0
30	1.4	3.5	-0.1	3.9
10	-2.1	7.1	0.2	6.5

Table 14

One spot filter retrieval errors, Dec. 5-8, 1975

Mid-scan
(Scan angle 3)

Pressure (mb)	Statistical D		Kalman-Bucy	
	Mean Error (K)	RMS Error (K)	Mean Error (K)	RMS Error (K)
1000	6.7	5.8	4.1	3.8
850	2.1	3.1	2.4	2.3
700	1.2	1.6	1.7	1.4
500	-0.6	2.1	-0.2	1.4
400	-1.1	2.6	-0.4	1.6
300	-2.1	3.2	-1.1	3.0
250	-2.8	3.8	-1.9	3.4
200	-0.6	2.6	-2.0	3.2
150	1.4	2.3	-1.5	1.8
100	3.8	3.5	2.6	2.1
70	0.7	3.8	0.5	3.8
50	1.2	3.1	1.3	4.7
30	1.5	3.8	2.4	5.6
10	-0.3	6.4	4.3	7.9

Table 15

One spot filter retrieval errors, Dec. 5-8, 1975

Nadir
(Scan angle 6)

Pressure (mb)	Statistical D		Kalman-Bucy	
	Mean Error (K)	RMS Error (K)	Mean Error (K)	RMS Error (K)
1000	6.6	5.0	3.4	3.9
850	2.4	2.9	2.0	2.7
700	1.6	1.9	1.6	1.8
500	-0.3	2.0	-0.3	1.4
400	-1.0	2.6	-0.4	1.9
300	-2.5	3.7	-1.4	3.7
250	-3.2	4.1	-2.1	3.8
200	-0.8	2.6	-1.9	3.4
150	1.5	2.4	-1.3	1.7
100	3.9	4.1	2.9	2.5
70	0.8	4.4	0.8	4.7
50	1.3	3.6	1.7	6.1
30	1.6	4.0	2.7	6.8
10	0.2	6.7	4.8	9.5

Table 16

One spot filter retrieval errors, Jan. 24-25, 1976

Extreme scan
(Scan angle 0)

Pressure (mb)	Statistical D		Kalman-Bucy	
	Mean Error (K)	RMS Error (K)	Mean Error (K)	RMS Error (K)
1000	8.2	11.6	2.2	6.3
850	2.0	4.6	0.8	2.5
700	1.1	3.0	0.6	1.1
500	-0.7	2.8	-0.1	1.6
400	-1.2	3.0	0.9	1.4
300	-1.7	3.5	1.1	2.4
250	-1.9	3.9	-0.3	3.6
200	0.9	2.8	-1.6	3.0
150	3.1	1.9	-1.5	1.9
100	5.6	3.3	2.1	1.5
70	2.1	3.2	0.3	2.4
50	1.8	3.3	0.7	2.2
30	-1.2	4.6	-0.5	3.5
10	-10.1	6.6	-5.5	7.2

Table 17

One spot filter retrieval errors, Jan 24-25, 1976

Mid-scan
(Scan angle 3)

Pressure (mb)	Statistical D		Kalman-Bucy	
	Mean Error (K)	RMS Error (K)	Mean Error (K)	RMS Error (K)
1000	5.5	8.3	1.5	5.9
850	2.3	3.5	1.7	3.3
700	1.5	2.6	1.5	2.0
500	-0.7	2.7	-0.1	1.5
400	-1.6	3.3	0.5	2.2
300	-3.3	4.0	-0.2	3.2
250	-4.3	4.6	-1.6	4.2
200	-1.0	3.5	-2.6	3.1
150	2.8	2.3	-1.5	1.5
100	6.4	3.8	3.0	3.0
70	2.8	3.6	1.4	3.6
50	2.1	4.0	2.1	3.7
30	-1.5	4.8	0.4	4.6
10	-11.5	5.8	-4.5	7.5

Table 18

One spot filter retrieval errors, Jan. 24-25, 1976

Nadir
(Scan angle 6)

Pressure (mb)	Statistical D		Kalman-Bucy	
	Mean Error (K)	RMS Error (K)	Mean Error (K)	RMS Error (K)
1000	5.7	8.1	1.7	5.1
850	2.3	3.9	2.2	3.2
700	1.6	2.3	1.8	2.0
500	-0.5	2.6	0.1	1.3
400	-1.3	3.3	0.5	2.0
300	-2.8	4.0	-0.3	3.1
250	-4.1	4.6	-1.9	4.0
200	-1.3	3.0	-2.9	2.9
150	2.5	2.3	-1.4	1.4
100	5.9	3.7	3.3	2.8
70	2.6	4.1	1.5	3.5
50	2.1	4.5	1.9	3.7
30	-1.5	5.2	0.2	4.2
10	-12.3	5.9	-5.4	7.5

Table 19

One spot filter retrieval errors, Feb. 3-6, 1976

Extreme scan
(Scan angle 0)

Pressure (mb)	Statistical D		Kalman-Bucy	
	Mean Error (K)	RMS Error (K)	Mean Error (K)	RMS Error (K)
1000	6.7	9.4	0.3	3.9
850	1.0	3.7	0.5	2.3
700	0.5	2.4	1.0	1.7
500	-0.8	2.0	0.2	1.5
400	-1.0	2.2	1.0	1.8
300	-1.4	3.4	0.9	3.1
250	-1.5	3.9	-0.2	3.5
200	0.6	3.3	-1.7	2.8
150	1.9	2.4	-1.3	1.7
100	4.6	2.7	2.4	2.0
70	1.9	2.7	0.3	2.0
50	1.5	3.0	0.3	3.2
30	0.3	4.6	0.1	5.1
10	-6.8	9.1	-1.7	10.7

Table 20

One spot filter retrieval errors, Feb. 3-6, 1976

Mid-scan
(Scan angle 3)

Pressure (mb)	Statistical D		Kalman-Bucy	
	Mean Error (K)	RMS Error (K)	Mean Error (K)	RMS Error (K)
1000	4.6	7.5	-0.5	4.9
850	1.5	2.9	0.4	2.9
700	1.2	2.2	0.9	1.9
500	-0.4	2.4	-0.2	1.6
400	-1.1	2.7	0.5	2.1
300	-2.5	4.0	0.0	3.9
250	-3.0	4.1	-0.6	4.4
200	-0.9	3.0	-1.7	3.2
150	1.4	2.6	-1.1	1.5
100	4.8	3.6	3.0	2.8
70	2.3	3.6	0.6	4.1
50	1.9	3.4	1.2	5.9
30	0.7	4.9	1.3	7.7
10	-5.7	8.4	0.4	13.0

Table 21

One spot filter retrieval errors, Feb. 3-6, 1976

Nadir
(Scan angle 6)

Pressure (mb)	Statistical D		Kalman-Bucy	
	Mean Error (K)	RMS Error (K)	Mean Error (K)	RMS Error (K)
1000	4.6	7.5	-0.5	4.9
850	1.5	2.9	0.4	2.9
700	1.2	2.2	0.9	1.9
500	-0.4	2.4	-0.2	1.6
400	-1.1	2.7	0.5	2.1
300	-2.5	4.0	0.0	3.9
250	-3.0	4.1	-0.6	4.4
200	-0.9	3.0	-1.7	3.2
150	1.4	2.6	-1.1	1.5
100	4.8	3.6	3.0	2.8
70	2.3	3.6	0.6	4.1
50	1.9	3.4	1.2	5.9
30	0.7	4.9	1.3	7.7
10	-5.7	8.4	0.4	13.0

Table 22

Two spot filter retrieval errors, Aug. 7-9, 1975

Pressure (mb)	Extreme scan				Close scan			
	Scan angle 0		Scan angle 1		Scan angle 5		Scan angle 6	
	Mean Error (K)	RMS Error (K)	Mean Error (K)	RMS Error (K)	Mean Error (K)	RMS Error (K)	Mean Error (K)	RMS Error (K)
1000	0.0	2.9	0.0	3.2	2.3	2.6	2.6	2.6
850	0.7	2.1	0.6	2.2	1.5	1.8	1.6	1.8
700	0.6	1.4	0.4	1.5	0.4	1.2	0.5	1.3
500	0.5	1.1	0.1	1.1	-0.6	1.2	-0.6	1.4
400	-0.2	1.0	-0.5	0.8	-0.2	1.4	-0.2	1.5
300	-0.2	1.6	-0.4	1.2	0.4	2.2	0.5	2.4
250	0.3	2.1	0.3	1.7	0.1	2.9	0.0	3.0
200	0.4	2.1	0.6	2.3	-1.9	3.9	-1.9	3.9
150	0.1	2.7	0.1	2.0	-2.3	2.9	-2.3	2.8
100	1.2	1.8	1.6	1.4	1.3	2.8	1.3	2.7
70	-1.0	0.9	-0.7	1.2	0.8	3.5	0.6	3.6
50	-0.9	1.3	-0.8	1.5	1.4	4.8	1.2	4.8
30	-0.6	1.5	-0.5	1.6	2.3	6.1	2.2	6.1
10	0.2	1.9	0.3	2.1	6.7	7.0	6.5	7.0

Table 23

Two spot filter retrieval errors, Oct. 3-5, 1975

Pressure (mb)	Extreme scan				Close scan			
	Scan angle 0		Scan angle 1		Scan angle 5		Scan angle 6	
	Mean Error (K)	RMS Error (K)	Mean Error (K)	RMS Error (K)	Mean Error (K)	RMS Error (K)	Mean Error (K)	RMS Error (K)
1000	2.3	3.9	2.2	3.4	2.3	2.6	2.6	2.6
850	1.5	2.3	1.3	2.0	1.5	1.8	1.6	1.8
700	0.4	1.2	0.2	1.2	0.4	1.2	0.5	1.3
500	-0.3	1.4	-0.6	1.4	-0.6	1.2	-0.6	1.4
400	0.2	1.3	0.0	1.4	-0.2	1.4	-0.2	1.5
300	1.0	1.7	0.9	1.7	0.4	2.2	0.5	2.4
250	1.6	2.2	1.4	2.2	0.1	2.9	0.0	3.0
200	-1.2	2.7	-1.4	2.4	-1.9	3.9	-1.9	3.9
150	-2.9	2.9	-2.5	2.9	-2.3	2.9	-2.3	2.8
100	0.7	2.4	1.2	2.5	1.3	2.8	1.3	2.7
70	0.7	1.9	0.8	2.0	0.8	3.5	0.6	3.6
50	1.3	2.9	1.2	3.0	1.4	4.8	1.2	4.8
30	2.8	4.1	2.6	4.2	2.3	6.1	2.2	6.1
10	7.6	5.6	7.3	5.6	6.7	7.0	6.5	7.0

Table 24

Two spot filter retrieval errors, Oct. 22-25, 1975

Pressure (mb)	Extreme scan				Close scan			
	Scan angle 0		Scan angle 1		Scan angle 5		Scan angle 6	
	Mean Error (K)	RMS Error (K)	Mean Error (K)	RMS Error (K)	Mean Error (K)	RMS Error (K)	Mean Error (K)	RMS Error (K)
1000	4.6	3.3	5.1	2.9	4.9	3.4	4.8	3.4
850	1.0	1.9	1.3	1.8	1.1	2.1	1.1	2.2
700	0.1	1.2	0.3	1.0	0.2	1.1	0.2	1.2
500	0.3	1.6	0.4	1.5	0.2	1.6	0.2	1.6
400	1.3	1.7	1.2	1.5	0.9	1.6	0.9	1.7
300	1.5	1.8	1.2	1.9	0.8	2.0	0.7	2.1
250	0.1	3.1	-0.1	3.3	-0.4	3.4	-0.3	3.5
200	-2.7	3.5	-2.7	3.4	-2.5	3.0	-2.5	3.0
150	-4.5	2.3	-4.5	2.3	-4.2	2.0	-4.3	2.0
100	1.3	1.5	1.2	1.5	1.3	1.8	1.3	1.7
70	0.6	2.9	0.7	3.1	0.5	3.3	0.5	3.2
50	1.7	4.7	2.0	5.0	1.7	4.8	1.6	4.6
30	4.0	6.6	4.4	7.0	4.0	6.4	3.8	6.2
10	10.0	9.8	10.4	10.0	9.7	9.3	9.4	8.9

Table 25

Two spot filter retrieval errors, Dec. 5-8, 1975

Pressure (mb)	Extreme scan				Close scan			
	Scan angle 0		Scan angle 1		Scan angle 5		Scan angle 6	
	Mean Error (K)	RMS Error (K)	Mean Error (K)	RMS Error (K)	Mean Error (K)	RMS Error (K)	Mean Error (K)	RMS Error (K)
1000	3.4	3.6	3.2	3.8	3.3	3.7	2.9	5.2
850	2.0	2.0	1.7	2.0	1.8	2.5	1.4	3.6
700	1.5	1.5	1.3	1.4	1.3	1.8	1.1	2.0
500	0.1	1.3	-0.1	1.4	-0.5	1.5	-0.3	1.8
400	0.4	1.1	0.2	1.3	-0.6	1.7	0.2	2.5
300	-0.1	2.5	-0.2	2.3	-1.4	3.5	-0.3	4.2
250	-0.9	3.1	-1.0	2.9	-1.9	3.6	-0.8	4.5
200	-1.3	3.2	-1.3	3.2	-1.7	3.5	-0.9	4.2
150	-1.5	2.0	-1.5	2.0	-1.0	1.7	-0.9	2.3
100	1.8	2.1	1.9	1.9	3.2	2.4	2.3	3.3
70	-0.1	2.6	-0.2	2.7	0.8	4.6	-0.9	5.5
50	-0.2	3.3	-0.2	3.3	1.5	6.0	-0.7	7.6
30	0.2	4.2	0.3	4.4	2.2	7.0	0.1	9.5
10	0.6	6.9	1.3	6.7	4.2	9.7	2.4	11.8

Table 26

Two spot filter retrieval errors, Jan. 24-25, 1976

Pressure (mb)	Extreme scan				Close scan			
	Scan angle 0		Scan angle 1		Scan angle 5		Scan angle 6	
	Mean Error (K)	RMS Error (K)	Mean Error (K)	RMS Error (K)	Mean Error (K)	RMS Error (K)	Mean Error (K)	RMS Error (K)
1000	2.2	6.1	2.2	6.1	1.5	4.9	1.9	5.0
850	0.8	2.2	1.5	2.3	2.0	3.1	2.3	3.0
700	0.6	1.0	1.3	1.4	1.7	2.1	1.8	1.9
500	-0.1	1.6	0.0	1.7	0.1	1.4	0.0	1.2
400	1.0	1.3	0.8	1.5	0.5	1.8	0.3	1.7
300	1.1	2.5	0.4	2.4	-0.2	3.1	-0.5	3.0
250	-0.3	3.9	-0.8	3.8	-1.7	4.1	-2.0	4.1
200	-1.6	3.3	-2.0	3.3	-2.6	2.9	-2.9	2.9
150	-1.5	2.2	-1.5	1.9	-1.4	1.4	-1.3	1.4
100	2.1	1.8	2.4	2.1	3.2	3.0	3.5	2.8
70	0.4	2.5	0.7	2.6	1.5	3.7	1.8	3.5
50	1.0	2.3	1.2	2.6	1.9	3.9	2.2	3.6
30	-0.1	3.6	-0.3	4.0	0.2	4.5	0.5	4.0
10	-5.0	7.7	-5.2	8.2	-5.2	7.2	-5.0	7.3

Table 27

Two spot filter retrieval errors, Feb. 3-6, 1976

Pressure (mb)	Extreme scan				Close scan			
	Scan angle 0		Scan angle 1		Scan angle 5		Scan angle 6	
	Mean Error (K)	RMS Error (K)	Mean Error (K)	RMS Error (K)	Mean Error (K)	RMS Error (K)	Mean Error (K)	RMS Error (K)
1000	0.6	4.1	0.3	4.3	-0.1	4.8	-0.3	5.1
850	0.7	2.3	0.8	2.1	0.6	2.9	0.5	3.0
700	1.1	1.6	1.1	1.5	1.0	1.9	0.9	1.9
500	0.2	1.5	0.1	1.4	-0.2	1.4	-0.3	1.5
400	0.9	1.6	0.8	1.6	0.4	2.0	0.3	2.0
300	0.8	3.0	0.5	2.9	-0.2	3.8	-0.2	3.9
250	-0.3	3.5	-0.2	3.4	-0.8	4.4	-0.7	4.5
200	-1.8	2.8	-1.7	2.6	-1.9	3.2	-1.7	3.3
150	-1.4	1.7	-1.2	1.5	-1.1	1.5	-1.0	1.6
100	2.3	2.1	2.5	2.0	3.0	2.7	3.1	2.7
70	0.3	2.0	0.4	2.2	0.8	4.0	0.8	4.3
50	0.4	3.3	0.6	3.4	1.5	5.8	1.3	6.2
30	0.3	5.2	0.4	5.3	1.7	7.7	1.5	8.3
10	-1.5	10.8	-1.2	10.6	1.0	12.9	0.5	13.5

Table 28

Three spot filter retrievals, Aug. 7-9, 1975

Extreme scan

Pressure (mb)	Scan angle 0		Scan angle 1		Scan angle 2	
	Mean Error (K)	RMS Error (K)	Mean Error (K)	RMS Error (K)	Mean Error (K)	RMS Error (K)
1000	-0.1	2.9	-0.1	2.9	0.1	2.9
850	0.6	2.0	0.5	2.0	0.6	2.0
700	0.6	1.4	0.4	1.3	0.4	1.4
500	0.5	1.1	0.2	1.1	0.1	1.2
400	-0.1	1.1	-0.4	0.8	-0.5	0.8
300	-0.1	1.6	-0.3	1.2	-0.5	1.2
250	0.4	2.1	0.3	1.6	0.1	1.7
200	0.4	2.0	0.5	2.2	0.3	2.4
150	0.1	2.7	0.0	2.0	0.0	1.9
100	1.2	1.8	1.5	1.4	1.7	1.6
70	-1.1	0.9	-0.7	1.2	-0.6	1.1
50	-1.0	1.3	-0.8	1.4	-0.9	1.4
30	-0.6	1.5	-0.5	1.6	-0.5	1.4
10	0.2	1.9	0.3	2.0	0.3	1.9

Table 29

Three spot filter retrieval errors, Aug. 7-9, 1975

Close scan

Pressure (mb)	Scan angle 5		Scan angle 6		Scan angle 7	
	Mean Error (K)	RMS Error (K)	Mean Error (K)	RMS Error (K)	Mean Error (K)	RMS Error (K)
1000	0.2	2.8	0.5	2.4	0.8	2.3
850	0.6	1.9	0.8	1.7	1.0	1.6
700	0.4	1.2	0.5	1.1	0.5	1.1
500	0.2	1.4	0.1	1.4	0.0	1.4
400	-0.1	1.1	-0.2	1.1	-0.2	1.2
300	0.0	1.3	0.0	1.3	0.0	1.4
250	0.7	1.9	0.6	1.9	0.6	2.0
200	0.4	2.0	0.3	2.1	0.3	2.2
150	-0.2	2.2	-0.2	2.3	-0.1	2.3
100	1.4	2.1	1.6	2.1	1.7	2.1
70	-1.0	1.4	-0.9	1.3	-0.8	1.3
50	-1.3	1.2	-1.3	1.1	-1.1	1.1
30	-1.0	1.0	-1.0	1.0	-0.9	1.0
10	-0.1	1.2	-0.1	1.3	0.0	1.3

Table 30

Three spot filter retrieval errors, Oct. 3-5, 1975

Extreme scan

Pressure (mb)	Scan angle 0		Scan angle 1		Scan angle 2	
	Mean Error (K)	RMS Error (K)	Mean Error (K)	RMS Error (K)	Mean Error (K)	RMS Error (K)
1000	2.2	4.0	2.2	3.5	2.1	3.4
850	1.3	2.4	1.3	2.1	1.2	2.1
700	0.4	1.2	0.3	1.1	0.2	1.1
500	-0.2	1.4	-0.5	1.2	-0.6	1.2
400	0.2	1.3	0.1	1.2	-0.1	1.4
300	1.0	1.6	0.9	1.6	0.9	1.9
250	1.6	2.2	1.4	2.2	1.2	2.3
200	-1.3	2.8	-1.5	2.5	-1.5	2.6
150	-3.0	2.9	-2.6	2.9	-2.2	2.8
100	0.7	2.4	1.2	2.4	1.4	2.4
70	0.6	1.9	0.8	1.8	0.9	1.9
50	1.3	2.9	1.3	2.9	1.3	3.1
30	2.9	4.1	2.6	4.2	2.6	4.3
10	7.7	5.6	7.4	5.6	7.4	5.6

Table 31

Three spot retrieval errors, Oct. 3-5, 1975

Close scan

Pressure (mb)	Scan angle 5		Scan angle 6		Scan angle 7	
	Mean Error (K)	RMS Error (K)	Mean Error (K)	RMS Error (K)	Mean Error (K)	RMS Error (K)
1000	2.0	2.5	2.2	2.4	2.2	2.6
850	1.2	1.7	1.3	1.7	1.3	1.9
700	0.4	1.2	0.4	1.2	0.3	1.4
500	-0.5	1.1	-0.5	1.2	-0.6	1.4
400	0.0	1.3	0.0	1.4	0.0	1.5
300	0.7	2.1	0.8	2.2	0.7	2.4
250	0.2	2.9	0.1	3.0	0.0	2.9
200	-1.8	3.9	-1.8	4.0	-1.8	3.8
150	-2.3	2.8	-2.4	2.8	-2.2	2.9
100	1.2	2.8	1.1	2.7	1.1	2.5
70	0.6	3.6	0.4	3.6	0.2	3.4
50	1.1	5.0	0.9	4.9	0.6	4.8
30	2.0	6.4	1.8	6.3	1.4	6.1
10	6.4	7.3	6.2	7.2	5.5	7.2

Table 32

Three spot filter retrieval errors, Oct. 22-25, 1975

Extreme scan

Pressure (mb)	Scan angle 0		Scan angle 1		Scan angle 2	
	Mean Error (K)	RMS Error (K)	Mean Error (K)	RMS Error (K)	Mean Error (K)	RMS Error (K)
1000	4.5	3.2	4.9	2.8	5.3	2.9
850	0.9	1.9	1.2	1.8	1.4	1.9
700	0.1	1.2	0.2	1.0	0.3	1.0
500	0.4	1.7	0.4	1.5	0.3	1.5
400	1.4	1.8	1.3	1.5	1.1	1.5
300	1.5	1.8	1.3	1.8	1.1	2.0
250	0.2	3.1	0.0	3.4	-0.1	3.4
200	-2.7	3.5	-2.7	3.5	-2.5	3.3
150	-4.6	2.3	-4.6	2.3	-4.4	2.2
100	1.3	1.5	1.1	1.6	1.1	1.5
70	0.5	2.9	0.6	3.0	0.6	3.3
50	1.7	4.8	1.9	5.0	1.9	5.2
30	4.1	6.9	4.4	7.1	4.3	7.3
10	10.2	10.2	10.5	10.3	10.4	10.4

Table 33

Three spot filter retrieval errors, Oct. 22-25, 1975

Close scan

Pressure (mb)	Scan angle 5		Scan angle 6		Scan angle 7	
	Mean Error (K)	RMS Error (K)	Mean Error (K)	RMS Error (K)	Mean Error (K)	RMS Error (K)
1000	4.6	3.5	4.5	3.5	4.4	3.5
850	0.9	2.2	0.9	2.2	0.8	2.2
700	0.2	1.1	0.2	1.2	0.1	1.2
500	0.3	1.5	0.3	1.5	0.2	1.5
400	1.0	1.6	1.1	1.6	1.1	1.6
300	0.9	2.0	0.9	2.0	1.1	2.1
250	-0.3	3.4	-0.2	3.5	0.1	3.5
200	-2.5	3.0	-2.5	3.0	-2.4	3.0
150	-4.2	2.0	-4.4	2.0	-4.4	2.0
100	1.3	1.9	1.2	1.7	1.0	1.5
70	0.5	3.5	0.3	3.4	0.1	3.3
50	1.7	5.1	1.4	4.9	1.2	4.9
30	3.9	6.8	3.6	6.6	3.3	6.4
10	9.7	9.7	9.3	9.2	8.8	8.8

Table 34

Three spot filter retrieval errors, Dec. 5-8, 1975

Extreme scan

Pressure (mb)	Scan angle 0		Scan angle 1		Scan angle 2	
	Mean Error (K)	RMS Error (K)	Mean Error (K)	RMS Error (K)	Mean Error (K)	RMS Error (K)
1000	3.4	3.5	3.5	3.6	3.7	3.6
850	2.0	1.9	2.0	1.9	2.1	1.9
700	1.5	1.5	1.5	1.3	1.5	1.2
500	0.1	1.3	0.0	1.2	-0.1	1.3
400	0.4	1.1	0.2	1.1	0.0	1.2
300	-0.1	2.6	-0.3	2.4	-0.5	2.4
250	-0.9	3.1	-1.1	2.9	-1.3	2.8
200	-1.3	3.2	-1.3	3.1	-1.5	3.0
150	-1.6	2.0	-1.5	1.9	-1.4	1.9
100	1.8	2.1	1.9	1.9	2.2	2.0
70	-0.1	2.7	-0.1	2.8	-0.1	2.9
50	-0.1	3.5	0.0	3.5	0.1	3.5
30	0.4	4.3	0.6	4.5	0.7	4.5
10	0.8	7.0	1.5	6.8	2.1	6.5

Table 35

Three spot filter retrieval errors, Dec. 5-8, 1975

Close scan

Pressure (mb)	Scan angle 5		Scan angle 6		Scan angle 7	
	Mean Error (K)	RMS Error (K)	Mean Error (K)	RMS Error (K)	Mean Error (K)	RMS Error (K)
1000	3.5	4.4	3.6	4.1	3.7	3.9
850	2.1	3.0	2.2	2.9	2.3	2.7
700	1.6	1.8	1.8	1.8	1.8	1.8
500	-0.2	1.1	-0.1	1.1	-0.1	1.1
400	-0.4	1.7	-0.3	1.6	-0.4	1.6
300	-1.3	3.6	-1.4	3.7	-1.6	3.7
250	-2.0	3.9	-2.2	3.9	-2.3	4.0
200	-2.0	3.6	-2.0	3.6	-2.1	3.7
150	-1.3	1.8	-1.3	1.7	-1.3	1.7
100	2.9	2.5	2.9	2.6	3.0	2.9
70	0.7	4.8	0.8	5.0	1.0	5.2
50	1.6	6.2	1.8	6.5	2.2	6.7
30	2.5	7.2	2.7	7.4	3.3	7.6
10	4.5	9.8	4.9	10.1	5.6	10.6

Table 36

Three spot filter retrieval errors, Jan. 24-25, 1976

Extreme scan

Pressure (mb)	Scan angle 0		Scan angle 1		Scan angle 2	
	Mean Error (K)	RMS Error (K)	Mean Error (K)	RMS Error (K)	Mean Error (K)	RMS Error (K)
1000	2.1	6.3	2.3	6.1	2.1	5.6
850	0.7	2.3	1.6	2.3	1.8	2.4
700	0.5	1.0	1.3	1.3	1.5	1.5
500	-0.2	1.6	-0.1	1.6	0.0	1.6
400	0.9	1.3	0.7	1.4	0.6	1.7
300	1.1	2.6	0.5	2.5	0.1	2.5
250	-0.2	4.0	-0.7	3.9	-1.2	3.8
200	-1.6	3.4	-1.9	3.3	-2.2	3.2
150	-1.4	2.2	-1.3	1.9	-1.4	1.9
100	2.1	1.8	2.5	2.2	2.7	2.5
70	0.5	2.5	0.7	2.7	0.9	2.9
50	1.0	2.4	1.2	2.6	1.4	2.9
30	-0.1	3.7	-0.3	3.9	-0.4	4.2
10	-5.1	7.7	-5.2	8.0	-5.3	8.5

Table 37

Three spot filter retrieval errors, Jan. 24-25, 1976

Close scan

Pressure (mb)	Scan angle 5		Scan angle 6		Scan angle 7	
	Mean Error (K)	RMS Error (K)	Mean Error (K)	RMS Error (K)	Mean Error (K)	RMS Error (K)
1000	1.6	4.8	2.0	4.7	2.3	5.2
850	2.1	3.0	2.4	2.9	2.6	3.1
700	1.7	2.1	1.9	1.9	2.0	1.9
500	0.0	1.3	-0.1	1.1	-0.1	1.2
400	0.5	1.7	0.3	1.6	0.1	1.7
300	-0.3	3.2	-0.5	3.1	-0.7	3.1
250	-1.8	4.2	-2.1	4.2	-2.3	4.2
200	-2.7	3.0	-2.9	2.9	-3.1	2.9
150	-1.4	1.5	-1.3	1.4	-1.2	1.5
100	3.3	3.0	3.5	2.8	3.8	2.7
70	1.6	3.7	1.9	3.5	2.1	3.3
50	2.1	4.1	2.3	3.7	2.5	3.5
30	0.5	4.7	0.6	4.2	0.8	3.9
10	-4.9	7.2	-4.8	7.2	-4.7	7.1

Table 38

Three spot filter retrieval errors, Feb. 3-6, 1976

Extreme scan

Pressure (mb)	Scan angle 0		Scan angle 1		Scan angle 2	
	Mean Error (K)	RMS Error (K)	Mean Error (K)	RMS Error (K)	Mean Error (K)	RMS Error (K)
1000	0.8	4.3	0.5	4.5	0.3	4.3
850	0.9	2.4	0.9	2.3	0.9	2.3
700	1.2	1.7	1.2	1.5	1.1	1.6
500	0.2	1.5	0.1	1.5	0.0	1.4
400	0.9	1.5	0.7	1.6	0.6	1.5
300	0.7	3.0	0.4	3.0	0.3	3.0
250	-0.4	3.5	-0.3	3.5	-0.3	3.6
200	-1.9	2.8	-1.8	2.7	-1.7	2.5
150	-1.5	1.8	-1.3	1.6	-1.2	1.4
100	2.3	2.1	2.5	2.1	2.6	2.1
70	0.3	2.1	0.4	2.2	0.4	2.5
50	0.5	3.3	0.7	3.3	0.8	3.8
30	0.5	5.3	0.5	5.2	0.7	5.7
10	-1.2	11.0	-1.0	10.7	-0.6	10.7

Table 39

Three spot filter retrieval error, Feb. 3-6, 1976

Close scan

Pressure (mb)	Scan angle 5		Scan angle 6		Scan angle 7	
	Mean Error (K)	RMS Error (K)	Mean Error (K)	RMS Error (K)	Mean Error (K)	RMS Error (K)
1000	0.0	5.0	-0.1	5.3	-0.2	5.3
850	0.8	3.1	0.7	3.2	0.5	3.2
700	1.0	1.9	1.0	1.9	0.9	2.0
500	-0.2	1.4	-0.3	1.4	-0.4	1.4
400	0.3	2.0	0.3	2.0	0.3	2.0
300	-0.3	3.8	-0.3	3.9	-0.3	4.1
250	-0.8	4.4	-0.8	4.6	-0.9	4.7
200	-1.9	3.2	-1.8	3.4	-1.8	3.5
150	-1.1	1.6	-1.0	1.6	-1.0	1.6
100	3.0	2.8	3.1	2.8	3.3	2.7
70	0.9	4.0	0.9	4.2	0.9	4.4
50	1.7	5.7	1.5	6.1	1.4	6.5
30	1.9	7.6	1.7	8.1	1.6	8.5
10	1.2	12.7	0.8	13.3	0.4	13.9

the temperature structure of which is the desired output product. The observation matrices are also less noisy since the assumptions made about the surface have less impact.

The second conclusion is that the filter performance improves with the number of scan angles used in the filter. This is an expected result. The atmosphere is basically a low pass process. The temperature profile at one spot contains a large amount of information about temperature profiles nearby in space. Thus, the filter is able to use this information for noise averaging. For multi-spot retrievals at the higher scan angles, a second important phenomenon enters to improve performance. As the scan angle increases, it has been mentioned that the weighting functions lift. The amount of increase in altitude between adjacent scan angles is highest at the extreme scan angles. The three spot inversion scheme at the extreme scan is thus able to view basically the same atmosphere with three different sets of weighting functions. At nadir, the three spot inversion looks at the atmosphere with what amounts to a single weighting function.

Seasonally, the Kalman filter shows the most improvement over the Statistical D method during the winter months. During this season the atmosphere exhibits large swings in temperature as weather systems move across the world. Within these systems the atmosphere is still

coherent spatially. The memory of the Kalman filter thus produces superior results at most levels of the atmosphere. During the summer, the atmosphere is relatively quiet and the temperature profile, in general, lies close to the prior mean. Thus, during the summer months both the Statistical D and the Kalman filter exhibit rms performance close to the inherent error of the standard of comparison. It is important to note that the Statistical D method contains a mean error that is generally absent in the Kalman filter.

The performance of the filter during the winter months deserves close attention since it discloses two deficiencies in the filter. The error performance at the highest levels (those above 70 mb) is poor at best. At these levels, the weighting functions do not contain appreciable energy and do not overlap. The filter receives little information about the temperature profile at these levels and relies heavily on its predictions. Errors in the state propagation procedure are thus magnified at these levels. Because the atmosphere is more varied in winter, this has a graphic effect on the error performance. These errors also could be observed in the innovations sequence of the filter. The innovations sequence of the highest altitude channel was generally negative and correlated.

The second effect that is shown by the winter data results is the lack of improvement over the Statistical D

method at the crossing point of the weighting functions for channels 4 and 5. While not strictly a deficiency in the filter, this demonstrates that even the multi-spot filter cannot overcome this redundancy of information.

Given these comparisons and observations, it is possible to speculate on which parts of the Kalman filter are most responsible for the improvement in performance over the Statistical D method. The general elimination of the mean error by the Kalman filter is most likely due to its correct treatment of the atmosphere as a non-stationary process. The Statistical D method coefficients have been historically been computed using an ensemble of radiosonde reports from a number of selected stations. This method thus treats the atmosphere as a globally stationary process whose mean and covariance are given by this ensemble. A change in the global statistics from one year or season to the next will yield mean errors with this method. Because the Kalman filter uses means and covariances conditioned on past data, these biases are generally absent after a short period of processing.

A second large contributor to the improvement seems to be the ability to use the low pass nature of the atmosphere to perform noise averaging. This is evidenced by the monotone increase in performance with the number of spots processed at nadir. It seems to be the case that doubling

the information available to the filter decreases its error by roughly ten percent.

The final source of improvement is the use of the different weighting functions of the instrument at the extreme scan. It is unclear, however, what portion of the improvement at the extreme scan comes from this source and how much comes from the reduced influence of the surface. It is also unclear to what extent the spatially varying weighting functions contribute to the overall improvement.

Section H. The non-causal experiment

The second experiment that was performed was the use of the filter in its non-causal mode. The forward-backward filter algorithm of Chapter III was used to perform this experiment. The results for the three merged tapes on which this experiment was run are given in Tables 40-51. Figures 7- 8 depict the improvement achieved on the October dataset. These results yield the expected conclusion that the non-causal filter gives superior performance when compared with the causal filter. The improvement in all scan angles and seasons is of the order of 10% in the rms and is often accompanied by a reduction in the mean error. This improvement is due to two causes. First, there is

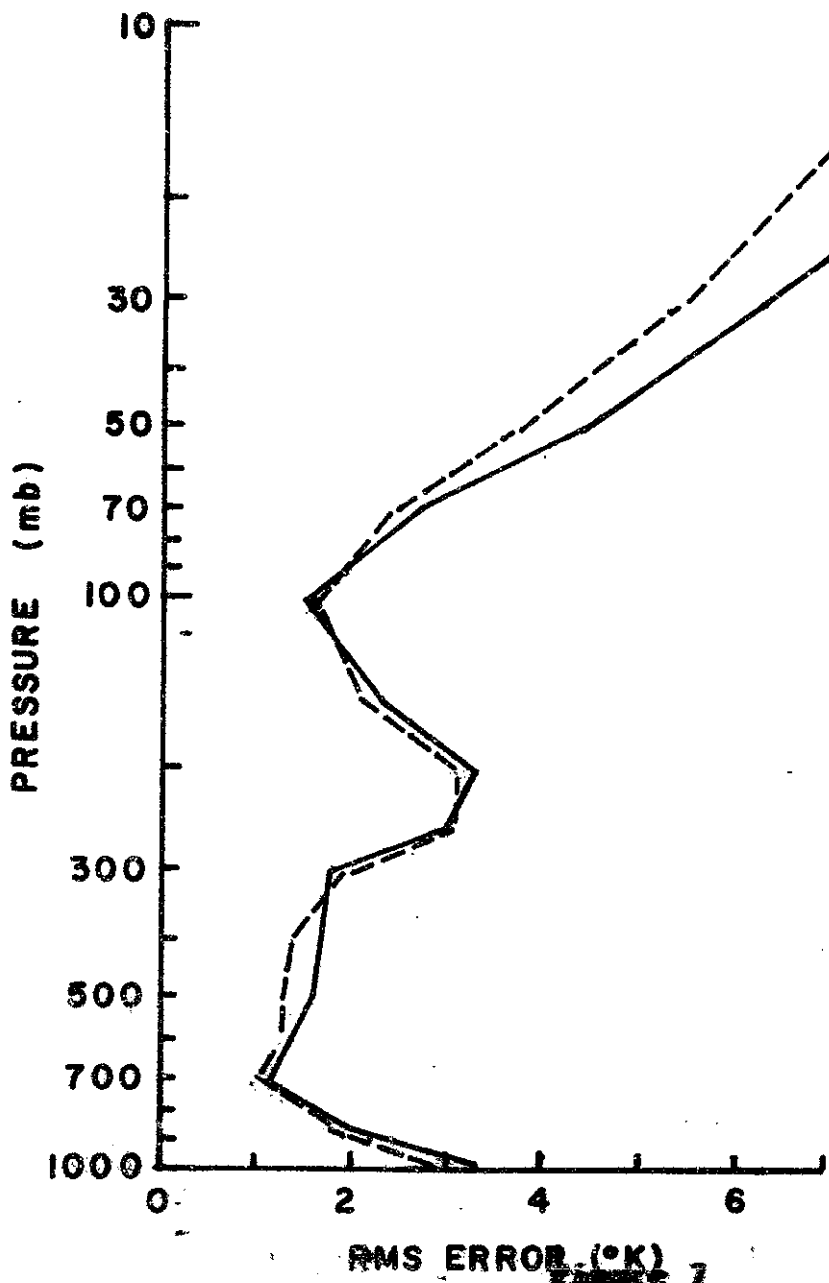


Figure 7
Causal versus Non-causal Filter Error Performance, October 22-25, 1975 ((One Spot Filter)) ((Solid line - causal filter, dashed line - non-causal filter))

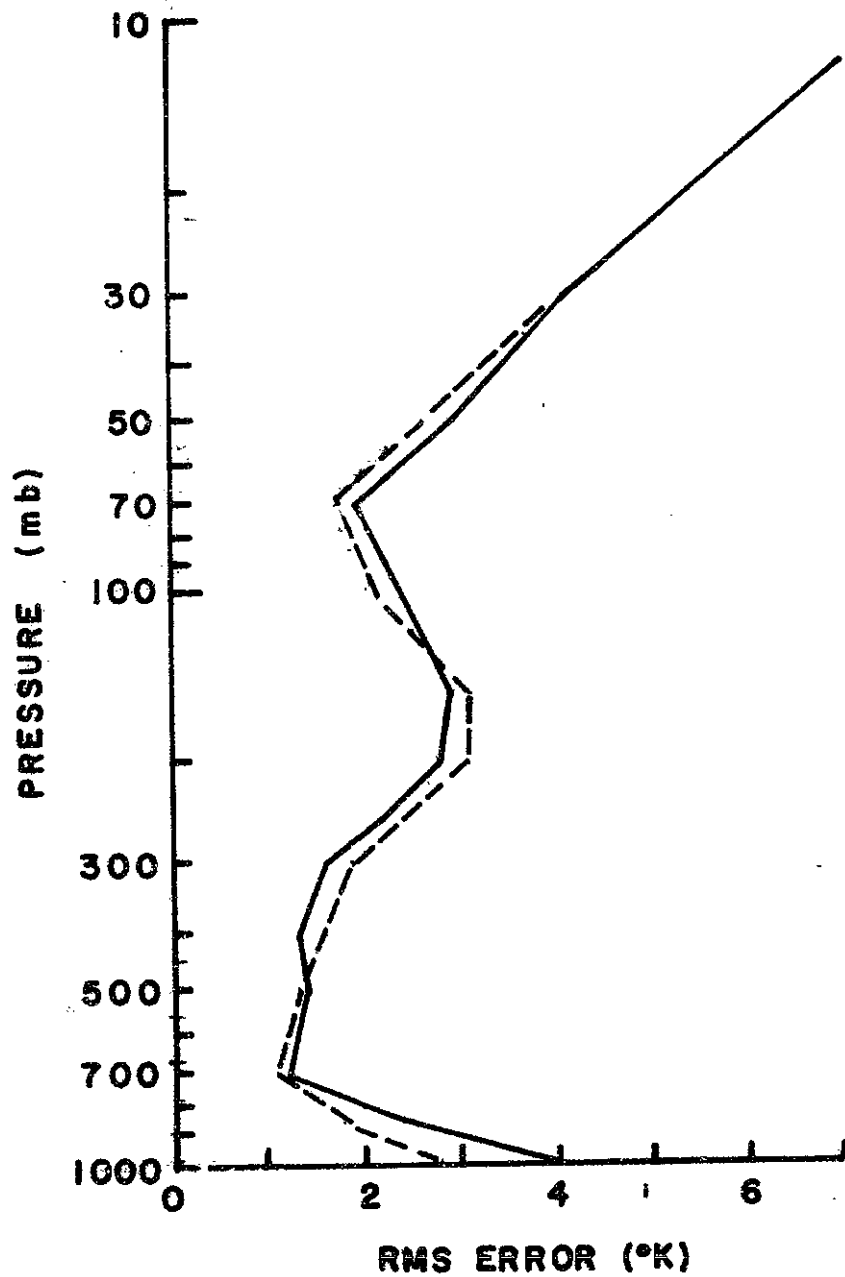


Figure 8
Causal versus Non-causal Filter Error Performance
October 22-25, 1975 (Three Spot Filter) (Solid
line - causal filter, dashed line - non-causal filter)

Table 40

One spot filter retrieval errors, Aug. 7-9, 1975

Non-causal filter

Pressure (mb)	Scan angle 0		Scan angle 3		Scan angle 6	
	Mean Error (K)	RMS Error (K)	Mean Error (K)	RMS Error (K)	Mean Error (K)	RMS Error (K)
1000	-0.1	2.9	-0.1	2.9	0.7	2.3
850	0.5	1.9	0.4	1.8	0.9	1.5
700	0.4	1.2	0.3	1.0	0.5	0.9
500	0.3	0.9	0.1	1.1	0.0	1.4
400	-0.3	0.9	-0.3	0.9	-0.3	1.1
300	-0.2	1.5	-0.2	1.2	-0.1	1.2
250	0.6	2.2	0.6	1.9	0.6	1.9
200	0.9	2.1	0.7	2.2	0.6	2.0
150	0.5	2.6	0.2	2.0	0.1	2.3
100	1.3	1.7	1.4	1.9	1.7	2.2
70	-1.1	0.7	-1.1	1.1	-1.0	1.4
50	-1.2	0.8	-1.5	0.9	-1.6	1.2
30	-0.9	1.1	-1.2	0.8	-1.4	1.1
10	-0.1	2.0	-0.3	1.4	-0.5	1.4

Table 41

One spot filter retrieval error, Oct. 22-25, 1975

Non-causal filter

Pressure (mb)	Scan angle 0		Scan angle 3		Scan angle 6	
	Mean Error (K)	RMS Error (K)	Mean Error (K)	RMS Error (K)	Mean Error (K)	RMS Error (K)
1000	4.7	2.9	5.3	2.9	3.0	3.1
850	1.2	1.8	1.4	1.8	0.9	1.9
700	0.2	1.1	0.3	1.0	0.7	1.2
500	0.4	1.3	0.2	1.3	0.2	1.3
400	1.3	1.4	0.9	1.4	0.4	1.5
300	1.5	1.9	1.0	2.1	0.1	1.9
250	0.4	3.1	0.1	3.3	-0.5	2.4
200	-2.3	3.1	-2.1	2.7	-1.3	2.4
150	-4.1	2.1	-4.0	1.8	-1.9	1.9
100	1.6	1.6	1.3	1.8	2.1	1.7
70	0.4	2.4	0.4	2.7	-1.3	2.8
50	1.0	3.7	1.2	3.6	-1.6	3.8
30	2.9	5.3	3.2	5.0	-1.4	4.5
10	8.7	8.3	9.0	7.7	0.4	6.4

Table 42

One spot filter retrieval errors, Jan 24-25, 1976

Non-causal filter

Pressure (mb)	Scan angle 0		Scan angle 3		Scan angle 6	
	Mean Error (K)	RMS Error (K)	Mean Error (K)	RMS Error (K)	Mean Error (K)	RMS Error (K)
1000	2.2	6.4	1.5	5.7	1.6	5.2
850	1.0	2.7	1.8	3.1	2.2	3.2
700	0.9	1.0	1.6	1.9	1.9	1.9
500	0.1	1.4	0.2	1.5	0.1	1.2
400	1.1	1.6	0.7	2.2	0.6	2.0
300	1.0	2.4	0.0	3.0	-0.2	3.0
250	-0.5	3.3	-1.6	3.7	-1.8	3.7
200	-1.9	2.7	-2.6	2.7	-2.8	2.6
150	-1.6	1.6	-1.4	1.5	-1.3	1.4
100	2.1	1.5	3.1	2.7	3.3	2.6
70	0.7	1.9	1.5	3.1	1.6	3.3
50	1.3	1.3	2.3	2.5	1.8	3.0
30	0.3	2.2	0.6	3.2	0.0	3.4
10	-4.6	5.9	-4.2	5.8	-5.5	5.6

Table 43

Two spot filter retrieval errors, Aug. 7-9, 1975

Pressure (mb)	Non-causal filter (Extreme scan)				Non-causal filter (Close scan)			
	Scan angle 0		Scan angle 1		Scan angle 5		Scan angle 6	
	Mean Error (K)	RMS Error (K)	Mean Error (K)	RMS Error (K)	Mean Error (K)	RMS Error (K)	Mean Error (K)	RMS Error (K)
1000	-0.2	2.5	-0.1	3.0	0.3	2.6	0.6	2.2
850	0.4	1.6	0.4	2.0	0.6	1.7	0.8	1.5
700	0.4	1.0	0.3	1.2	0.4	1.0	0.5	0.9
500	0.3	1.0	0.1	0.9	0.1	1.2	0.0	1.3
400	-0.2	0.9	-0.5	0.7	-0.2	0.9	-0.3	1.0
300	-0.2	1.5	-0.3	1.1	-0.1	1.1	-0.1	1.2
250	0.6	2.1	0.5	1.7	0.7	1.8	0.6	1.9
200	0.8	2.0	1.0	2.3	0.6	2.0	0.5	2.0
150	0.4	2.6	0.3	1.9	0.1	2.2	0.0	2.3
100	1.2	1.8	1.5	1.4	1.5	2.0	1.7	2.1
70	-1.2	0.7	-0.9	1.0	-1.1	1.3	-1.0	1.3
50	-1.2	0.8	-1.2	0.9	-1.6	1.1	-1.5	1.1
30	-0.9	1.0	-0.9	1.0	-1.3	1.0	-1.3	1.0
10	-0.1	1.9	-0.1	1.8	-0.5	1.3	-0.4	1.3

Table 44

Two spot filter retrieval errors, Oct. 22-25, 1975

Pressure (mb)	Non-causal filter (Extreme scan)				Non-causal filter (Close scan)			
	Scan angle 0		Scan angle 1		Scan angle 5		Scan angle 6	
	Mean Error (K)	RMS Error (K)	Mean Error (K)	RMS Error (K)	Mean Error (K)	RMS Error (K)	Mean Error (K)	RMS Error (K)
1000	4.6	2.8	5.1	2.5	4.8	3.1	4.7	3.1
850	1.0	1.7	1.4	1.6	1.1	2.0	1.0	2.0
700	0.1	1.1	0.4	1.0	0.2	1.0	0.2	1.1
500	0.3	1.4	0.5	1.2	0.2	1.3	0.3	1.3
400	1.3	1.5	1.3	1.2	1.0	1.5	1.0	1.5
300	1.5	1.9	1.4	2.0	1.0	1.9	1.0	1.9
250	0.4	3.1	0.2	3.4	0.1	3.2	0.2	3.3
200	-2.3	3.1	-2.3	3.0	-2.0	2.6	-2.0	2.7
150	-4.1	2.1	-4.1	2.0	-3.8	1.8	-3.9	1.9
100	1.5	1.6	1.4	1.7	1.4	1.8	1.3	1.8
70	0.4	2.6	0.5	2.8	0.0	2.9	0.0	2.8
50	1.0	4.0	1.3	4.3	0.7	3.8	0.6	3.7
30	2.9	5.6	3.2	6.1	2.4	5.0	2.3	4.9
10	8.8	8.7	9.1	9.0	8.0	7.8	7.8	7.5

Table 45

Two spot filter retrieval errors, Jan. 24-25, 1976

Pressure (mb)	Non-causal filter (Extreme scan)				Non-causal filter (Close scan)			
	Scan angle 0		Scan angle 1		Scan angle 5		Scan angle 6	
	Mean Error (K)	RMS Error (K)	Mean Error (K)	RMS Error (K)	Mean Error (K)	RMS Error (K)	Mean Error (K)	RMS Error (K)
1000	2.1	6.0	2.1	6.1	1.5	4.8	1.7	4.9
850	0.9	2.2	1.5	2.6	2.0	2.9	2.3	2.9
700	0.9	0.8	1.4	1.2	1.8	1.9	1.9	1.8
500	0.2	1.5	0.2	1.4	0.2	1.3	0.0	1.2
400	1.1	1.4	0.9	1.7	0.7	1.8	0.4	1.7
300	1.0	2.4	0.5	2.5	-0.1	2.8	-0.4	2.9
250	-0.6	3.5	-1.0	3.5	-1.7	3.8	-2.0	3.8
200	-2.0	2.9	-2.2	2.8	-2.6	2.5	-2.9	2.5
150	-1.8	1.8	-1.5	1.6	-1.4	1.5	-1.3	1.5
100	2.0	1.6	2.6	1.9	3.3	2.7	3.5	2.7
70	0.7	2.0	1.1	2.1	1.5	3.4	1.8	3.3
50	1.4	1.4	1.8	1.7	2.0	3.0	2.3	2.8
30	0.5	2.3	0.5	2.8	0.3	3.5	0.6	3.2
10	-4.4	6.4	-4.3	6.6	-5.1	5.3	-4.8	5.4

Table 46

Three spot filter retrieval error, Aug. 7-9, 1975

Pressure (mb)	Non-causal filter (Extreme scan)					
	Scan angle 0		Scan angle 1		Scan angle 2	
	Mean Error (K)	RMS Error (K)	Mean Error (K)	RMS Error (K)	Mean Error (K)	RMS Error (K)
1000	-0.3	2.5	-0.2	2.8	0.0	2.7
850	0.4	1.6	0.4	1.9	0.5	1.8
700	0.4	1.0	0.3	1.2	0.3	1.2
500	0.3	1.0	0.1	0.9	0.0	1.0
400	-0.2	1.0	-0.4	0.6	-0.6	0.7
300	-0.1	1.5	-0.3	1.1	-0.5	1.1
250	0.6	2.1	0.5	1.6	0.2	1.7
200	0.8	2.1	0.9	2.3	0.6	2.4
150	0.3	2.6	0.3	1.9	0.2	1.7
100	1.2	1.8	1.5	1.4	1.6	1.6
70	-1.3	0.7	-1.0	1.0	-0.9	1.0
50	-1.3	0.9	-1.2	0.9	-1.2	0.8
30	-1.0	1.1	-0.9	1.0	-0.9	0.8
10	-0.1	1.9	-0.1	1.8	-0.1	1.6

Table 47

Three spot filter retrieval error, Aug. 7-9, 1975

Non-causal filter
(Close scan)

Pressure (mb)	Scan angle 5		Scan angle 6		Scan angle 7	
	Mean Error (K)	RMS Error (K)	Mean Error (K)	RMS Error (K)	Mean Error (K)	RMS Error (K)
1000	0.3	2.6	0.5	2.3	0.8	2.1
850	0.6	1.7	0.8	1.5	1.0	1.4
700	0.4	1.0	0.5	1.0	0.5	0.9
500	0.1	1.2	0.0	1.2	0.0	1.2
400	-0.2	0.9	-0.2	0.9	-0.3	1.0
300	0.0	1.0	-0.1	1.1	-0.1	1.2
250	0.7	1.8	0.7	1.8	0.7	2.0
200	0.6	2.0	0.5	2.0	0.5	2.2
150	0.1	2.2	0.0	2.2	0.1	2.3
100	1.4	2.0	1.6	2.0	1.7	2.0
70	-1.2	1.4	-1.1	1.3	-1.0	1.3
50	-1.6	1.2	-1.6	1.1	-1.5	1.1
30	-1.4	1.0	-1.4	1.0	-1.3	1.0
10	-0.5	1.3	-0.4	1.3	-0.4	1.3

Table 48

Three spot filter retrieval error, Oct. 22-25, 1975

Non-causal filter
(Extreme scan)

Pressure (mb)	Scan angle 0		Scan angle 1		Scan angle 2	
	Mean Error (K)	RMS Error (K)	Mean Error (K)	RMS Error (K)	Mean Error (K)	RMS Error (K)
1000	4.5	2.8	4.9	2.4	5.2	2.5
850	1.0	1.7	1.2	1.6	1.4	1.7
700	0.1	1.1	0.3	1.0	0.4	1.0
500	0.4	1.4	0.5	1.2	0.4	1.2
400	1.3	1.6	1.3	1.2	1.2	1.2
300	1.6	1.9	1.4	2.0	1.3	2.2
250	0.4	3.1	0.2	3.4	0.2	3.5
200	-2.3	3.1	-2.3	3.1	-2.1	3.0
150	-4.2	2.1	-4.2	2.0	-4.0	1.9
100	1.5	1.7	1.4	1.7	1.3	1.7
70	0.3	2.6	0.4	2.8	0.4	3.1
50	1.0	4.0	1.2	4.3	1.2	4.5
30	3.0	5.7	3.2	6.1	3.2	6.3
10	8.8	8.8	9.1	9.0	9.1	9.1

Table 49

Three spot filter retrieval error, Oct. 22-25, 1975

Non-causal filter
(Close scan)

Pressure (mb)	Scan angle 5		Scan angle 6		Scan angle 7	
	Mean Error (K)	RMS Error (K)	Mean Error (K)	RMS Error (K)	Mean Error (K)	RMS Error (K)
1000	4.6	3.1	4.5	3.1	4.3	3.1
850	1.0	2.0	0.9	2.1	5.8	2.0
700	0.2	1.0	0.2	1.1	0.1	1.1
500	0.3	1.3	0.3	1.3	0.2	1.2
400	1.1	1.4	1.1	1.4	1.1	1.4
300	1.1	1.8	1.1	1.9	1.2	2.0
250	0.2	3.2	0.2	3.3	0.5	3.2
200	-2.0	2.6	-2.0	2.7	-1.9	2.6
150	-3.9	1.8	-4.0	1.8	-4.1	1.8
100	1.3	1.9	1.2	1.8	1.1	1.7
70	0.0	3.0	-0.1	3.0	-0.3	3.0
50	0.6	4.0	0.5	4.0	0.4	4.0
30	2.4	5.2	2.2	5.2	2.0	5.1
10	7.9	8.0	7.6	7.7	7.4	7.4

Table 50

Three spot filter retrieval error, Jan. 24-25, 1976

Non-causal filter
(Extreme scan)

Pressure (mb)	Scan angle 0		Scan angle 1		Scan angle 2	
	Mean Error (K)	RMS Error (K)	Mean Error (K)	RMS Error (K)	Mean Error (K)	RMS Error (K)
1000	2.2	6.1	2.3	6.0	1.9	5.5
850	0.9	2.2	1.7	2.4	1.7	2.5
700	0.9	0.9	1.5	1.1	1.6	1.4
500	0.1	1.5	0.2	1.3	0.2	1.4
400	1.1	1.4	0.9	1.5	0.8	1.8
300	1.0	2.4	0.4	2.4	0.1	2.5
250	-0.6	3.6	-1.0	3.5	-1.4	3.4
200	-2.0	2.9	-2.3	2.8	-2.4	2.7
150	-1.8	1.8	-1.5	1.7	-1.5	1.7
100	2.0	1.6	2.6	2.0	2.8	2.2
70	0.7	2.1	1.1	2.2	1.3	2.4
50	1.4	1.4	1.7	1.7	1.9	1.9
30	0.5	2.4	0.4	2.7	0.3	3.1
10	-4.4	6.3	-4.4	6.5	-4.5	6.8

Table 51

Three spot filter retrieval error, Jan. 24-25, 1976

Non-causal filter
(Close scan)

Pressure (mb)	Scan angle 5		Scan angle 6		Scan angle 7	
	Mean Error (K)	RMS Error (K)	Mean Error (K)	RMS Error (K)	Mean Error (K)	RMS Error (K)
1000	1.5	4.8	1.9	4.7	2.1	5.2
850	2.0	2.9	2.3	2.8	2.5	3.0
700	1.7	1.9	1.9	1.8	1.9	1.7
500	0.1	1.3	0.0	1.1	-0.1	1.2
400	0.6	1.7	0.4	1.6	0.2	1.8
300	-0.1	2.9	-0.4	2.9	-0.6	3.0
250	-1.6	3.9	-1.9	3.9	-2.2	3.9
200	-2.5	2.5	-2.8	2.5	-3.0	2.5
150	-1.3	1.5	-1.2	1.5	-1.1	1.5
100	3.3	2.8	3.5	2.7	3.8	2.7
70	1.5	3.4	1.7	3.2	1.9	3.1
50	1.9	3.1	2.1	2.9	2.2	2.8
30	0.1	3.6	0.4	3.3	0.4	3.2
10	-5.3	5.2	-5.1	5.3	-5.0	5.2

additional information brought into the filter by the "future" observations. Secondly, there is "noise averaging" in the observation matrices over ocean. For this surface, the observation matrices are a function of the predicted surface temperature. The observation matrix error produced by a descending orbit (one traversing a cold ocean to a warm ocean) help cancel those of an ascending orbit (one traversing a warm ocean to a cold one).

Section I. The precomputed sub-optimal filter experiment

The one great disadvantage of the Kalman filter is its computational burden. For the cases investigated in this chapter, the complexity of the algorithm is dominated by the cube of the number of temperatures estimated. For this reason, it is useful to consider ways in which this complexity may be reduced. One method is, of course, a reduction in the number of state variables. Studies made in the earlier stages of this thesis indicate that this is an ultimate possibility. The covariance matrix of a the temperature profile at a single spot and the plant noise contain eight eigenvectors having significant energy. The second method, and the one adopted for this thesis, was to

use the approach of operating a sub-optimal filter that used a nominal gain or error covariance history. For the case in which the nominal error covariance history is used, the entire process of error covariance propagation is eliminated. Further, since we may just as well precompute the square root of the covariance, the gain computation is simplified. The sub-optimal filter that uses precomputed gains is vastly more simple than the standard filter. In this case, the filter need only compute the innovations, update and propagate the state. The cost of this simplicity is that data reasonableness testing cannot be easily done since the gains have been computed off line and the error covariance matrix is not available.

An examination of the error covariance and gain history of the causal filter suggested that either or both of the precomputed sub-optimal filters might perform adequately. Examples of typical gain and error covariance histories of the causal filter are given in Figures 9 - 11. These figures depict the gain, error and covariance history of the 850 mb level of a single spot filter for two ascending orbits starting at 30 degrees latitude. These orbits were separated by about 100 degrees of longitude. In these cases, the filter has reached a steady state after a short period. After this point, the behaviour of the filter is dominated by the plant noise.

ALIGNMENT ON GRID LINE
NON-REPRODUCIBLE
10 5001
MILITARY

- 172 -

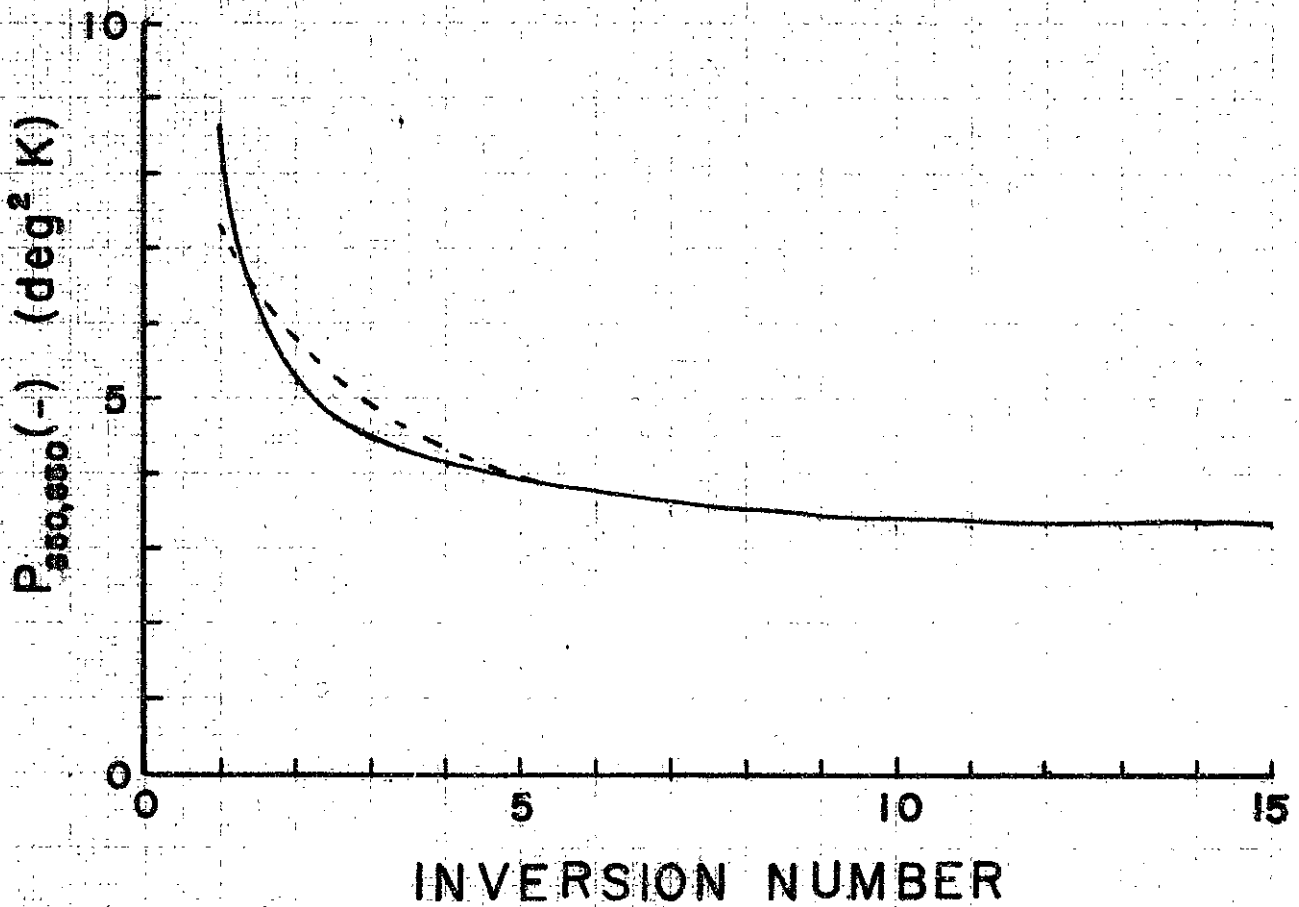


FIGURE 9
Typical 850 mb Error Covariance History - 30° Latitude

ARUPILL & EASER CO.
MADE IN U.S.A.

ALWAYS USE GUIDE LINE
NON-REPRODUCIBLE

10 9961
MILWAUKEE

- 173 -

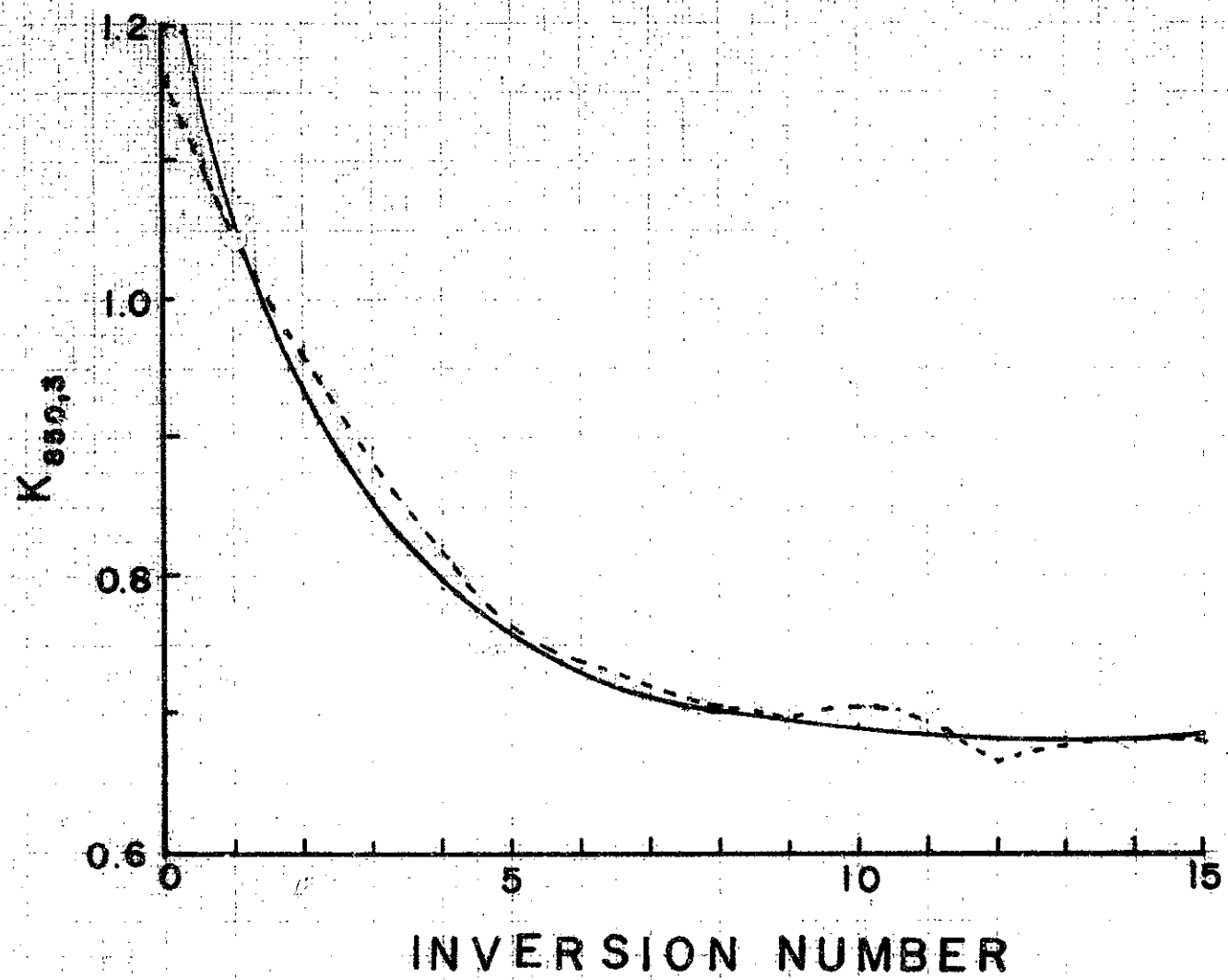


Figure 16
Typical 850 mb Rainfall Rate History - 30° Latitude

KELFELL & ESSER CO.
MILWAUKEE, WIS.

- 174 -

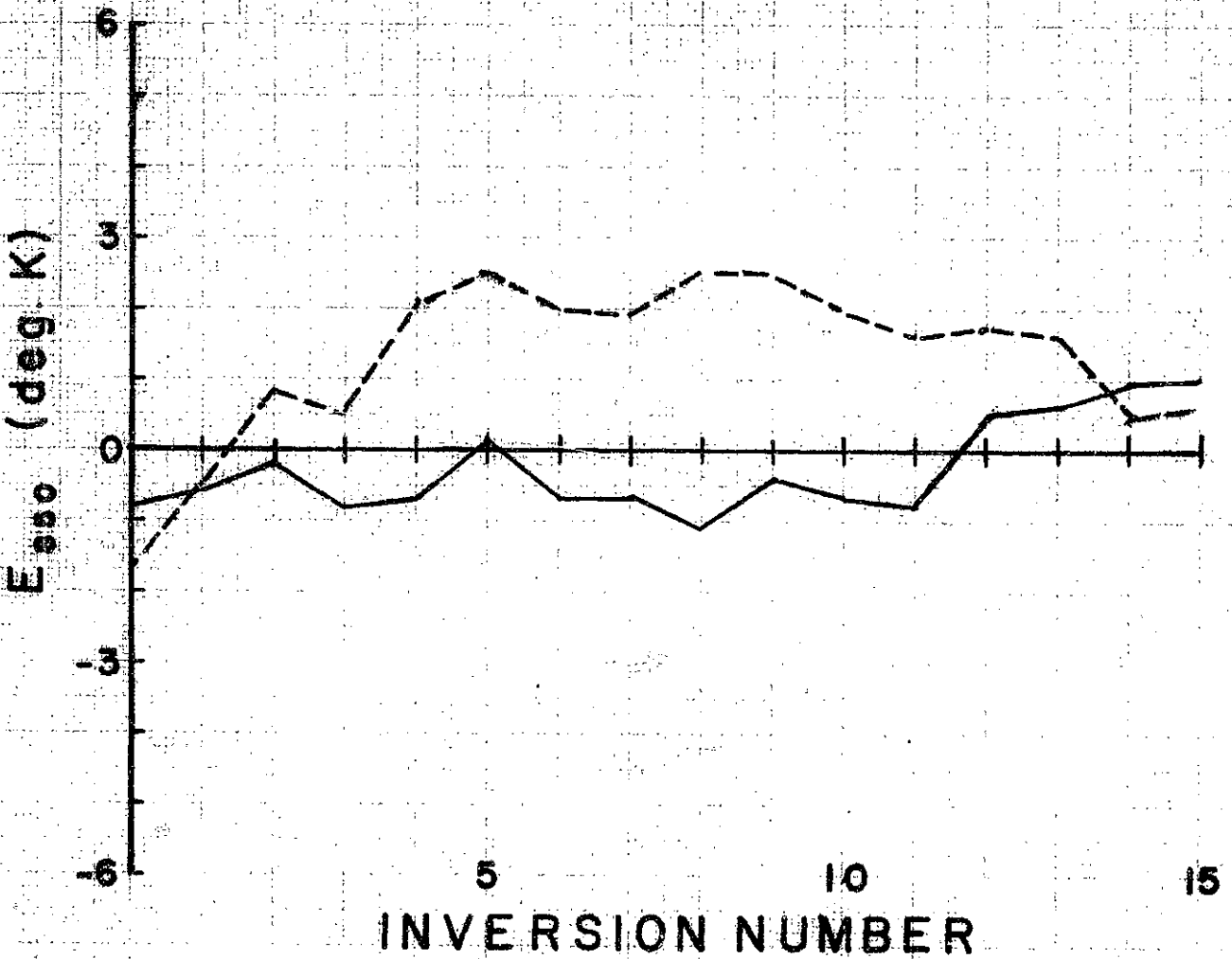


FIGURE 11
Typical 950 mμ BEER HISTORY - 30° LATITUDE

The experiment of this section thus consisted of running the full filter for a period of five frames and then switching to either a precomputed gain or precomputed covariance strategy. The precomputed gains and covariances that were used were obtained from the datasets in the non-causal experiment. The January matrices were used in December and February, one October dataset produced the data for the other and the August dataset was run on itself since this was the only dataset that used the summer plant matrices. In all cases, the matrices were averaged in 5 latitude bins.

The error performances of the two filters are given in Tables 52- 83. The comparative timings of the causal and precomputed matrix filters are given in Table 84. It is quite surprising that the performance of the precomputed gain filter seems to be better than that of the precomputed error covariance filter. In fact, the performance of the precomputed gain filter approaches that of the full causal filter. One possible explanation of this is the fact that the data used in this experiment is heavily weighted toward land areas. The filter is linear for such cases. A second possible explanation is that the ordering of the observation processing has reduced the non-linear aspects of the filtering process to the point where they are no longer important. Finally, there is the possibility that the

Table 52

One spot filter retrieval errors, Aug. 7-9, 1975

Precomputed error covariance

Pressure (mb)	Scan angle 0		Scan angle 3		Scan angle 6	
	Mean Error (K)	RMS Error (K)	Mean Error (K)	RMS Error (K)	Mean Error (K)	RMS Error (K)
1000	0.2	3.4	-0.1	3.1	0.7	2.5
850	0.8	2.4	0.4	2.1	0.9	1.7
700	0.6	1.6	0.4	1.3	0.5	1.2
500	0.4	1.1	0.2	1.2	0.0	1.5
400	-0.2	1.1	-0.2	1.0	-0.3	1.3
300	-0.3	1.7	-0.1	1.2	-0.1	1.4
250	0.3	2.2	0.5	1.9	0.6	1.9
200	0.5	2.2	0.4	2.3	0.4	2.1
150	0.2	2.6	0.0	2.0	-0.1	2.4
100	1.3	1.8	1.4	1.8	1.7	2.2
70	-0.9	0.9	-0.9	1.1	-0.8	1.4
50	-0.9	1.2	-1.2	1.1	-1.2	1.2
30	-0.6	1.3	-0.8	1.0	-1.0	1.1
10	0.3	1.8	0.1	1.4	-0.1	1.3

Table 53

One spot filter retrieval error, Aug. 7-9, 1975

Precomputed Kalman gain

Pressure (mb)	Scan angle 0		Scan angle 3		Scan angle 6	
	Mean Error (K)	RMS Error (K)	Mean Error (K)	RMS Error (K)	Mean Error (K)	RMS Error (K)
1000	0.2	3.4	-0.1	3.1	0.7	2.5
850	0.8	2.5	0.4	2.1	0.9	1.8
700	0.6	1.6	0.4	1.3	0.5	1.2
500	0.4	1.1	0.2	1.2	0.1	1.5
400	-0.2	1.1	-0.2	1.0	-0.3	1.3
300	-0.3	1.7	-0.1	1.2	-0.1	1.4
250	0.3	2.2	0.5	1.9	0.6	1.9
200	0.5	2.2	0.4	2.3	0.3	2.1
150	0.2	2.6	0.0	2.0	-0.1	2.4
100	1.3	1.8	1.5	1.9	1.7	2.2
70	-0.9	0.9	-0.9	1.1	-0.8	1.4
50	-0.8	1.2	-1.2	1.1	-1.2	1.2
30	-0.5	1.3	-0.8	1.0	-1.0	1.1
10	0.3	1.8	0.1	1.4	-0.1	1.3

Table 54

One spot filter retrieval error, Oct. 3-5, 1975

Precomputed error covariance

Pressure (mb)	Scan angle 0		Scan angle 3		Scan angle 6	
	Mean error (K)	RMS Error (K)	Mean Error (K)	RMS Error (K)	Mean Error (K)	RMS Error (K)
1000	2.5	3.8	2.4	3.3	2.8	2.6
850	1.6	2.3	1.4	2.1	1.8	1.8
700	0.4	1.3	0.3	1.1	0.5	1.3
500	-0.3	1.4	-0.7	1.2	-0.7	1.4
400	0.1	1.4	-0.3	1.4	-0.3	1.6
300	0.9	1.8	0.4	2.0	0.4	2.4
250	1.5	2.3	0.4	2.7	-0.2	3.0
200	-1.2	2.8	-1.8	3.5	-2.0	3.9
150	-2.8	3.0	-2.1	2.9	-2.4	2.9
100	0.8	2.5	1.6	2.9	1.3	2.8
70	0.7	2.0	1.1	2.8	0.8	3.5
50	1.2	2.9	1.5	4.0	1.5	4.8
30	2.7	4.2	2.7	5.1	2.6	6.1
10	7.5	5.6	7.4	6.1	7.0	7.1

Table 55

One spot rilter retrieval error, Oct. 3-5, 1975

Precomputed Kalman gain

Pressure (mb)	Scan angle 0		Scan angle 3		Scan angle 6	
	Mean Error (K)	RMS Error (K)	Mean error (K)	RMS Error (K)	Mean Error (K)	RMS Error (K)
1000	2.6	3.8	2.4	3.3	3.0	3.0
850	1.6	2.3	1.4	2.1	1.9	2.1
700	0.5	1.3	0.3	1.2	0.6	1.5
500	-0.3	1.4	-0.7	1.2	-0.6	1.6
400	0.1	1.3	-0.4	1.4	-0.2	1.8
300	0.9	1.8	0.4	2.0	0.5	2.7
250	1.5	2.3	0.4	2.7	-0.1	3.2
200	-1.2	2.7	-1.8	3.5	-1.8	4.1
150	-2.9	3.0	-2.1	2.9	-2.2	3.0
100	0.8	2.5	1.6	2.9	1.4	2.8
70	0.7	2.1	1.1	2.8	0.9	3.5
50	1.3	3.0	1.6	4.0	1.5	4.8
30	2.8	4.1	2.8	5.0	2.5	6.1
10	7.6	5.5	7.4	6.0	6.8	7.2

Table 56

One spot filter retrieval error, Dec. 5-8, 1975

Precomputed error covariance

Pressure (mb)	Scan angle 0		Scan angle 3		Scan angle 6	
	Mean Error (K)	RMS Error (K)	Mean Error (K)	RMS Error (K)	Mean Error (K)	RMS Error (K)
1000	3.2	3.7	4.1	3.8	3.4	3.9
850	1.8	2.1	2.4	2.3	2.0	2.7
700	1.4	1.6	1.7	1.4	1.5	1.8
500	0.0	1.5	-0.2	1.4	-0.3	1.4
400	0.4	1.3	-0.4	1.6	-0.4	1.9
300	0.0	2.5	-1.1	3.0	-1.4	3.7
250	-0.7	3.0	-1.9	3.4	-2.1	3.8
200	-1.1	3.2	-2.0	3.3	-1.9	3.4
150	-1.4	2.0	-1.5	1.8	-1.3	1.6
100	1.9	2.0	2.6	2.1	2.9	2.5
70	-0.2	2.4	0.6	3.8	0.7	4.7
50	-0.4	3.0	1.4	4.8	1.7	6.1
30	-0.1	3.9	2.5	5.7	2.7	6.9
10	0.2	6.6	4.4	8.0	4.8	9.6

Table 57

One spot filter retrieval error, Dec. 5-8, 1975

Precomputed Kalman gain

Pressure (mb)	Scan angle 0		Scan angle 3		Scan angle 6	
	Mean Error (K)	RMS Error (K)	Mean Error (K)	RMS Error (K)	Mean Error (K)	RMS Error (K)
1000	5.3	3.7	4.2	3.8	3.4	4.0
850	1.8	2.1	2.5	2.3	2.0	2.7
700	1.4	1.6	1.8	1.4	1.6	1.8
500	0.0	1.5	-0.2	1.4	-0.2	1.4
400	0.4	1.3	-0.4	1.6	-0.4	1.9
300	0.0	2.5	-1.1	3.0	-1.4	3.7
250	-0.8	3.0	-1.9	3.4	-2.1	3.8
200	-1.1	3.2	-2.0	3.3	-1.9	3.4
150	-1.4	2.1	-1.5	1.8	-1.3	1.6
100	1.9	2.0	2.6	2.1	2.9	2.6
70	-0.2	2.4	0.6	3.8	0.7	4.8
50	-0.4	3.0	1.4	4.8	1.7	6.1
30	-0.1	3.9	2.4	5.7	2.6	6.9
10	0.2	6.5	4.4	8.0	4.8	9.6

Table 58

One spot retrieval error, Feb. 3-6, 1976

Precomputed error covariance

Pressure (mb)	Scan angle 0		Scan angle 3		Scan angle 6	
	Mean Error (K)	RMS Error (K)	Mean Error (K)	RMS Error (K)	Mean Error (K)	RMS Error (K)
1000	0.3	3.9	0.3	4.3	-0.5	4.9
850	0.5	2.3	1.0	2.7	0.4	2.9
700	1.0	1.7	1.2	1.8	0.9	1.9
500	0.2	1.4	-0.1	1.5	-0.2	1.6
400	1.0	1.7	0.5	1.9	0.5	2.1
300	0.9	3.1	0.2	3.7	-0.1	3.8
250	-0.2	3.5	-0.4	4.3	-0.6	4.4
200	-1.7	2.8	-1.7	3.1	-1.6	3.1
150	-1.3	1.7	-1.1	1.5	-1.0	1.5
100	2.4	2.0	2.7	2.5	3.0	2.8
70	0.3	2.0	0.5	3.5	0.6	4.0
50	0.3	3.2	1.0	5.0	1.1	5.8
30	0.0	5.1	1.1	7.0	1.2	7.6
10	-1.8	10.7	0.0	12.4	0.2	13.0

Table 59

One spot filter retrieval error, Feb. 3-6, 1976

Precomputed Kalman gain

Pressure (mb)	Scan angle 0		Scan angle 3		Scan angle 6	
	Mean Error (K)	RMS Error (K)	Mean Error (K)	RMS Error (K)	Mean Error (K)	RMS Error (K)
1000	0.3	3.9	0.3	4.4	-0.5	4.9
850	0.6	2.3	1.0	2.7	0.4	2.9
700	1.0	1.7	1.2	1.8	1.0	1.9
500	0.2	1.4	0.0	1.5	-0.1	1.6
400	1.0	1.7	0.5	1.9	0.6	2.1
300	0.9	3.1	0.2	3.6	0.0	3.9
250	-0.2	3.5	-0.4	4.3	-0.6	4.3
200	-1.7	2.8	-1.8	3.1	-1.7	3.1
150	-1.3	1.7	-1.2	1.5	-1.1	1.5
100	2.4	2.1	2.7	2.5	3.0	2.8
70	0.3	2.0	0.5	3.5	0.6	4.0
50	0.3	3.2	1.1	5.0	1.1	5.7
30	0.1	5.2	1.1	7.0	1.3	7.6
10	-1.7	10.7	0.1	12.4	0.3	12.9

Table 60

Two spot filter retrieval error, Aug. 7-9, 1975

Pressure (mb)	Precomputed error covariance (Extreme scan)				Precomputed error covariance (Close scan)			
	Scan angle 0		Scan angle 1		Scan angle 5		Scan angle 6	
	Mean Error (K)	RMS Error (K)	Mean Error (K)	RMS Error (K)	Mean Error (K)	RMS Error (K)	Mean Error (K)	RMS Error (K)
1000	0.0	3.5	0.0	3.5	0.2	3.0	0.7	3.2
850	0.6	2.5	0.6	2.6	0.6	2.1	0.9	2.1
700	0.5	1.7	0.4	1.6	0.3	1.3	0.6	1.3
500	0.3	1.2	0.2	1.0	0.0	1.3	0.1	1.5
400	-0.3	1.1	-0.4	0.9	-0.2	1.0	-0.2	1.5
300	-0.2	1.5	-0.3	1.4	-0.1	1.2	-0.1	1.6
250	0.4	2.1	0.4	1.8	0.6	1.9	0.5	1.9
200	0.7	2.3	0.6	2.3	0.5	2.1	0.2	2.1
150	0.4	2.7	0.0	2.1	0.0	2.4	-0.3	2.3
100	1.4	1.9	1.5	1.5	1.6	2.1	1.6	2.3
70	-1.0	1.0	-0.8	1.3	-0.8	1.3	-0.9	1.7
50	-1.0	1.3	-0.9	1.3	-1.2	1.2	-1.3	1.4
30	-0.7	1.4	-0.6	1.3	-0.9	1.1	-1.0	1.2
10	0.1	1.8	0.2	1.8	0.0	1.4	-0.1	1.5

Table 61

Two spot filter retrieval error, Aug. 7-9, 1975

Pressure (mb)	Precomputed Kalman gain (Extreme scan)				Precomputed Kalman gain (Close scan)			
	Scan angle 0		Scan angle 1		Scan angle 5		Scan angle 6	
	Mean Error (K)	RMS Error (K)	Mean Error (K)	RMS Error (K)	Mean Error (K)	RMS Error (K)	Mean Error (K)	RMS Error (K)
1000	0.1	2.9	0.1	3.2	0.3	2.8	0.7	2.4
850	0.7	2.1	0.6	2.3	0.7	1.9	0.9	1.7
700	0.6	1.4	0.4	1.5	0.4	1.2	0.5	1.2
500	0.4	1.1	0.1	1.1	0.2	1.4	0.1	1.4
400	-0.2	1.0	-0.5	0.8	-0.2	1.2	-0.2	1.2
300	-0.2	1.6	-0.5	1.2	-0.1	1.3	-0.1	1.3
250	0.3	2.1	0.3	1.6	0.6	1.9	0.5	1.9
200	0.5	2.1	0.5	2.4	0.3	2.0	0.3	2.1
150	0.2	2.7	0.1	2.1	-0.1	2.3	-0.1	2.4
100	1.3	1.8	1.6	1.4	1.5	2.1	1.7	2.2
70	-1.0	1.0	-0.6	1.2	-0.9	1.4	-0.8	1.4
50	-0.9	1.3	-0.8	1.5	-1.2	1.2	-1.2	1.2
30	-0.6	1.4	-0.5	1.6	-0.9	1.1	-0.9	1.1
10	0.2	1.8	0.3	2.0	0.1	1.4	0.0	1.4

Table 62

Two spot filter retrieval error, Oct. 3-5, 1975

Pressure (mb)	Precomputed error covariance (Extreme scan)				Precomputed error covariance (Close scan)			
	Scan angle 0		Scan angle 1		Scan angle 5		Scan angle 6	
	Mean Error (K)	RMS Error (K)	Mean Error (K)	RMS Error (K)	Mean Error (K)	RMS Error (K)	Mean Error (K)	RMS Error (K)
1000	2.4	4.1	1.9	4.4	2.3	2.4	2.3	3.6
850	1.5	2.4	1.1	2.7	1.4	1.6	1.5	2.4
700	0.3	1.2	0.0	1.8	0.3	1.2	0.6	1.4
500	-0.4	1.4	-0.7	2.0	-0.8	1.3	-0.4	1.6
400	0.1	1.4	0.0	1.7	-0.4	1.5	0.2	1.9
300	0.9	1.7	1.2	1.8	0.3	2.2	0.9	2.6
250	1.5	2.1	2.0	2.6	0.0	2.9	0.3	3.3
200	-1.2	2.9	-0.8	3.4	-1.9	3.9	-1.6	4.0
150	-2.9	3.2	-2.0	3.6	-2.3	3.0	-2.3	3.3
100	0.7	2.6	1.4	2.5	1.4	2.9	1.1	2.9
70	0.7	2.0	0.4	2.5	0.9	3.5	0.2	4.3
50	1.3	3.1	0.2	4.9	1.5	5.0	0.6	6.6
30	2.8	4.5	0.9	7.3	2.5	6.5	1.6	8.9
10	7.6	6.0	5.3	9.2	6.9	7.4	6.1	10.5

Table 63

Two spot filter retrieval errors, Oct. 3-5, 1975

Pressure (mb)	Precomputed Kalman gain (Extreme scan)				Precomputed Kalman gain (Close scan)			
	Scan angle 0		Scan angle 1		Scan angle 5		Scan angle 6	
	Mean Error (K)	RMS Error (K)	Mean Error (K)	RMS Error (K)	Mean Error (K)	RMS Error (K)	Mean Error (K)	RMS Error (K)
1000	2.4	3.9	2.3	3.3	2.3	2.6	2.8	3.0
850	1.5	2.3	1.4	2.0	1.4	1.8	1.8	2.2
700	0.4	1.2	0.3	1.2	0.4	1.2	0.6	1.5
500	-0.3	1.4	-0.6	1.4	-0.6	1.2	-0.5	1.6
400	0.1	1.3	0.0	1.4	-0.2	1.4	0.0	1.8
300	1.0	1.7	0.9	1.7	0.5	2.2	0.7	2.7
250	1.6	2.2	1.4	2.2	0.1	3.0	0.2	3.5
200	-1.2	2.8	-1.4	2.4	-1.8	4.0	-1.6	4.4
150	-2.9	2.9	-2.5	2.8	-2.3	2.9	-2.2	3.0
100	0.7	2.4	1.2	2.5	1.3	2.9	1.3	2.8
70	0.7	1.9	0.8	2.0	0.8	3.7	0.6	3.7
50	1.3	2.9	1.2	3.1	1.3	5.1	1.1	5.1
30	2.8	4.2	2.6	4.3	2.2	6.5	2.0	6.5
10	7.6	5.6	7.3	5.7	6.6	7.4	6.2	7.6

Table 64

Two spot filter retrieval error, Dec. 5-8, 1975

Pressure (mb)	Precomputed error covariance (Extreme scan)				Precomputed error covariance (Close scan)			
	Scan angle 0		Scan angle 1		Scan angle 5		Scan angle 6	
	Mean Error (K)	RMS Error (K)	Mean Error (K)	RMS Error (K)	Mean Error (K)	RMS Error (K)	Mean Error (K)	RMS Error (K)
1000	2.7	3.8	3.3	4.2	3.3	3.7	3.0	5.2
850	1.3	2.4	1.7	2.3	1.8	2.5	1.4	3.7
700	0.9	1.9	1.2	1.7	1.3	1.8	1.1	2.0
500	-0.3	1.5	-0.1	1.7	-0.6	1.5	-0.3	1.8
400	0.4	1.3	0.4	1.5	-0.6	1.7	0.2	2.5
300	0.2	2.6	0.0	2.6	-1.4	3.5	-0.3	4.4
250	-0.5	3.2	-0.9	3.8	-1.8	3.7	-0.7	4.7
200	-0.8	3.4	-1.3	4.4	-1.6	3.6	-0.8	4.3
150	-1.2	2.2	-1.6	3.1	-1.0	1.7	-0.8	2.3
100	1.9	2.0	1.6	2.2	3.1	2.4	2.3	3.4
70	-0.4	2.5	-0.3	3.6	0.7	4.7	-1.0	5.7
50	-0.8	3.5	0.1	6.0	1.3	6.1	-0.8	7.9
30	-0.7	4.6	1.1	8.4	2.0	7.2	0.0	9.7
10	-0.6	7.2	2.3	11.0	3.9	9.9	2.3	12.0

Table 65

Two spot filter retrieval error, Dec. 5-8, 1975

Pressure (mb)	Precomputed Kalman gain (Extreme scan)				Precomputed Kalman gain (Close scan)			
	Scan angle 0		Scan angle 1		Scan angle 5		Scan angle 6	
	Mean Error (K)	RMS Error (K)	Mean Error (K)	RMS Error (K)	Mean Error (K)	RMS Error (K)	Mean Error (K)	RMS Error (K)
1000	3.5	3.6	3.2	3.8	3.7	4.3	3.6	4.0
850	2.0	2.0	1.8	2.1	2.2	2.9	2.2	2.7
700	1.5	1.5	1.3	1.4	1.7	1.7	1.7	1.7
500	0.1	1.3	-0.1	1.4	-0.2	1.2	-0.2	1.2
400	0.4	1.1	0.2	1.3	-0.4	1.7	-0.5	1.8
300	-0.1	2.5	-0.3	2.3	-1.4	3.6	-1.6	3.7
250	-0.9	3.0	-1.0	2.9	-2.1	3.9	-2.3	3.9
200	-1.2	3.2	-1.2	3.2	-2.0	3.6	-2.1	3.6
150	-1.5	2.0	-1.4	2.0	-1.3	1.7	-1.4	1.7
100	1.9	2.1	1.9	2.0	3.0	2.5	3.0	2.6
70	-0.1	2.6	-0.2	2.6	0.9	4.8	0.9	4.9
50	-0.3	3.3	-0.2	3.4	1.8	6.2	2.0	6.4
30	0.1	4.3	0.2	4.5	2.8	7.1	3.1	7.3
10	0.4	7.0	1.1	6.8	5.0	9.7	5.2	10.0

Table 66

Two spot filter retrieval error, Feb. 3-6, 1976

Pressure (mb)	Precomputed error covariance (Extreme scan)				Precomputed error covariance (Close scan)			
	Scan angle 0		Scan angle 1		Scan angle 5		Scan angle 6	
	Mean Error (K)	RMS Error (K)	Mean Error (K)	RMS Error (K)	Mean Error (K)	RMS Error (K)	Mean Error (K)	RMS Error (K)
1000	0.4	4.0	0.7	4.8	-0.2	4.4	-0.6	6.5
850	0.6	2.4	1.2	2.7	0.5	2.7	0.1	4.2
700	1.0	1.9	1.3	2.0	0.9	1.9	0.5	2.8
500	0.2	1.6	0.1	1.8	-0.2	1.5	-0.5	2.1
400	1.1	1.7	0.5	1.7	0.5	2.0	0.4	2.7
300	1.0	3.1	0.1	3.2	0.0	3.8	0.1	5.0
250	-0.2	3.7	-0.7	4.3	-0.5	4.4	-0.2	6.0
200	-1.7	3.0	-2.0	3.7	-1.7	3.1	-1.1	4.9
150	-1.4	1.8	-1.3	2.8	-1.0	1.5	-0.6	3.0
100	2.3	2.0	2.6	2.4	2.8	2.7	3.0	3.2
70	0.2	2.1	0.7	2.8	0.5	4.0	0.2	5.6
50	0.3	3.4	0.9	5.3	1.0	5.7	0.2	9.2
30	0.2	5.3	0.6	8.7	1.1	7.7	0.0	13.1
10	-1.6	10.9	-1.0	13.8	0.2	12.8	-1.2	17.9

Table 67

Two spot filter retrieval error, Feb. 3-6

Pressure (mb)	Precomputed Kalman gain (Extreme scan)				Precomputed Kalman gain (Close scan)			
	Scan angle 0		Scan angle 1		Scan angle 5		Scan angle 6	
	Mean Error (K)	RMS Error (K)	Mean Error (K)	RMS Error (K)	Mean Error (K)	RMS Error (K)	Mean Error (K)	RMS Error (K)
1000	0.6	4.1	0.3	4.3	0.0	4.9	-0.2	5.1
850	0.8	2.3	0.8	2.2	0.7	2.9	0.6	3.0
700	1.1	1.6	1.1	1.5	1.1	1.9	1.0	1.9
500	0.2	1.5	0.1	1.4	-0.2	1.5	-0.3	1.5
400	0.9	1.6	0.8	1.6	0.4	2.0	0.3	2.0
300	0.8	2.9	0.5	2.9	-0.2	3.8	-0.3	3.9
250	-0.4	3.5	-0.3	3.4	-0.8	4.4	-0.8	4.5
200	-1.8	2.8	-1.7	2.6	-1.9	3.2	-1.8	3.3
150	-1.4	1.7	-1.3	1.5	-1.1	1.5	-1.1	1.5
100	2.3	2.1	2.5	2.0	3.0	2.8	3.1	2.7
70	0.3	2.0	0.4	2.2	0.9	4.0	0.8	4.2
50	0.4	3.3	0.6	3.4	1.6	5.7	1.4	6.1
30	0.3	5.2	0.4	5.2	1.9	7.6	1.6	8.2
10	-1.5	10.8	-1.2	10.5	1.2	12.8	0.7	13.4

Table 68

Three spot filter retrieval error, Aug. 7-9, 1975

Precomputed error covariance
(Extreme scan)

Pressure (mb)	Scan angle 0		Scan angle 1		Scan angle 2	
	Mean Error (K)	RMS Error (K)	Mean Error (K)	RMS Error (K)	Mean Error (K)	RMS Error (K)
1000	-0.1	3.5	-0.1	3.3	-0.1	3.3
850	0.5	2.5	0.5	2.5	0.5	2.3
700	0.5	1.7	0.3	1.6	0.4	1.5
500	0.4	1.2	0.2	1.1	0.1	1.1
400	-0.2	1.1	-0.4	0.9	-0.4	1.1
300	-0.2	1.6	-0.3	1.4	-0.4	1.5
250	0.4	2.1	0.4	1.9	0.2	1.9
200	0.6	2.3	0.6	2.3	0.3	2.4
150	0.3	2.7	-0.1	2.0	-0.1	1.9
100	1.4	1.9	1.4	1.5	1.5	1.8
70	-1.0	0.9	-0.8	1.3	-0.8	1.3
50	-0.9	1.3	-0.9	1.3	-1.0	1.3
30	-0.7	1.4	-0.6	1.3	-0.6	1.2
10	0.2	1.8	0.2	1.8	0.3	1.7

Table 69

Three spot filter retrieval error, Aug. 7-9, 1975

Precomputed error covariance
(Close scan)

Pressure (mb)	Scan angle 5		Scan angle 6		Scan angle 7	
	Mean Error (K)	RMS Error (K)	Mean Error (K)	RMS Error (K)	Mean Error (K)	RMS Error (K)
1000	0.0	2.9	-0.1	2.9	0.1	2.9
850	0.7	2.0	0.5	2.1	0.6	2.0
700	0.6	1.4	0.4	1.4	0.4	1.4
500	0.5	1.1	0.2	1.1	0.0	1.2
400	-0.1	1.1	-0.4	0.8	-0.6	0.8
300	-0.2	1.6	-0.4	1.2	-0.6	1.2
250	0.3	2.1	0.3	1.6	0.0	1.7
200	0.4	2.1	0.5	2.3	0.3	2.5
150	0.1	2.7	0.0	2.0	0.0	1.9
100	1.2	1.8	1.5	1.4	1.7	1.6
70	-1.0	1.0	-0.7	1.2	-0.6	1.2
50	-1.0	1.3	-0.8	1.5	-0.8	1.4
30	-0.6	1.4	-0.5	1.6	-0.4	1.4
10	0.2	1.8	0.4	2.0	0.4	1.9

Table 70

Three spot filter retrieval error, Aug. 7-9, 1975

Precomputed Kalman gain
(Extreme scan)

Pressure (mb)	Scan angle 0		Scan angle 1		Scan angle 2	
	Mean Error (K)	RMS Error (K)	Mean Error (K)	RMS Error (K)	Mean Error (K)	RMS Error (K)
1000	0.0	2.9	-0.1	2.9	0.1	2.9
850	0.7	2.0	0.5	2.1	0.6	2.0
700	0.6	1.4	0.4	1.4	0.4	1.4
500	0.5	1.1	0.2	1.1	0.0	1.2
400	-0.1	1.1	-0.4	0.8	-0.6	0.8
300	-0.2	1.6	-0.4	1.2	-0.6	1.2
250	0.3	2.1	0.3	1.6	0.0	1.7
200	0.4	2.1	0.5	2.3	0.3	2.5
150	0.1	2.7	0.0	2.0	0.0	1.9
100	1.2	1.8	1.5	1.4	1.7	1.6
70	-1.0	1.0	-0.7	1.2	-0.6	1.2
50	-1.0	1.3	-0.8	1.5	-0.8	1.4
30	-0.6	1.4	-0.5	1.6	-0.4	1.4
10	0.2	1.8	0.4	2.0	0.4	1.9

Table 71

Three spot filter retrieval error, Aug. 7-9, 1975

Precomputed Kalman gain
(Close scan)

Pressure (mb)	Scan angle 5		Scan angle 6		Scan angle 7	
	Mean Error (K)	RMS Error (K)	Mean Error (K)	RMS Error (K)	Mean Error (K)	RMS Error (K)
1000	0.3	2.8	0.5	2.5	0.8	2.4
850	0.6	1.9	0.8	1.7	0.9	1.6
700	0.5	1.2	0.5	1.2	0.5	1.2
500	0.2	1.3	0.1	1.4	0.0	1.4
400	-0.1	1.1	-0.2	1.2	-0.3	1.2
300	0.0	1.3	0.0	1.3	-0.1	1.4
250	0.7	1.9	0.6	1.9	0.6	2.0
200	0.4	2.0	0.3	2.1	0.3	2.2
150	-0.2	2.2	-0.2	2.3	-0.1	2.3
100	1.4	2.0	1.6	2.1	1.7	2.1
70	-1.0	1.4	-0.9	1.4	-0.8	1.3
50	-1.3	1.2	-1.3	1.2	-1.1	1.1
30	-1.0	1.0	-1.0	1.1	-0.9	1.0
10	-0.1	1.3	-0.1	1.3	0.0	1.3

Table 72

Three spot filter retrieval error, Oct. 3-5, 1975

Precomputed error covariance
(Extreme scan)

Pressure (mb)	Scan angle 0		Scan angle 1		Scan angle 2	
	Mean Error (K)	RMS Error (K)	Mean Error (K)	RMS Error (K)	Mean Error (K)	RMS Error (K)
1000	2.2	4.1	1.7	4.2	2.3	4.4
850	1.4	2.5	0.9	2.5	1.3	2.6
700	0.3	1.3	-0.1	1.7	0.1	1.6
500	-0.4	1.5	-0.7	2.0	-0.7	1.6
400	0.1	1.4	0.1	1.6	0.0	1.4
300	0.9	1.7	1.2	1.7	1.1	2.0
250	1.6	2.1	2.0	2.8	1.6	3.2
200	-1.2	2.9	-0.8	3.4	-1.0	4.1
150	-2.9	3.2	-2.1	3.6	-2.0	3.7
100	0.7	2.6	1.3	2.5	1.4	2.4
70	0.6	2.0	0.4	2.6	0.5	3.1
50	1.3	3.1	0.3	5.0	0.6	6.0
30	2.9	4.5	1.1	7.4	1.4	8.7
10	7.7	6.1	5.6	9.9	5.9	10.9

Table 73

Three spot filter retrieval error, Oct. 3-5, 1975

Precomputed error covariance
(Close scan)

Pressure (mb)	Scan angle 5		Scan angle 6		Scan angle 7	
	Mean Error (K)	RMS Error (K)	Mean Error (K)	RMS Error (K)	Mean Error (K)	RMS Error (K)
1000	2.2	2.3	1.9	3.8	1.7	3.5
850	1.3	1.5	1.1	2.5	0.9	2.4
700	0.3	1.2	0.3	1.4	0.1	1.6
500	-0.8	1.4	-0.5	1.5	-0.5	1.6
400	-0.3	1.5	0.3	1.8	0.5	1.8
300	0.4	2.2	1.2	2.6	1.5	2.8
250	0.0	2.9	0.8	3.3	1.0	3.5
200	-1.8	3.9	-1.2	4.2	-1.0	4.4
150	-2.2	3.0	-2.0	3.3	-1.9	3.4
100	1.4	2.9	1.0	3.0	0.7	2.6
70	0.9	3.5	-0.3	4.5	-1.1	4.4
50	1.5	5.0	-0.3	6.8	-1.3	7.2
30	2.5	6.5	0.1	9.0	-1.0	9.5
10	6.9	7.6	4.0	11.5	2.9	11.4

Table 74

Three spot retrieval error, Oct. 3-5, 1975

Precomputed Kalman gain
(Extreme scan)

Pressure (mb)	Scan angle 0		Scan angle 1		Scan angle 2	
	Mean Error (K)	RMS Error (K)	Mean Error (K)	RMS Error (K)	Mean Error (K)	RMS Error (K)
1000	2.2	4.0	2.2	3.5	2.2	3.4
850	1.4	2.4	1.3	2.0	1.2	2.1
700	0.4	1.2	0.3	1.1	0.2	1.1
500	-0.3	1.4	-0.5	1.2	-0.6	1.2
400	0.2	1.2	0.0	1.2	-0.1	1.4
300	1.0	1.6	0.9	1.6	0.8	1.9
250	1.6	2.2	1.4	2.2	1.2	2.3
200	-1.2	2.8	-1.5	2.5	-1.4	2.6
150	-3.0	2.9	-2.6	2.9	-2.2	2.8
100	0.7	2.4	1.2	2.4	1.5	2.4
70	0.6	1.9	0.8	1.9	0.9	1.9
50	1.3	2.9	1.3	3.0	1.3	3.1
30	2.8	4.1	2.6	4.2	2.6	4.3
10	7.6	5.6	7.4	5.6	7.3	5.6

Table 75

Three spot retrieval error, Oct. 3-5, 1975

Precomputed Kalman gain
(Close scan)

Pressure (mb)	Scan angle 5		Scan angle 6		Scan angle 7	
	Mean Error (K)	RMS Error (K)	Mean Error (K)	RMS Error (K)	Mean Error (K)	RMS Error (K)
1000	2.0	2.5	2.4	3.0	2.4	3.1
850	1.2	1.7	1.5	2.1	1.5	2.3
700	0.4	1.2	0.5	1.5	0.4	1.7
500	-0.5	1.1	-0.4	1.5	-0.5	1.6
400	0.0	1.4	0.2	1.7	0.2	1.8
300	0.7	2.1	1.0	2.7	0.9	2.7
250	0.2	2.9	0.4	3.5	0.2	3.5
200	-1.6	4.0	-1.5	4.5	-1.6	4.4
150	-2.4	2.8	-2.2	3.1	-2.1	3.2
100	1.2	2.9	1.2	2.8	1.2	2.7
70	0.6	3.7	0.4	3.7	0.2	3.5
50	1.1	5.2	0.8	5.1	0.5	5.0
30	2.0	6.5	1.7	6.5	1.2	6.3
10	6.4	7.5	5.9	7.7	5.3	7.6

Table 76

Three spot filter retrieval error, Dec. 5-8, 1975

Precomputed error covariance
(Extreme scan)

Pressure (mb)	Scan angle 0		Scan angle 1		Scan angle 2	
	Mean Error (K)	RMS Error (K)	Mean Error (K)	RMS Error (K)	Mean Error (K)	RMS Error (K)
1000	2.6	3.7	3.9	4.2	3.6	4.2
850	1.3	2.3	2.3	2.2	2.2	2.5
700	0.9	1.9	1.8	1.6	1.8	1.7
500	-0.3	1.6	0.3	1.7	0.2	1.6
400	0.3	1.2	0.4	1.4	0.2	1.3
300	0.1	2.6	-0.3	2.6	-0.7	3.1
250	-0.5	3.2	-1.4	3.9	-1.8	4.5
200	-0.9	3.4	-1.8	4.3	-2.2	4.9
150	-1.2	2.2	-2.0	3.0	-2.0	3.2
100	1.9	2.0	1.6	2.2	2.0	2.1
70	-0.3	2.5	0.1	3.6	0.4	4.5
50	-0.7	3.5	0.8	5.8	1.5	7.6
30	-0.5	4.5	1.9	8.4	2.9	10.5
10	-0.3	7.2	3.1	11.8	4.7	13.5

Table 77

Three spot filter retrieval error, Dec. 5-8, 1975

Precomputed error covariance
(Close scan)

Pressure (mb)	Scan angle 5		Scan angle 6		Scan angle 7	
	Mean Error (K)	RMS Error (K)	Mean Error (K)	RMS Error (K)	Mean Error (K)	RMS Error (K)
1000	3.3	3.7	4.2	5.7	3.1	5.3
850	1.8	2.6	2.6	3.8	1.9	3.7
700	1.2	1.8	2.0	2.0	1.6	2.0
500	-0.6	1.5	0.0	1.8	-0.1	1.5
400	-0.7	1.7	-0.2	2.4	0.0	2.2
300	-1.5	3.4	-1.1	4.1	-0.9	4.1
250	-2.0	3.5	-1.7	4.5	-1.4	4.8
200	-1.8	3.5	-1.6	4.2	-1.3	4.5
150	-1.0	1.6	-1.0	2.2	-1.0	2.2
100	3.3	2.4	2.9	3.1	2.6	3.2
70	1.0	4.5	0.2	5.5	-0.1	5.8
50	1.8	5.9	0.6	7.7	0.5	8.4
30	2.7	6.8	0.8	9.9	1.3	10.6
10	4.7	9.4	2.3	13.0	3.4	13.6

Table 78

Three spot filter retrieval error, Dec. 5-8, 1975

Precomputed Kalman gain
(Extreme scan)

Pressure (mb)	Scan angle 0		Scan angle 1		Scan angle 2	
	Mean Error (K)	RMS Error (K)	Mean Error (K)	RMS Error (K)	Mean Error (K)	RMS Error (K)
1000	3.5	3.5	3.5	3.6	3.8	3.6
850	2.0	1.9	2.0	1.9	2.1	1.9
700	1.5	1.5	1.5	1.3	1.5	1.2
500	0.1	1.3	0.0	1.2	-0.1	1.3
400	0.4	1.1	0.2	1.1	0.0	1.3
300	-0.1	2.5	-0.3	2.3	-0.5	2.4
250	-0.9	3.1	-1.0	2.9	-1.3	2.8
200	-1.3	3.2	-1.3	3.2	-1.5	3.0
150	-1.6	2.0	-1.5	2.0	-1.4	1.9
100	1.8	2.1	1.9	2.0	2.2	2.0
70	-0.1	2.7	-0.1	2.8	-0.1	2.9
50	-0.1	3.5	0.0	3.5	0.1	3.6
30	0.3	4.4	0.5	4.5	0.7	4.6
10	0.7	7.1	1.5	6.9	2.1	6.7

Table 79

Three spot filter retrieval error, Dec. 5-8, 1975

Precomputed Kalman gain
(Close scan)

Pressure (mb)	Scan angle 5		Scan angle 6		Scan angle 7	
	Mean Error (K)	RMS Error (K)	Mean Error (K)	RMS Error (K)	Mean Error (K)	RMS Error (K)
1000	3.5	4.4	3.6	4.2	3.7	4.0
850	2.1	3.0	2.2	2.9	2.3	2.8
700	1.6	1.7	1.8	1.8	1.9	1.8
500	-0.2	1.2	-0.1	1.1	-0.1	1.2
400	-0.3	1.7	-0.3	1.7	-0.3	1.7
300	-1.3	3.6	-1.4	3.7	-1.6	3.7
250	-2.0	3.9	-2.1	4.0	-2.3	4.0
200	-2.0	3.7	-2.0	3.7	-2.1	3.7
150	-1.3	1.8	-1.4	1.7	-1.3	1.7
100	2.9	2.5	2.9	2.7	2.9	2.9
70	0.7	4.8	0.8	5.0	1.0	5.2
50	1.6	6.3	1.8	6.5	2.2	6.7
30	2.5	7.3	2.7	7.5	3.3	7.6
10	4.6	9.9	4.9	10.2	5.6	10.6

Table 80

Three spot filter retrieval error, Feb. 3-6, 1976

Precomputed error covariance
(Extreme scan)

Pressure (mb)	Scan angle 0		Scan angle 1		Scan angle 2	
	Mean Error (K)	RMS Error (K)	Mean Error (K)	RMS Error (K)	Mean Error (K)	RMS Error (K)
1000	0.4	4.0	0.6	4.9	0.6	5.2
850	0.6	2.5	1.1	2.8	1.1	3.2
700	1.0	1.9	1.2	2.0	1.2	2.2
500	0.3	1.6	0.1	2.0	0.0	1.8
400	1.1	1.7	0.6	1.7	0.5	1.7
300	1.0	3.1	0.2	3.1	0.1	3.6
250	-0.2	3.7	-0.7	4.3	-0.6	4.9
200	-1.8	3.0	-2.1	3.9	-1.9	4.1
150	-1.5	1.8	-1.4	2.9	-1.2	2.8
100	2.2	2.0	2.5	2.3	2.7	2.4
70	0.2	2.1	0.7	2.8	0.6	3.7
50	0.4	3.4	1.1	5.6	0.9	6.5
30	0.3	5.4	1.0	8.9	0.7	9.7
10	-1.4	11.0	-0.5	14.2	-0.6	14.8

Table 81

Three spot filter retrieval error, Feb. 3-6, 1976

Precomputed error covariance
(Close scan)

Pressure (mb)	Scan angle 5		Scan angle 6		Scan angle 7	
	Mean Error (K)	RMS Error (K)	Mean Error (K)	RMS Error (K)	Mean Error (K)	RMS Error (K)
1000	-0.3	4.5	-0.1	6.8	0.0	6.8
850	0.5	2.8	0.5	4.5	0.5	4.3
700	0.9	2.0	0.8	2.8	0.7	2.7
500	-0.2	1.6	-0.5	2.2	-0.5	2.0
400	0.5	2.0	0.3	2.6	0.2	2.7
300	0.0	3.7	-0.2	4.8	-0.3	5.1
250	-0.6	4.4	-0.5	5.9	-0.7	6.0
200	-1.7	3.1	-1.4	4.8	-1.5	4.8
150	-1.1	1.5	-0.8	2.9	-0.7	2.7
100	2.8	2.8	3.1	3.1	3.3	2.9
70	0.6	4.0	0.5	5.5	0.7	5.6
50	1.1	5.8	0.8	9.1	0.9	9.2
30	1.3	7.7	0.7	12.8	0.9	12.8
10	0.4	12.7	-0.3	17.5	-0.4	17.8

Table 82

Three spot filter retrieval error, Feb. 3-6, 1976

Precomputed Kalman gain
(Extreme scan)

Pressure (mb)	Scan angle 0		Scan angle 1		Scan angle 2	
	Mean Error (K)	RMS Error (K)	Mean Error (K)	RMS Error (K)	Mean Error (K)	RMS Error (K)
1000	0.8	4.3	0.5	4.5	0.3	4.3
850	0.9	2.4	0.9	2.3	0.9	2.4
700	1.2	1.7	1.2	1.6	1.2	1.6
500	0.2	1.5	0.1	1.5	0.0	1.3
400	0.9	1.5	0.7	1.6	0.6	1.5
300	0.7	3.0	0.4	3.0	0.3	3.0
250	-0.4	3.5	-0.4	3.6	-0.4	3.6
200	-1.9	2.8	-1.8	2.7	-1.8	2.5
150	-1.5	1.8	-1.3	1.6	-1.2	1.4
100	2.3	2.1	2.5	2.1	2.6	2.1
70	0.3	2.1	0.5	2.2	0.4	2.5
50	0.5	3.3	0.7	3.3	0.8	3.8
30	0.5	5.3	0.5	5.2	0.7	5.6
10	-1.3	10.9	-1.0	10.7	-0.6	10.6

Table 83

Three spot filter retrieval error, Feb. 3-6, 1976

Precomputed Kalman gain
(Close scan)

Pressure (mb)	Scan angle 5		Scan angle 6		Scan angle 7	
	Mean Error (K)	RMS Error (K)	Mean Error (K)	RMS Error (K)	Mean Error (K)	RMS Error (K)
1000	0.0	5.1	-0.1	5.4	-0.2	5.4
850	0.8	3.1	0.7	3.2	0.5	3.2
700	1.1	1.9	1.0	1.9	0.9	2.0
500	-0.2	1.5	-0.3	1.4	-0.3	1.4
400	0.4	2.0	0.3	2.0	0.3	2.0
300	-0.3	3.8	-0.4	3.9	-0.3	4.2
250	-0.9	4.4	-0.9	4.6	-1.0	4.7
200	-2.0	3.2	-1.9	3.3	-1.8	3.5
150	-1.2	1.6	-1.1	1.6	-1.0	1.6
100	3.0	2.8	3.1	2.8	3.3	2.7
70	1.0	4.0	0.9	4.2	0.9	4.3
50	1.8	5.6	1.6	6.0	1.5	6.4
30	2.1	7.5	1.8	8.0	1.8	8.4
10	1.4	12.6	0.9	13.2	0.6	13.8

Table 84

Execution times of various filters (sec.)

	Causal	Precomputed P(-)	Precomputed Gain
One Spot	0.04	0.02	0.01
Two Spot	0.14	0.07	0.01
Three Spot	0.55	0.20	0.02

observation matrices themselves are noise because of improper elevation of emissivity estimates. The averaging done in the precomputation of the gain has possibly reduced this error.

Chapter V

The Water Vapor and Liquid Water Experiment

Section A. General description

In order to further investigate the capabilities of the extended Kalman-Bucy filter, it was decided to implement it as an inversion scheme for retrieval of liquid water and water vapor column using the two window channels of SCAMS. This is a more substantially non-linear problem than the temperature problem. Besides the quadratic term in the absorption coefficient of water vapor, the two variables interact significantly with themselves and each other. As an example, a heavy cloud deck will obscure the radiation from its lower levels and from the water vapor beneath it. In the extreme, an increase in the liquid column will produce a decrease in the observed brightness temperature since the opaque cloud will penetrate further into the colder high atmosphere.

It is unfortunate, but this experiment could not be run on actual SCAMS data. While there are independent estimates

of water vapor columns available, there is no corresponding ground truth for liquid water. The filter was thus evaluated on a synthetic dataset constructed to be as close to reality as possible. While this implies perfect knowledge of the plant, it is felt that the conclusions of this chapter are still valid.

Section B of this chapter discusses the problem of the identification of the plant for this filter. The synthesis of the observation matrices and the evaluation of the equations of the equations of radiative transfer at the prior are discussed in Section C. A description of the dataset synthesis is given in Section D. Section E presents the results of the experiment.

Section B. System identification

Because of the lack of independent measurements, the problem of system identification was a rather difficult one. The only estimate of liquid water and water vapor columns available on a large scale are those produced by the inversions of SCAMS itself. It was thus this data that formed the dataset used in the system identification.

A dataset consisting of three days of August 1975 data

was processed to extract all those scans in which all thirteen spots were over water, thus allowing water vapor and liquid water to be estimated. This extracted dataset was then divided into latitude bands and the mean in each band computed. The mean of the water vapor showed the expected behaviour, peaking at about 40 mm precipitable water at the equator and tapering off to about 10 mm at 60 latitude. Liquid water columns showed no particular latitudinal pattern. The mean over the latitudes examined was approximately 0.2 mm. There was a mild peak of 0.3 to 0.4 mm near the intertropical convergence zone.

Using an interpolation in latitude of the water vapor means and a mean of 0.2 mm for the liquid water columns, the dataset was then processed to yield the covariance of the liquid water and water vapor along a scan and the cross-covariance between a scan and the one following in space. It was expected that a simple stepwise regression of one scan on the other would produce a state transition matrix. Such a regression was attempted. However, when the results of this regression were used in the simulation of Section D, certain states began to grow without limit after roughly 20 scans of pure prediction. Because the intended use of the plant was both in the filter and in the simulation, this state transition matrix was discarded. The state transition matrix that was finally used was a result

of the first step of the regression. The regression coefficient for the water vapor states was about 0.95, and that for the liquid water states was about 0.90. Since there is no a priori reason to suspect that one spot will be different from another, these values were used for all spots in the matrix. The dataset was then reprocessed using this matrix in the prediction scheme to produce an estimate of the plant noise. Both the covariance of the prior and this plant noise were produced in 10 degree latitude bands.

Section C. Observations and observation matrices

As mentioned earlier in this chapter, the forward problem for water vapor and liquid water is more non-linear than the forward problem for oxygen. This is further compounded by the fact that estimates for liquid water and water vapor can be reliably produced only when they can be observed in emission against the cold background of the ocean. The temperature effects of the sea surface reflectivity thus enter the problem as do the effects of sea state. To overcome these problems, an approach believed novel in remote sensing has been developed and will be presented in this section.

The first consideration in the observation process is to factor out the effect of the surface. Examining the equation of radiative transfer, we find that the observed brightness temperature is composed of three parts: the radiation produced by the atmosphere and observed directly by the satellite, the radiation produced by the atmosphere and observed by the satellite after it has been reflected from the surface, and finally, the emission from the surface after it has been attenuated by the atmosphere. This is expressed by the equation:

$$\begin{aligned}
 T_B = & \int_{H_s}^H T(h) K(\nu, h) \tau(h, H) dh \\
 & + R(\nu) \int_{H_s}^H T(h) K(\nu, h) \tau(h, H) \tau(H_s, H) dh \quad 5.1 \\
 & + (1 - R(\nu)) T_s \tau(H_s, H)
 \end{aligned}$$

This implies that we may compute the observed brightness temperature for an arbitrary surface temperature and emissivity if we know the values of the two integrals and the absorption through the atmosphere.

Having factored out the state of the surface from the equation of radiative transfer, we now seek a fast method for evaluating the two integrals and the atmospheric attenuation. There is, of course, no method to do this exactly. For a given atmospheric structure, these

quantities must be evaluated using the full integrals. Therefore, we will seek a reasonable approximation to the integrals instead. To accomplish this, we will first examine the problem to discover if we may make any simplifying assumptions about the atmosphere.

Assuming that the hydrostatic equation is valid, there are three quantities that will specify the absorptions in the integrals of 5.1: temperature, water vapor concentration, and liquid water concentration. The liquid water and water vapor are primarily located in the region of the atmosphere below tropopause. There are rare occasions in which extreme weather occasions will pump significant water vapor into the upper atmosphere, but these conditions are the exception rather than the rule. The same may be said of liquid water. If the total bandpass of the radiometer is large enough so that the total brightness temperature is unaffected by any possible spike in the spectrum at 22.235 GHz., it is reasonable to assume that the region above tropopause is totally dry. We may then fracture the integrals into upper and lower atmosphere

pieces. Doing this we obtain:

$$\begin{aligned}
 T_B = & I_1 + \tau(H_T, H) I_2 + R(\nu) \left\{ \tau^2(H_S, H_T) \tau(H_T, H) I_3 \right. \\
 & \left. + \tau(H_S, H_T) \tau(H_T, H) I_4 \right\} \\
 & + (1 - R(\nu)) T_S \tau(H_S, H_T) \tau(H_T, H)
 \end{aligned} \tag{5.2}$$

where

$$I_1 = \int_{H_T}^H T(h) K(\nu, h) \tau(h, H) dh \tag{5.3}$$

$$I_2 = \int_{H_S}^{H_T} T(h) K(\nu, h) \tau(H_S, h) dh \tag{5.4}$$

and

$$I_3 = \int_{H_T}^H T(h) K(\nu, h) \tau(h, H) dh \tag{5.5}$$

$$I_4 = \int_{H_S}^{H_T} T(h) K(\nu, h) \tau(h, H) dh \tag{5.6}$$

where H_T is the height of the tropopause. Of the quantities in 5.2, I_1 , I_3 , and $\tau(H_T, H)$ are unaffected by liquid water and water vapor because of our assumption of a dry troposphere. Their values are affected solely by the

temperature structure above tropopause. Since the frequencies used by SCAMS for water vapor and liquid water estimates are in the far wings of the oxygen complex, the atmosphere is very nearly transparent above this level. This leads to the conclusion that it will have little ultimate impact if the temperature structure above tropopause is only grossly approximated. For such an approximation, it is more than reasonable to use the standard supplemental atmospheres.

To deal with I_2 , I_4 , and $\tau(H_S, H_T)$ requires further assumptions about the structure of the atmosphere. In the case of the vertical distribution of water vapor, it is often reasonable to assume that its concentration decays exponentially with altitude. The scale height usually associated with this decay is 2.2 km, although a figure of 2.0 km is sometimes used. Under this assumption, approximately 86 percent of the total water vapor lies in the bottom 4.4 km of the atmosphere.

The vertical distribution of liquid water is best described by its distribution within the many varieties of clouds that occur in the atmosphere. While clouds display a continuous behaviour in altitude and liquid water concentrations, it is possible to classify them into general categories or cloud models. It is thus common in meteorology to talk of an alto-stratus, fair weather

cumulus, etc. cloud. A catalog of some of the more common cloud types with their altitudes, drop size distributions, and densities has been compiled by Reifenstein and Gaut (1971). To approximate the distribution of liquid water for a given column it is reasonable to select a cloud model with a column close to that desired and vary its density slightly.

The final approximation needed is one for the temperature structure of the lower atmosphere. Since the region of greatest concern is below 4 km, it is reasonable to assume that the temperature in this portion of the atmosphere is given by the temperature at a level such as 850 mb and a lapse rate. The lapse rate used should be a function of the temperature itself. As an example, a temperature typical of a sub-arctic winter would imply a lapse rate typical of that atmosphere.

Given these assumptions, it is possible to evaluate the integrals I_2 , I_4 and $\tau(H_S, H_T)$ for a choice of temperature and liquid water and water vapor columns. This is still a rather time-consuming process if it is necessary each time a retrieval is performed. Thus, we will require a further level of approximation.

This approximation will be to evaluate the various parts of 5.1 by means of a bicubic spline in water vapor and liquid water. The spline coefficients used will be provided

by an interpolation of those produced for two temperatures surrounding the desired temperature profile. Thus, we evaluate a spline for each of the quantities:

$$S_1 = I_1 + \tau(H_T, H) I_2 \quad 5.7$$

$$S_2 = \tau^2(H_S, H_T) \tau(H_T, H) I_3 + \tau(H_S, H_T) \tau(H_T, H) I_4 \quad 5.8$$

$$S_3 = \tau(H_S, H_T) \tau(H_T, H) \quad 5.9$$

and then combine them with the surface temperature and reflectivity at run time to produce the brightness temperature as a function of the prediction.

The knots of the spline were chosen to be on the mesh (L_j, W_j) , where L_j was the liquid water column from the set $\{0., 0.2, 0.4, 0.6, 0.8, 1.0, 4.0, 8.0, 16.0, 20.0\}$ mm precipitable water and W_j was the water vapor column in the set $\{0.0, 10.0, 20.0, 30.0, 40.0, 50.0, 60.0, 70.0, 80.0, 90.0, 100.0\}$ mm precipitable water vapor. These spline coefficients were evaluated for temperatures at 1013 mb from -20.0 to 40.0 degrees centigrade in 5 degree steps. It should be recognized that certain of these atmospheres are physically impossible. As an example, a zero water vapor column will never occur in conjunction with a 20 mm liquid water column. These knots were evaluated simply to mechanize the entire process. It should also be noted that

the values of I_1 , I_2 , and $\tau(H_T, H)$ need be evaluated only once for the knot mesh, thus reducing the total computation required.

Because the predicted brightness temperature is produced in terms of this bicubic spline, it is a simple matter to produce the partial derivatives needed for the evaluation of:

$$H_i(\hat{X}_i(-)) = \left. \frac{\partial}{\partial X} h_i(X) \right|_{X=\hat{X}_i(-)} \quad \begin{array}{l} 3.62 \\ \text{(REPEATED)} \end{array}$$

The partial derivatives of each of the splines with respect to liquid water and water vapor columns are well defined. One need only combine them in terms of the surface reflectivity and temperature.

Section D. The simulation

Given the choice of the plant, the simulation of the observed brightness temperatures is more or less mechanical. The "orbit" was chosen to be successive passes from -59° to 59° latitude with all spots at the same latitude. The temperature of the atmosphere was given by the interpolated standard atmospheres. The values of liquid

water and water vapor were produced by decomposing the plant noise covariance matrix, Q_i , into its eigenvectors and eigenvalues and then driving the eigenvectors with Gaussian random numbers having variance equal to the eigenvalues. The surface temperature was taken to be the temperature at 1013 mb, but no less than 273.15°K. The dataset produced for the experiment was the "position" of the satellite, the brightness temperatures at all 13 spots corrupted by 0.2°K rms independent Gaussian random variables and a noisy value of the atmospheric and surface temperature. These two temperatures will never be known perfectly to an inversion scheme. The noise processes added to these temperatures were chosen to be independent on each surface and atmospheric temperature. Since the errors in the temperature estimates will not be white, the errors were produced by a plant with $\Phi = 0.98I$ and $Q = (0.57)^2 I$. These statistics were chosen to give a 4°K rms error in each temperature.

To randomize the initial state, the simulation was run for 60 "frames" before actual data was produced.

Section E. Results

The results of the inversion of 400 frames of synthetic data produced by the simulation are given in Tables 85-86. For purposes of comparison, a regression inversion was also produced for this experiment. This regression inversion was obtained by regressing the values of liquid water and water vapor against the brightness temperatures for scan angles 0 through 6 for three orbits of the simulation (368 frames). Since the D matrix constants are symmetric about nadir, the constant for scan angle 5 may be used at scan angle 7, and those for scan angle 0 for scan angle 12, etc. Because the regressions were performed using the statistics for spots 0 through 6, the error statistics of spots 7 through 12 represent errors obtained on an independent dataset.

Even with this highly inbred standard of comparison, the extended Kalman-Bucy filter shows its ability to track the non-linear aspects of the physics. The rms errors of the filter are roughly one third of the regression inversion. To show this more graphically, another simulation with an inbred regression inversion was run with the plant producing liquid water in cm rather than in mm. The mean was thus 2mm rather than 0.2 mm. The results of this simulation are given in Tables 87-88. The error in water

Table 85

Water Vapor Retrieval Error

Scan Angle	Kalman-Bucy		Statistical D	
	Mean	RMS	Mean	RMS
	Error	Error	Error	Error
	(mm)	(mm)	(mm)	(mm)
0	0.246	0.678	0.046	1.517
1	-0.297	1.064	0.159	2.621
2	0.054	0.793	0.199	2.013
3	-0.227	0.684	0.179	2.061
4	-0.714	0.929	0.260	2.427
5	-0.452	1.051	0.460	3.260
6	-0.039	0.801	0.195	2.733
7	-0.210	0.830	1.895	2.835
8	-0.643	0.808	1.594	2.340
9	0.250	0.650	0.945	1.698
10	-0.272	0.757	0.967	1.684
11	-0.274	0.500	0.524	2.698
12	0.738	0.861	0.301	1.565

Table 86

Liquid Water Retrieval Error

Scan Angle	Kalman-Bucy		Statistical D	
	Mean	RMS	Mean	RMS
	Error	Error	Error	Error
	(mm)	(mm)	(mm)	(mm)
0	-0.007	0.018	0.004	0.044
1	0.013	0.027	-0.004	0.065
2	0.002	0.021	-0.004	0.063
3	0.005	0.025	-0.004	0.058
4	0.010	0.023	-0.007	0.060
5	0.010	0.029	-0.020	0.091
6	-0.001	0.024	-0.009	0.087
7	0.006	0.028	-0.047	0.088
8	0.024	0.027	-0.033	0.077
9	-0.009	0.020	0.000	0.065
10	0.006	0.020	-0.019	0.055
11	0.009	0.015	-0.012	0.059
12	-0.020	0.027	-0.006	0.041

Table 87

Water Vapor Retrieval Error
(High Liquid Water Experiment)

Scan Angle	Kalman-Bucy		Statistical D	
	Mean	RMS	Mean	RMS
	Error	Error	Error	Error
	(mm)	(mm)	(mm)	(mm)
0	-0.556	1.609	-0.093	4.614
1	-0.666	1.809	-0.002	4.946
2	-0.691	1.771	0.158	4.584
3	-0.705	1.866	0.349	4.702
4	-1.191	1.865	0.196	5.314
5	-1.237	2.276	0.760	7.250
6	-1.147	2.957	0.319	6.342
7	-0.503	2.632	3.614	7.156
8	-0.644	2.295	2.791	5.302
9	-0.579	1.645	1.922	4.279
10	-0.696	1.394	1.025	4.283
11	-0.555	1.272	1.204	5.557
12	-0.497	2.325	1.646	5.597

Table 88

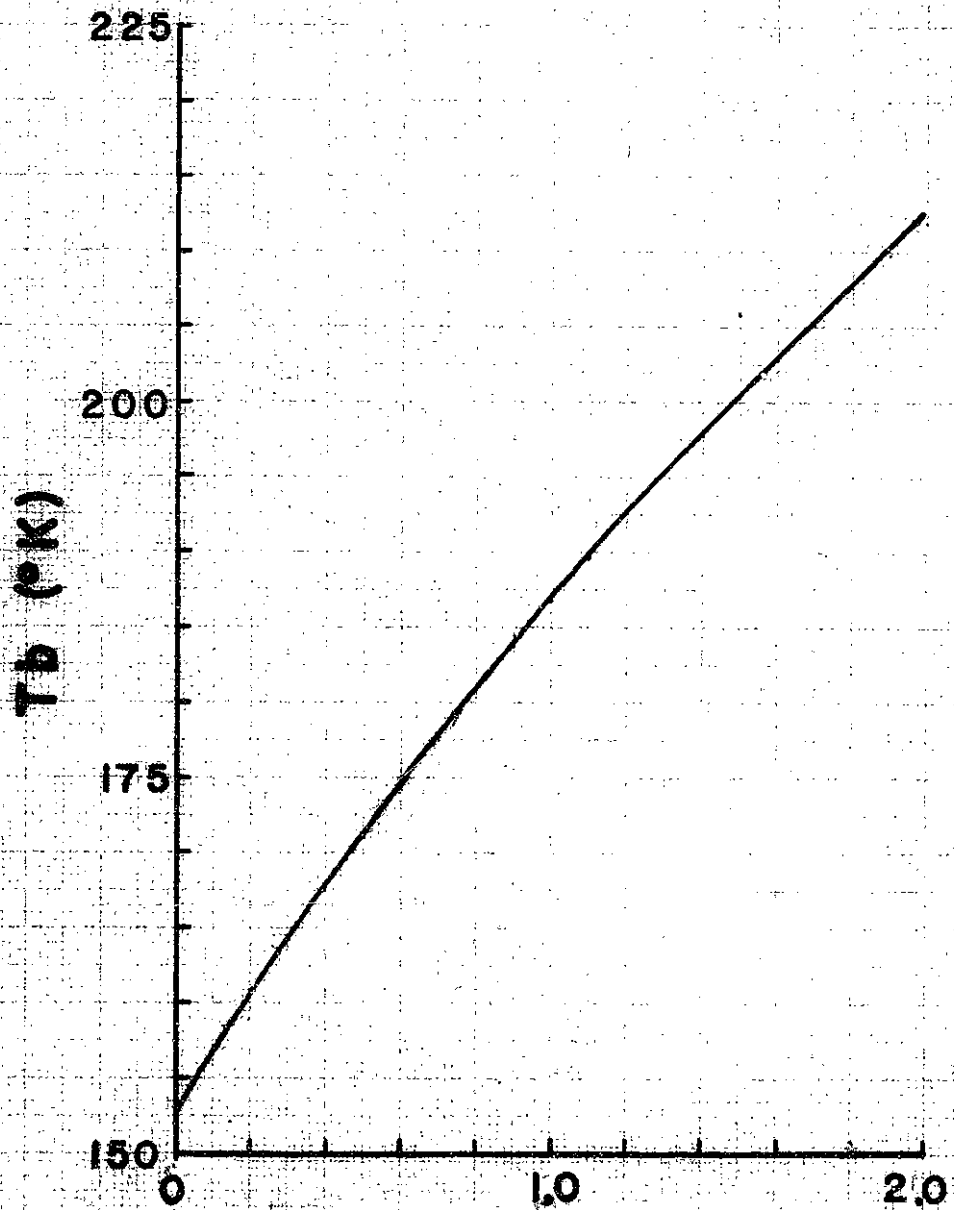
Liquid Water Retrieval Error
(High Liquid Water Experiment)

Scan Angle	Kalman-Bucy		Statistical D	
	Mean	RMS	Mean	RMS
	Error	Error	Error	Error
	(mm)	(mm)	(mm)	(mm)
0	-0.01	0.06	-0.02	0.42
1	0.03	0.08	0.01	0.57
2	0.02	0.07	0.02	0.67
3	0.01	0.08	0.01	0.61
4	0.02	0.08	-0.01	0.52
5	0.01	0.19	-0.19	0.97
6	0.02	0.10	-0.07	0.64
7	0.00	0.14	-0.18	0.84
8	0.01	0.35	-0.16	0.93
9	-0.02	0.09	0.17	0.58
10	0.02	0.07	0.00	0.64
11	0.03	0.07	-0.06	0.78
12	0.00	0.15	-0.14	0.59

vapor is still one third of the regression inversion, but the error in liquid water is now one seventh that of the regression.

To show the value of this non-linear tracking ability, we may consider the plot of Figure 12. This is a plot of the channel two brightness temperatures as a function of liquid water for a water vapor column of 25 mm. Assuming that the liquid water mean is 0.2 mm and that the water vapor is invariant, a regression inversion will produce an estimate essentially based on the slope of this curve at 0.2 mm. This estimate will be approximately $L = 0.02687(T - 160.9) + 0.2$. A received brightness temperature of 180.9°K will generate an estimate of 0.74 mm for an error of -0.06 mm. The Kalman filter used in the experiment exhibited innovations in the order of several degrees. For the purposes of this argument, we will assume that the prediction was 0.6 mm. The Kalman estimate is thus roughly $L = 0.02988(T - 174.6) + 0.6$. For a 180.9°K received brightness temperature, the estimate will be 0.79 mm for an error of -0.01 mm. The tracking ability and the ability to evaluate the derivatives at the prior thus yields significant advantages.

Since these improvements seem so large, it is reasonable to inquire beyond the above simple analysis as to their source. One question that should be asked is how easy



LIQUID WATER (mm)

Figure 12
 Boiling Point Temperature at 31.65 mm.
 Vacuum Liquid Water Column at 25 mm
 Water Vapor Column

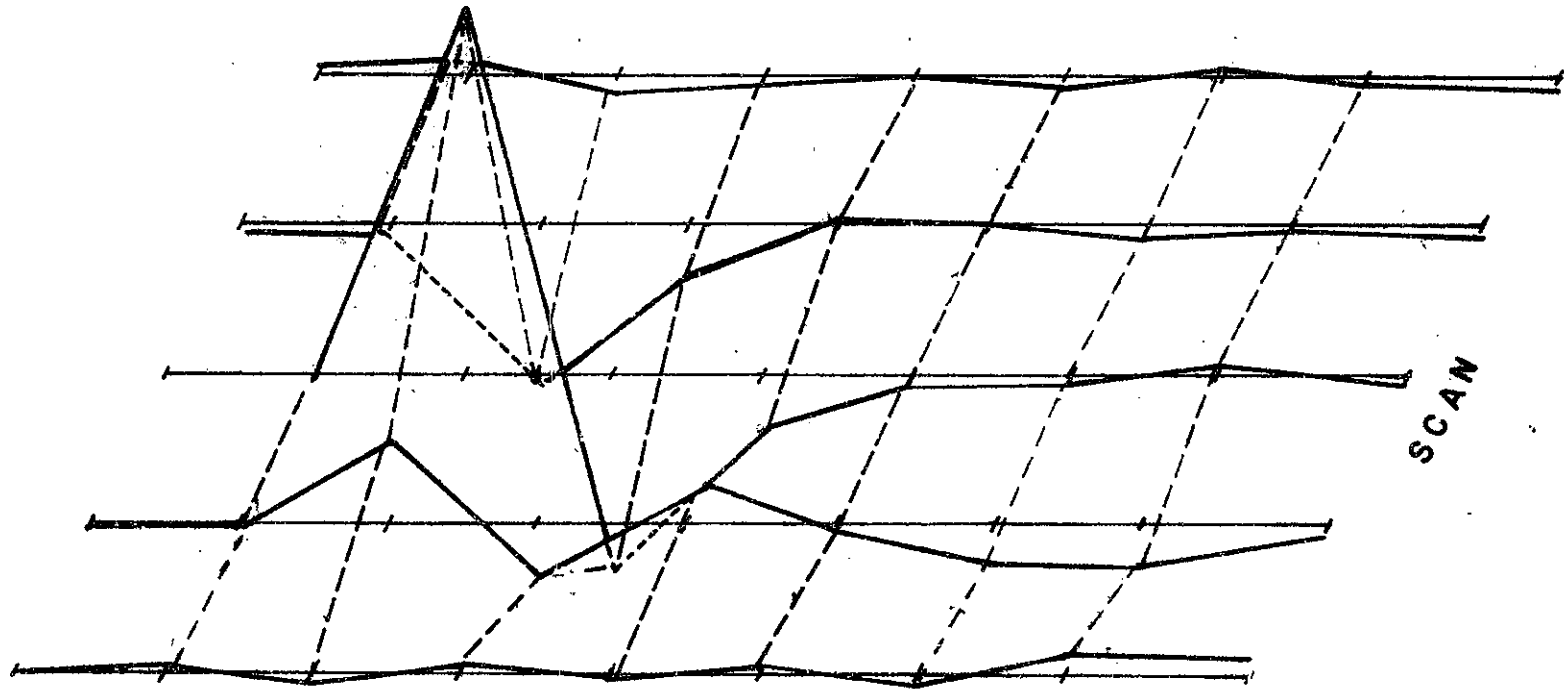
- 20 -

it is to "derail" the non-linear processing. This question was addressed by running the filter for a period of time and then injecting one gram (10mm) of liquid water into the nadir spot for a period of one frame. The resulting error performances are plotted in Figures 13-14. It should be noted that the filter has recovered in approximately three frames and has resumed nominal error performance.

A second question is how critical the estimates of the surface and atmospheric temperature are to the estimation process. To investigate this effect, the filter was run with a constant atmospheric and surface temperature estimate of 293.15° K. The results of this experiment are given in Tables 89-90. It may be seen that when the filter is denied temperature information, the performance is degraded to that of the Statistical D method. The question is now which of the two temperatures is more critical to the processing. To answer this, the experiment was re-run with the filter being denied either the atmospheric temperature or the surface temperature. The results of these two experiments are given in Tables 91-94. The conclusion that may be made from these experiments is that the knowledge of the atmospheric temperature is more important than the knowledge of the surface temperature, but that if either is lacking, the performance is seriously degraded.

A final issue that must be addressed is the sensitivity

ERROR

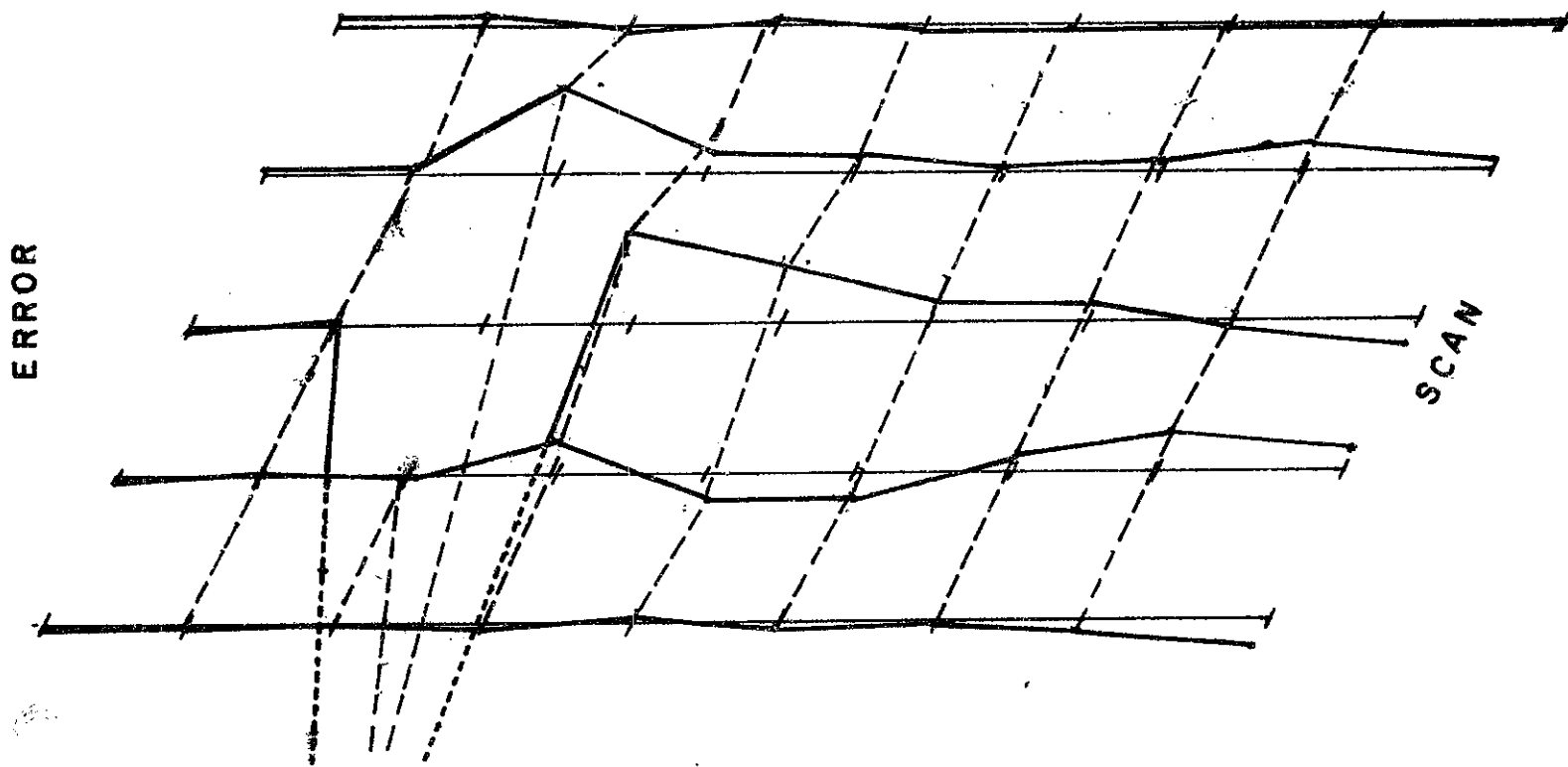


INVERSION NUMBER

SCAN

Figure 13

Water Vapor Error Response to a Liquid Water Impulse



INVERSION NUMBER

Figure 14

Liquid Water Error Response to a Liquid Water Impulse

Table 89

Water Vapor Retrieval Error
(No Temperature Knowledge Experiment)

Scan Angle	Kalman-Bucy		Statistical D	
	Mean	RMS	Mean	RMS
	Error	Error	Error	Error
	(mm)	(mm)	(mm)	(mm)
0	1.370	1.292	0.046	1.517
1	0.443	2.954	0.159	2.621
2	1.512	2.607	0.199	2.013
3	1.751	3.519	0.179	2.061
4	2.362	4.632	0.260	2.427
5	2.260	5.936	0.460	3.620
6	2.460	4.145	0.195	2.733
7	2.052	4.946	1.859	2.835
8	1.656	4.130	1.594	2.340
9	1.216	3.254	0.945	1.698
10	0.980	2.371	0.967	1.684
11	0.258	2.593	0.524	2.698
12	1.242	1.187	0.301	1.565

Table 90

Liquid Water Retrieval Error
(No Temperature Knowledge Experiment)

Scan Angle	Kalman-Bucy		Statistical D	
	Mean	RMS	Mean	RMS
	Error	Error	Error	Error
	(mm)	(mm)	(mm)	(mm)
0	-0.002	0.460	-0.004	0.044
1	0.010	0.101	-0.004	0.065
2	-0.001	0.103	-0.004	0.063
3	-0.005	0.122	-0.004	0.058
4	-0.004	0.141	-0.007	0.060
5	-0.004	0.162	-0.020	0.091
6	-0.008	0.150	-0.009	0.087
7	0.004	0.153	-0.047	0.088
8	0.009	0.136	-0.033	0.077
9	0.011	0.126	0.000	0.065
10	0.007	0.095	-0.019	0.055
11	0.015	0.094	-0.012	0.059
12	0.004	0.046	-0.006	0.041

Table 91

Water Vapor Retrieval Error
 (No Atmospheric Temperature Knowledge Experiment)

Scan Angle	Kalman-Bucy		Statistical D	
	Mean	RMS	Mean	RMS
	Error	Error	Error	Error
	(mm)	(mm)	(mm)	(mm)
0	1.398	2.147	0.046	1.517
1	1.447	1.971	0.159	2.621
2	1.552	2.454	0.199	2.013
3	1.697	2.452	0.179	2.061
4	1.809	2.930	0.260	2.427
5	1.910	3.631	0.460	3.620
6	1.643	2.872	0.195	2.733
7	1.591	3.281	1.859	2.835
8	1.510	2.629	1.594	2.340
9	1.222	2.267	0.945	1.698
10	1.023	2.297	0.967	1.684
11	1.204	1.872	0.524	2.698
12	1.413	2.016	0.301	1.565

Table 92

Liquid Water Retrieval Error
(No Atmospheric Temperature Knowledge Experiment)

Scan Angle	Kalman-Bucy		Statistical D	
	Mean	RMS	Mean	RMS
	Error	Error	Error	Error
	(mm)	(mm)	(mm)	(mm)
0	-0.024	0.061	-0.004	0.044
1	-0.026	0.063	-0.004	0.065
2	-0.024	0.078	-0.004	0.063
3	-0.035	0.086	-0.004	0.058
4	-0.033	0.096	-0.007	0.060
5	-0.036	0.101	-0.020	0.091
6	-0.033	0.101	-0.009	0.087
7	-0.017	0.107	-0.047	0.088
8	-0.018	0.085	-0.033	0.077
9	-0.016	0.086	0.000	0.065
10	-0.017	0.069	-0.019	0.055
11	-0.020	0.062	-0.012	0.059
12	-0.018	0.065	-0.006	0.041

Table 93

Water Vapor Retrieval Error
(No Surface Temperature Knowledge Experiment)

Scan Angle	Kalman-Bucy		Statistical D	
	Mean Error (mm)	RMS Error (mm)	Mean Error (mm)	RMS Error (mm)
0	0.333	1.646	0.046	1.517
1	-1.379	1.817	0.159	2.621
2	-0.026	0.797	0.199	2.013
3	-0.295	1.324	0.179	2.061
4	-0.415	1.729	0.260	2.427
5	-0.460	2.386	0.460	3.620
6	0.625	1.450	0.195	2.733
7	0.035	2.358	1.859	2.835
8	-0.684	1.765	1.594	2.340
9	0.124	1.503	0.945	1.698
10	-0.340	0.724	0.967	1.684
11	-1.263	1.651	0.524	2.698
12	0.668	1.517	0.301	1.565

Table 94

Liquid Water Retrieval Error
(No Surface Temperature Knowledge Experiment)

Scan Angle	Kalman-Bucy		Statistical D	
	Mean	RMS	Mean	RMS
	Error	Error	Error	Error
	(mm)	(mm)	(mm)	(mm)
0	0.017	0.026	-0.004	0.044
1	0.044	0.043	-0.004	0.065
2	0.021	0.032	-0.004	0.063
3	0.030	0.043	-0.004	0.058
4	0.034	0.046	-0.007	0.060
5	0.034	0.050	-0.020	0.091
6	0.018	0.046	-0.009	0.087
7	0.022	0.056	-0.047	0.088
8	0.044	0.051	-0.033	0.077
9	0.013	0.045	0.000	0.065
10	0.027	0.035	-0.019	0.055
11	0.042	0.038	-0.012	0.059
12	0.005	0.025	-0.006	0.041

of the observation matrices to the assumptions made in their construction. In particular, their sensitivity to the assumed water vapor scale height requires attention. To investigate this, two additional sets of splines were constructed that represent extreme conditions in the atmosphere. One set of splines had an assumed water vapor scale height of 1.0 km and the other had an assumed water vapor scale height of 3.0 km. These splines were then used to create two new synthetic datasets. The filter was then run on these datasets using the 2.2 km splines for the forward model. The results of these experiments are given in Tables 95 - 98. The conclusion that may be drawn from these experiments is that the scale height of water vapor is a significant factor in the non-linear processing of the filter. To further test this behaviour, a mixed synthetic dataset was constructed in which records were randomly selected from the 2.2 km synthetic dataset with probability 0.6 and from the 1.0 km or 3.0 km dataset with probability 0.2. The filter was then run on this dataset using the 2.2 km splines. The result of this experiment is given in Tables 99-100. In this more realistic (but still extreme) experiment, the filter still continues to perform better than the Statistical D method retrievals constructed for the mixed dataset. This improvement is by no means as marked as when the water vapor scale height was known a priori. It

Table 95

Water Vapor Retrieval Error
(3.0 km Water Vapor Scale Height Experiment)

Scan Angle	Kalman-Bucy		Statistical D	
	Mean	RMS	Mean	RMS
	Error	Error	Error	Error
	(mm)	(mm)	(mm)	(mm)
0	1.984	1.123	1.553	1.645
1	1.322	0.936	1.071	2.623
2	1.706	1.207	1.279	2.090
3	1.299	0.818	0.998	2.106
4	0.854	0.871	0.992	2.457
5	1.309	1.459	1.232	3.276
6	1.832	1.008	1.147	2.799
7	1.294	1.044	2.598	2.866
8	0.784	0.827	2.322	2.386
9	1.754	0.866	1.786	1.725
10	1.207	1.083	2.044	1.819
11	1.221	0.689	1.420	2.796
12	2.358	1.367	1.799	1.842

Table 96

Liquid Water Retrieval Error
(3.0 km Water Vapor Scale Height Experiment)

Scan Angle	Kalman-Bucy		Statistical D	
	Mean	RMS	Mean	RMS
	Error	Error	Error	Error
	(mm)	(mm)	(mm)	(mm)
0	-0.054	0.034	-0.044	0.046
1	-0.039	0.025	-0.032	0.063
2	-0.045	0.036	-0.036	0.063
3	-0.042	0.039	-0.031	0.057
4	-0.039	0.033	-0.043	0.060
5	-0.044	0.034	-0.047	0.090
6	-0.060	0.037	-0.038	0.087
7	-0.042	0.040	-0.072	0.088
8	-0.023	0.028	-0.058	0.078
9	-0.053	0.034	-0.026	0.065
10	-0.036	0.033	-0.049	0.597
11	-0.035	0.028	-0.039	0.059
12	-0.062	0.046	-0.045	0.047

Table 97

Water Vapor Retrieval Error
(1.0 km Water Vapor Scale Height Experiment)

Scan Angle	Kalman-Bucy		Statistical D	
	Mean	RMS	Mean	RMS
	Error	Error	Error	Error
	(mm)	(mm)	(mm)	(mm)
0	-4.358	1.917	-4.269	1.842
1	-4.754	2.703	-2.495	2.865
2	-4.628	2.194	-2.988	2.332
3	-4.583	2.471	-2.320	2.309
4	-5.387	2.836	-2.145	2.593
5	-5.546	2.774	-2.134	3.375
6	-5.387	2.660	-3.450	2.930
7	-4.635	2.072	-0.523	2.868
8	-4.708	2.099	-0.675	2.327
9	-3.952	1.748	-1.551	1.910
10	-4.271	1.591	-2.063	1.618
11	-4.296	1.986	-2.018	2.619
12	-3.072	1.530	-3.938	1.340

Table 98

Liquid Water Retrieval Error
(1.0 km Water Vapor Scale Height Experiment)

Scan Angle	Kalman-Bucy		Statistical D	
	Mean Error (mm)	RMS Error (mm)	Mean Error (mm)	RMS Error (mm)
0	0.127	0.072	0.096	0.056
1	0.149	0.095	0.065	0.075
2	0.138	0.082	0.076	0.075
3	0.138	0.082	0.063	0.069
4	0.157	0.097	0.061	0.069
5	0.167	0.102	0.048	0.096
6	0.157	0.094	0.063	0.094
7	0.142	0.079	0.013	0.095
8	0.153	0.083	0.029	0.079
9	0.112	0.060	0.066	0.070
10	0.124	0.064	0.054	0.059
11	0.131	0.069	0.054	0.066
12	0.101	0.052	0.091	0.044

Table 99

Water Vapor Retrieval Error
(Mixed Water Vapor Scale Height Experiment)

Scan Angle	Kalman-Bucy		Statistical D	
	Mean	RMS	Mean	RMS
	Error	Error	Error	Error
	(mm)	(mm)	(mm)	(mm)
0	-0.527	1.827	0.113	2.447
1	-0.926	2.317	0.171	2.880
2	-0.791	2.124	0.217	2.499
3	-0.889	2.239	0.173	2.423
4	-1.475	2.478	0.295	2.779
5	-1.394	2.575	0.524	3.616
6	-0.976	2.503	0.233	3.119
7	-0.883	2.283	1.974	3.088
8	-1.170	2.057	1.661	2.574
9	-0.484	1.921	0.939	2.120
10	-0.897	1.899	0.831	2.180
11	-0.890	1.978	0.388	3.002
12	0.003	1.793	0.306	2.361

Table 100

Liquid Water Retrieval Error
(Mixed Water Vapor Scale Height Experiment)

Scan Angle	Kalman-Bucy		Statistical D	
	Mean	RMS	Mean	RMS
	Error	Error	Error	Error
	(mm)	(mm)	(mm)	(mm)
0	0.013	0.052	-0.006	0.061
1	0.030	0.069	-0.005	0.071
2	0.025	0.064	-0.005	0.072
3	0.023	0.068	-0.004	0.067
4	0.033	0.075	-0.008	0.073
5	0.034	0.080	-0.021	0.102
6	0.023	0.073	-0.010	0.093
7	0.026	0.068	-0.051	0.094
8	0.039	0.065	-0.036	0.084
9	0.011	0.056	0.000	0.071
10	0.024	0.056	-0.016	0.065
11	0.026	0.059	-0.029	0.072
12	-0.002	0.049	-0.007	0.066

must then be concluded that the performance achieved in which the water vapor scale height was known exactly may be overly optimistic.

In summary, the Extended Kalman-Bucy filter appears to be a valuable means of producing estimates of liquid water and water vapor from satellite data. To fully utilize its potential, it is necessary to incorporate estimates of the temperature profile and ocean surface temperature. It will also be desirable to incorporate estimates of the sea surface state as this parameter also affects the reflectivity of the sea surface. Finally, the assumptions made about the water vapor scale height have a critical role in its performance.

Chapter VI

Summary and Recommendations for Future Research

The basic conclusions that may be reached from the experiments conducted in this thesis are: The extended Kalman-Bucy filter offers an improvement in estimation accuracy over a presently used inversion method for parameters sensed from passive remote sounders. This improvement is greatest in the more non-linear problem of estimating liquid water and water vapor. The degree of improvement is sufficient to warrant the increased computational burden.

There are several areas in which further research should be fruitful: The system identification procedures used to identify the plant in the filters developed were specific to the instrument and not very satisfactory. A more adequate and general identification will be warranted before such filters are used operationally. The temperature filter implemented did not use the two low frequency channels of SCAMS. Since these two channels contain quite a bit of information about the surface temperature over land, one should be able to improve the performance of the filter

further by including them in an inversion scheme. The filter should be tried in a number of the other more non-linear problems of the field. Some of these might include: temperature inversion using sensors in the infrared spectrum, a combined inversion using both microwave and infrared sensors, estimation of sea state in conjunction with water vapor and liquid water, and liquid water and water vapor profiling. Finally, the problem of state reduction for the atmosphere is highly important to reduce the number of states in the filters used.

Appendix A

Comparisons Between Point and Area Sounders

One of the problems of the analysis of the results of any experiment with any passive remote sounder such as SCAMS is the lack of independent verification data corresponding to the parameters being estimated. Historically, the independent verification sources have been taken to be either radiosonde reports or an analysis grid such as the NMC K27 grid used in this thesis. A passive sounder such as SCAMS measures the parameters of interest averaged over the antenna beam pattern which has an area on the earth of over 17,000 square kilometers. The radiosonde report consists of an area average of perhaps a few square centimeters along its line of flight. Because of the manner in which analysis grids are produced, it is unclear what sort of area average they represent.

The purpose of this appendix is an attempt to quantify the apparent error between a comparison of a perfect point sounding and a perfect area sounding in a homogeneous isotropic atmosphere. That is, we desire a numerical value of $E\{[P_A(\sigma_1) - P_P(\sigma_2)]^2\}$, where $P_A(\sigma_1)$ is a perfect area

sounding of some parameter centered at location σ_1 and $P_p(\sigma_2)$ is a perfect point sounding of the same parameter centered at σ_2 . We will define the area sounding as:

$$P_A(\sigma_1) = \int_{\omega_1} G(\sigma) P(\sigma) d\sigma \quad A.1$$

where $G(\sigma)$ is the antenna beam pattern and ω_1 is the physical space seen by the beam. Taking the expectation of both sides of A.1, we obtain:

$$E\{P_A(\sigma_1)\} = \int_{\omega_1} G(\sigma) E\{P_p(\sigma)\} d\sigma \quad A.2$$

Since we have assumed a homogeneous field, $E\{P_p(\sigma)\}$ is a constant and may be moved out of the integral. Then assuming that:

$$\int_{\omega_1} G(\sigma) d\sigma = 1 \quad A.3$$

we obtain:

$$E\{P_A(\sigma_1)\} = E\{P_p(\sigma_2)\} \quad A.4$$

Without loss of generality, we will assume these processes to be zero mean.

Defining e as our error measure, we expand it to

obtain:

$$e = E\{P_P^2(\sigma_2)\} - 2 E\{P_A(\sigma_1) P_P(\sigma_2)\} + E\{P_A^2(\sigma_1)\} \quad A.5$$

The quantity $E\{P_P^2(\sigma_2)\}$ is simply the variance of $P_P(\sigma_2)$ and is a constant for all σ due to the assumption of a homogeneous atmosphere. We will define this as $\text{Var}(P_P)$.

Substituting the definition of the area sounding (A.1) into A.5 and bringing the expectation into the integrals, we obtain:

$$e = \text{Var}(P_P) - 2 \int_{\omega_1} G(\sigma) E\{P_P(\sigma) P_P(\sigma_2)\} d\sigma + \int_{\omega_1} \int_{\omega_1} G(\sigma') G(\sigma'') E\{P(\sigma') P(\sigma'')\} d\sigma' d\sigma'' \quad A.6$$

Factoring out $\text{Var}(P_P)$ from this expression yields:

$$e = \text{Var}(P_P) \left[1 - 2 \int_{\omega_1} G(\sigma) R(\sigma, \sigma_2) d\sigma + \int_{\omega_1} \int_{\omega_1} G(\sigma') G(\sigma'') R(\sigma', \sigma'') d\sigma' d\sigma'' \right] \quad A.7$$

where $R(\sigma', \sigma'')$ is the correlation coefficient between

$P_p(\sigma')$ and $P_p(\sigma'')$. To evaluate A.7, we require an expression for $G(\sigma)$ and $R(\sigma', \sigma'')$.

In order to obtain an expression for $R(\sigma', \sigma'')$, a large number of radiosonde reports were examined. These radiosonde reports spanned the months of January and February, 1973, and represented the majority of the input from the global radiosonde network in the NMC analysis grids for these months. The number of synoptic reporting times in this data set was 109. As the number of radiosondes launched at each synoptic is approximately 800, it was decided to restrict the study to 300 stations in the United States and Canada. This smaller dataset was then subjected to a two-pass outlier rejection procedure to remove reports with data transmission or reporting errors. The sample mean and standard deviation was computed for each station and data points that were further than three standard deviations from the sample mean were removed.

The dataset was then fractioned into four latitude bands in which the most populous band had roughly 100 stations. The purpose of this step was to attempt to assure the homogeneity of the statistics within each band. These bands were located at latitudes below 34° , 34° to 44° , 44° to 54° , and above 54° . Pairwise correlations within each band were then performed using the local sample statistics for each station. The distance between each of the stations

and all others in the latitude band were then computed. The distances were partitioned into bins of 40 km, and a weighted average of the asymptotically normal statistic:

$$Z_{ij} = \text{Ln} \frac{1 + R_{ij}}{1 - R_{ij}} \quad \text{A.8}$$

was performed, where R_{ij} is the sample correlation coefficient between station i and j . The variance of this sample statistic is approximately:

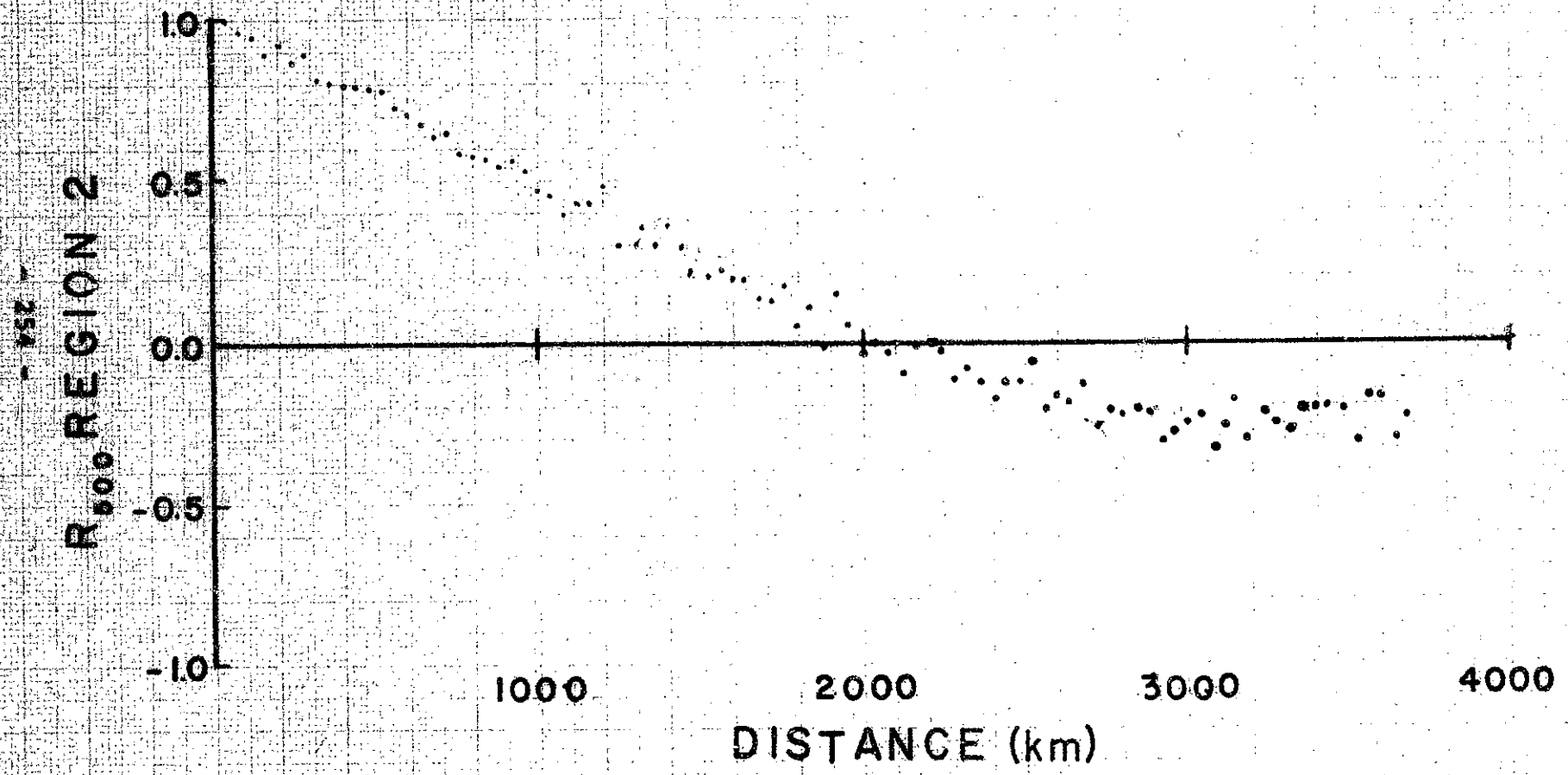
$$\text{Var}(Z_{ij}) \approx \frac{1}{N_{ij} - 3} \quad \text{A.9}$$

where N_{ij} is the number of i, j comparisons entering into the sample. The weight of each of the Z_{ij} was the inverse of this variance.

Several plots of this estimate of the correlation coefficient as a function of distance are given in Figures 15-17. The trend of these curves is consistent with the behaviour that one expects in the atmosphere. The curves drop to zero fastest at pressure levels near the surface and tropopause. They become very long in the atmosphere above tropopause and generally increase in correlation length as one moves toward the equator.

The shape of these curves is suggestive of one of several functions: a polynomial in distance, a

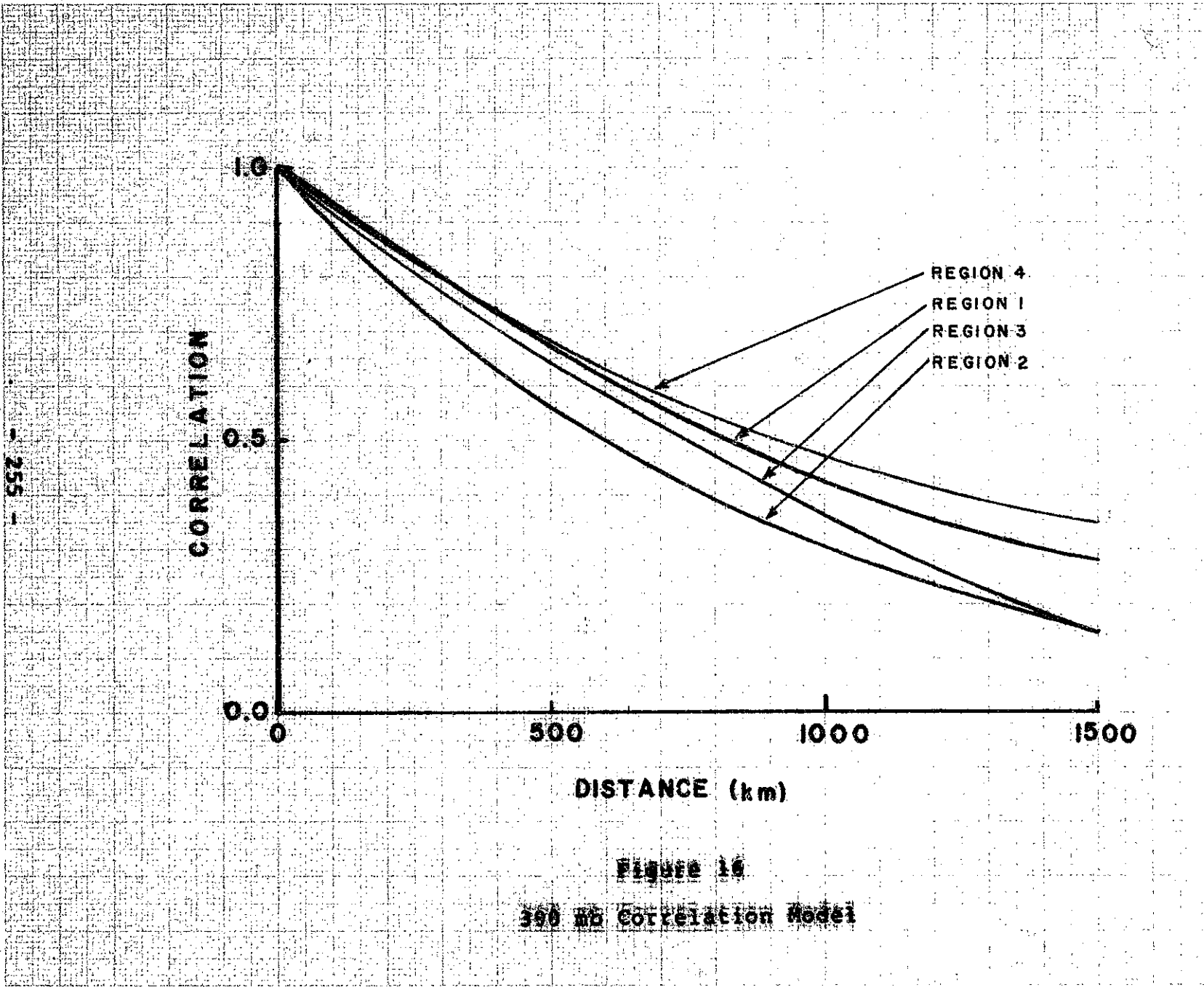
ACQUAINTANCE & GUIDE LINE
NON-REPRODUCIBLE
10 FOOT
MILLIMETER



KUHFRELL & ESSER CO.
MADE IN U.S.A.

Figure 15

500 mb Correlation Coefficient (Sample statistic - Region 2)



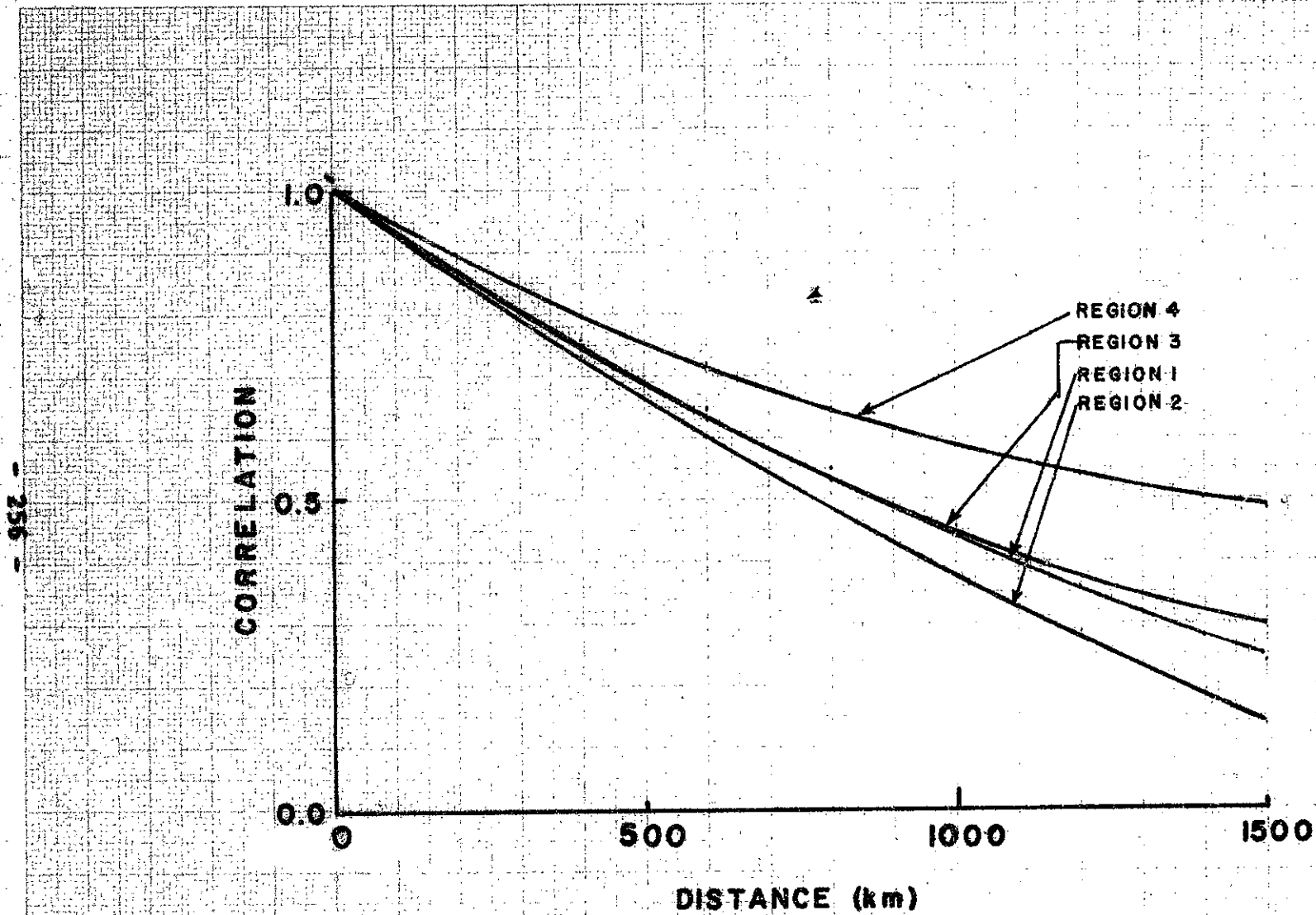


Figure 17

850 mb Correlation Model

sinc(distance) relationship, or a decaying exponential. At the time the database was first analysed, the immediate need was in terms of the discussion of this appendix. It was decided at that time to perform a weighted polynomial fit to the curves. A list of the regression coefficients produced by this procedure are given in Tables 101-104. For some of the cases investigated, the dataset was too sparse or the scatter too large to produce a significant fit. This occurred most often in region 4 (below 34° latitude) where the a priori variance is naturally low and few stations participated in the fit. For these cases, the table contains the entry "No Regression". The near field behaviour of all regressions accepted was generally linear.

In the context of producing estimated of the apparent error between a nearby radiosonde and a radiometer, it is reasonable to assume that the two are nearly co-incident in space and time for the comparison to be meaningful. Thus, it was assumed that the correlation coefficient between two points in the atmosphere was governed by the near field behaviour. This leads to a model of the correlation coefficient as:

$$R(\sigma', \sigma'') = 1 - \frac{|\sigma' - \sigma''|}{R_p} \quad \text{A.10}$$

Table 101

Region 1 Correlation Regression Coefficients

(Above 54° Latitude)

$$R(X) = A_0 + A_1 X + A_2 X^2 + A_3 X^3$$

Pressure Level	A ₀	A ₁ (10 ⁻³)	A ₂ (10 ⁻⁶)	A ₃ (10 ⁻¹⁰)
1000	0.9838	-0.8524	0.5572	-0.1708
850	1.0065	-0.6352	0.0823	0.0000
700	1.0573	-0.6193	0.0626	0.0000
500	1.0266	-0.5621	0.0519	0.0000
400	0.9737	-0.5111	0.0440	0.0000
300	0.8595	-0.6484	0.1559	0.0000
250	0.9585	-0.7175	0.1668	0.0000
200	1.0037	-0.4422	0.0737	0.0000
150	0.9863	-0.1950	0.0000	0.0000
100	0.9816	-0.1833	0.0000	0.0000
70	0.9547	-0.1864	0.0000	0.0000

Table 102

Region 2 Correlation Regression Coefficients

(Between 54° and 44° Latitude)

$$R(X) = A_0 + A_1 X + A_2 X^2 + A_3 X^3$$

Pressure Level	A ₀	A ₁ (10 ⁻³)	A ₂ (10 ⁻⁶)	A ₃ (10 ⁻¹⁰)
1000	No Regression			
850	0.9934	-0.6479	0.0522	0.0000
700	1.0616	-0.5744	0.0000	0.0000
500	1.0406	-0.6061	0.0475	0.0000
400	1.0087	-0.6618	0.0857	0.0000
300	0.9839	-1.1430	0.6032	-1.4209
250	0.9775	-0.9721	0.3595	-0.4669
200	1.0280	-0.6170	0.1567	0.0000
150	1.0643	-0.4346	0.1164	0.0000
100	0.9759	-0.1307	0.0000	0.0000
70	No Regression			

Table 103

Region 3 Correlation Regression Coefficients

(Between 44° and 34° Latitude)

$$R(X) = A_0 + A_1 X + A_2 X^2 + A_3 X^3$$

Pressure Level	A ₀	A ₁ (10 ⁻³)	A ₂ (10 ⁻⁶)	A ₃ (10 ⁻¹⁰)
1000	No Regression			
850	0.9534	-0.7408	0.2748	-0.5492
700	1.0847	-0.6511	0.1085	0.0000
500	0.9546	-0.6574	0.0997	0.0000
400	0.9819	-0.6950	0.1053	0.0000
300	0.9741	-0.7431	0.1245	0.0000
250	1.0084	-0.9525	0.1920	0.0000
200	0.9913	-0.6179	0.1024	0.0000
150	0.9069	-0.5185	0.0000	0.0000
100	0.7852	-0.3024	0.0000	0.0000
70	No Regression			

Table 104

Region 4 Correlation Regression Coefficients

(Below 34° Latitude)

$$R(X) = A_0 + A_1 X + A_2 X^2 + A_3 X^3$$

Pressure Level	A ₀	A ₁ (10 ⁻³)	A ₂ (10 ⁻⁶)	A ₃ (10 ⁻¹⁰)
1000	No Regression			
850	0.8986	-0.4830	0.1138	0.0000
700	0.8651	-0.3346	0.0000	0.0000
500	1.0902	-0.8574	0.1854	0.0000
400	0.9136	-0.6633	0.1132	0.0000
300	0.8033	-0.5795	0.1528	0.0000
250	No Regression			
200	No Regression			
150	No Regression			
100	0.8751	-0.3372	-0.0175	0.0000
70	No Regression			

where R_p is the correlation distance characteristic of the pressure level. A list of the near field R_p values for the various levels and regions are given in Table 105.

Having chosen a model for the correlation coefficients, we now need a model for the antenna pattern. Many radiometers such as the Nimbus E Microwave Spectrometer (NEMS) and SCAMS have circular antennas. The beam patterns are therefore best described by modified first order Bessel functions. However, the use of such an exact expression was not deemed justified in view of the uncertainties in the correlation coefficient expression. It was rather chosen to approximate the beam gain by:

$$G(r, \theta) = \frac{\text{sinc}^2(r/X)}{1.2188148} \quad \text{A.11}$$

where X is the distance from the center of the beam to its first null. This function is much easier to compute in practice than the Bessel functions. The units of this gain are inverse beam radii squared.

Having specified the necessary quantities, we may now

Table 105

Near Field Correlation Lengths
(km)

Pressure Level (mb)	Region 1	Region 2	Region 3	Region 4
1000	1154	954	NR	NR
850	1548	1533	1287	1860
700	1707	1847	1557	2585
500	1826	1717	1452	1271
400	1905	1524	1412	1377
300	1325	861	1310	1386
250	1336	1005	1058	NR
200	2261	1666	1604	NR
150	5045	2448	1749	NR
100	5345	7479	2595	2379
70	5124	NR	NR	NR

NR implies no regression fit.

return to A.7 and substitute them to yield the expression:

$$\begin{aligned}
 e = \text{Var}(P_p) \left[1 \right. \\
 - 2 \int_0^{2\pi} \int_0^1 \frac{\text{sinc}^2(r')}{1.218815} \left(1 - \frac{\sqrt{r'^2 + \tilde{r}_p^2 - 2r'\tilde{r}_p \cos(\theta)}}{\tilde{R}_p} \right) r' dr' d\theta \quad \text{A.12} \\
 \left. + \int_0^{2\pi} \int_0^1 \int_0^{2\pi} \int_0^1 \frac{\text{sinc}^2(r')}{1.218815} \frac{\text{sinc}^2(r'')}{1.218815} \left(1 - \frac{\sqrt{r'^2 + r''^2 - 2r'r'' \cos(\theta - \varphi)}}{\tilde{R}_p} \right) r'r'' dr' d\theta dr'' d\varphi \right]
 \end{aligned}$$

We have normalized all distances in this equation by the beam radius X . R_p is thus the characteristic length in beam radii and r_p is the distance of the point sensor from the beam center in beam radii.

The expression A.12 may be evaluated numerically for various values of r_p . Before this is done, it is desirable to simplify this expression. Since the integral of the beam gain over the beam area is one, we find:

$$e = \frac{\text{Var}(P_p)}{\tilde{R}_p} (I_2(\tilde{r}_p) - I_1) \quad \text{A.13}$$

where

$$I_1 = \int_0^1 \int_0^1 \int_0^\pi \frac{4}{(1.218815)^2} \text{sinc}^2(r') \text{sinc}^2(r'') \sqrt{r'^2 + r''^2 - 2r'r'' \cos(\theta)} r'r'' d\theta dr' dr''$$

A.14

and

$$I_2(\tilde{r}_2) = \frac{4}{1.218815} \int_0^1 \int_0^\pi \text{sinc}^2(r) \sqrt{\tilde{r}_2^2 + r'^2 - 2\tilde{r}r' \cos(\theta)} r' dr' d\theta \quad \text{A.15}$$

Of these two integrals, only I_2 is dependent on the separation of the point sensor from the beam center. The integrals I_1 and I_2 are tabulated for several values of separation \tilde{r}_2 in Table 106.

To evaluate the expectation of the error variance between a point and area sensor, it is simply necessary to express the correlation distance and the distance from the beam center in beam radii and perform the calculation of A.13 using the values in Table 106. For convenience, it will be mentioned that to three significant digits, the distance of the first null of a $\text{sinc}^2(\bullet)$ function is 2.5 times the distance to the point where it is 0.5. It will also be cautioned that the near field assumption should not be violated. It is doubtful that the expression of A.13 has much value when the separation exceeds 500 km. It will be further noted that the assumptions of a homogeneous and isotropic atmosphere may be violated at even shorter separations at the higher latitudes. To assist in evaluating the apparent error, the value of a weighted

Table 106

Values of the Integrals I_1 and I_2

$$I_1 = .57335$$

r	$I_2(r)$
0.0	0.8205
0.1	0.8387
0.2	0.8923
0.3	0.9785
0.4	1.0931
0.5	1.2310
0.6	1.3869
0.7	1.5559
0.8	1.7339
0.9	1.9176
1.0	2.1051
1.1	2.2951
1.2	2.4869
1.3	2.6800
1.4	2.8741
1.5	3.0691
1.6	3.2647
1.7	3.4608
1.8	3.6574
1.9	3.8543
2.0	4.0516

average of the sample variances for the four regions are given in Table 107.

It is also possible to evaluate the apparent error between an area sounder and weighted average of point sensors in an arbitrary configuration using the integrals I_1 and I_2 . If the error statistic desired is:

$$e = E \left\{ \left[\sum_{i=1}^n \frac{P_{Pi}}{W_i} - P_A \right]^2 \right\} \quad A.16$$

where W_i is the weight of the i^{th} point sensor, we arrive at the expression:

$$e = \left[\sum_{i=1}^n \sum_{j=1}^n \frac{1 - \tilde{D}_{ij}/\tilde{R}_p}{W_i W_j} + I_1 - 1 - \sum_{i=1}^n I_2(\tilde{r}_i) \right] \text{Var}(P_p) \quad A.17$$

where \tilde{D}_{ij} is the distance between the i^{th} and j^{th} point sensor.

There is an additional statistic that could in theory be derived from the analysis of the radiosonde dataset discussed in this appendix. If we model a radiosonde as a noisy measurement, the intercept values of the correlation model will give us a value for the error between two

Table 107

Sample Variances of Temperatures in the
 Atmosphere by Latitude Region
 (degrees square Kelvin)

Pressure Level (mb)	Region 1	Region 2	Region 3	Region 4
1000	59.5	26.8	13.8	13.5
850	31.8	19.2	21.9	13.5
700	26.8	22.1	24.1	11.7
500	26.2	22.8	17.4	12.4
400	20.9	18.6	14.7	11.9
300	10.5	9.4	11.3	14.2
250	21.7	18.5	20.0	9.8
200	37.4	36.9	23.6	7.0
150	36.4	29.7	14.5	6.7
100	42.4	23.1	10.5	11.1
70	62.2	30.1	10.3	14.1

radiosondes launched at the same point as:

$$\text{Var}(N) = \text{Var}(P_p) [1 - R(0,0)] \quad \text{A.18}$$

As an exercise, this quantity has been tabulated for three of the latitude regions in Table 108. The values for the lowest latitude region were not computed because of the relatively small number of radiosondes in that latitude band and resulting uncertainty in the value of the intercept. The values used for the zero separation coefficients were produced by a separate polynomial regression on the statistic Z of A.8. The reader is cautioned that the quantities in Table 108 are an extrapolation and that they are conditioned on the validity of the model. It is perhaps questionable to consider the model as valid through zero distance as this would imply identical mesoscale and microscale behaviour in the atmosphere. The use of the model for this purpose will probably yield an overly large estimate of the radiosonde error.

Although it was not done for the temperature filter of this thesis, an analysis of the sort performed in this appendix may provide a more accurate system identification for the temperature inverting Kalman filter. If we care to generate models for the cross-covariances of temperatures with distance, it will be possible to construct matrices

Table 108

Apparent Radiosonde Error Variance
(degree square Kelvin)

Pressure Level (mb)	Region 1	Region 2	Region 3	Region 4
1000	6.63	4.46	2.04	1.97
850	3.52	1.39	2.44	2.10
700	1.35	0.62	0.93	1.13
500	1.74	0.90	1.65	0.56
400	2.35	0.97	1.09	1.61
300	1.70	0.74	0.78	1.71
250	2.21	2.04	1.02	3.11
200	1.62	1.43	1.42	2.45
150	1.45	0.59	1.48	1.17
100	2.27	0.71	1.79	1.39
70	5.90	1.57	1.99	4.01

cross-covariance matrices of temperatures at one remote spot with another. The elements of this matrix are:

$$P_{ij} = \sqrt{\text{Var}(P_i) \text{Var}(P_j)} \int_{\omega_1} \int_{\omega_2} G(\sigma_1) G(\sigma_2) R_{ij}(\sigma_1, \sigma_2) d\sigma_1 d\sigma_2 \quad \text{A.19}$$

This formula also gives the covariance matrix of temperatures at a single spot when the areas ω_1 and ω_2 are the same.

This approach was considered at times during this work. It was discarded for the reason that it is a rather expensive and time-consuming operation. The purpose of this thesis was what is sometimes called a feasibility study. It was felt that the available resources were better spent in building a Kalman filter that worked and then exploring the nature of its behaviour in various configurations, seasons, etc., than performing an elaborate system identification.

A further possible use of the cross-covariance elements of temperature would be for "Gandin weighting". One of the persistent problems in the production of synoptic analyses is the interpolation of reports to produce a value assigned to a mesh gridpoint. One method proposed by Gandin (1963) is basically a regression procedure. For this procedure to operate successfully, the correlation of and between levels as a function of distance is required. The author is unaware of any study other than the one that appears in this

appendix that has attempted to address even a portion of the problem.

Appendix B

Sensitivity of Oxygen Absorption and Weighting Functions to Temperature

The temperature weighting function is defined in terms of the absorption coefficient of the atmosphere and the reflectivity of the surface. For channels whose weighting functions peak high in the atmosphere, the water vapor component of the absorption and the reflectivity of the surface have little effect. It is therefore instructive to examine the sensitivity of their weighting functions and oxygen absorption to temperature.

The off resonance absorption of oxygen is due to collisional broadening. It is therefore the case that it will be affected by temperature. Two approaches have been taken to quantify this effect. The first is the experimental measurement of the absorption by Liebe (1975). The second is presented in this appendix.

The approach taken here was to perform an analytic differentiation of the oxygen lineshape of Rosenkranz (1975) with regards to temperature. To do this, the absorption routine O2ABSB was entered symbolically in the mathematical

symbolic manipulation language MACSYMA. It was then expanded in terms of its arguments and differentiated with regards to temperature. This differentiated expression was then constructed into a function, translated into LISP, and eventually into machine language.

The relative sensitivity of the oxygen absorption to temperature obtained by this method over a range of frequencies, temperatures, and pressures are given in Tables 109 - 117. The figures here appear to be in excellent agreement with those determined by Liebe.

To demonstrate the insensitivity of the weighting function to temperature, we will make use of a result by Poon (1974). This result is that, under certain assumptions, the peak of the weighting function occurs when the optical depth of the atmosphere is one neper or:

$$\int_h^H K(\nu, h'') dh'' = 1 \quad \text{B.1}$$

where h is the height of the peak of the weighting function. We will now consider the case in which the entire temperature profile above the peak increases in temperature by one degree. Examining Tables 109 - 117, we see that this implies a change in the absorption coefficient above the peak of roughly one percent. Re-evaluating B.1 after the

temperature change that this implies:

$$\int_h^H K'(\nu, h'') dh'' \approx 0.99 \quad \text{B.2}$$

where $K'(h)$ is the changed absorption coefficient. To find the new weighting function peak, we must find the height that is 0.01 neper deeper into the atmosphere. For specifics in numbers, we will state that the high altitude channel of SCAMS (55.45 GHz.) has an absorption coefficient that is roughly 0.24 neper/km at its peak. Thus, at least for this frequency, 0.01 neper is roughly 40m deeper into the atmosphere. This represents an insignificant change in the height of the peak of the weighting function when it is remembered that the weighting functions are several km wide. We thus conclude that the temperature weighting functions are insensitive to temperature.

Table 109

Sensitivity of Oxygen Absorption at 300 K, 720 Torr
(Percent change per degree Kelvin)

Freq. (GHz.)	0	1	2	3	4	5	6	7	8	9
10	-0.965	-0.965	-0.965	-0.965	-0.965	-0.965	-0.964	-0.964	-0.964	-0.964
20	-0.963	-0.963	-0.963	-0.962	-0.962	-0.961	-0.961	-0.960	-0.960	-0.959
30	-0.958	-0.957	-0.956	-0.955	-0.954	-0.953	-0.952	-0.950	-0.949	-0.947
40	-0.944	-0.942	-0.938	-0.934	-0.930	-0.923	-0.915	-0.903	-0.885	-0.855
50	-0.801	-0.717	-0.537	-0.383	-0.341	-0.402	-0.506	-0.629	-0.737	-0.807
60	-0.813	-0.768	-0.661	-0.549	-0.438	-0.341	-0.323	-0.427	-0.617	-0.738
70	-0.799	-0.848	-0.875	-0.892	-0.904	-0.913	-0.920	-0.926	-0.931	-0.935
80	-0.939	-0.943	-0.947	-0.951	-0.954	-0.958	-0.962	-0.966	-0.971	-0.975
90	-0.981	-0.986	-0.992	-0.999	-1.006	-1.013	-1.022	-1.031	-1.040	-1.051
100	-1.062	-1.074	-1.086	-1.100	-1.114	-1.128	-1.143	-1.158	-1.172	-1.186
110	-1.199	-1.210	-1.218	-1.220	-1.215	-1.196	-1.148	-1.036	-0.814	-0.713
120	-0.938	-1.104	-1.179	-1.211	-1.224	-1.227	-1.224	-1.218	-1.209	-1.200
130	-1.189	-1.178	-1.167	-1.156	-1.145	-1.133	-1.122	-1.112	-1.101	-1.091
140	-1.082	-1.072	-1.063	-1.055	-1.046	-1.038	-1.030	-1.023	-1.016	-1.009

Table 110

Sensitivity of Oxygen Absorption at 300 K, 360 Torr
(Percent change per degree Kelvin)

Freq. (GHz.)	0	1	2	3	4	5	6	7	8	9
10	-0.966	-0.966	-0.965	-0.965	-0.965	-0.965	-0.965	-0.964	-0.964	-0.964
20	-0.963	-0.963	-0.963	-0.962	-0.962	-0.961	-0.961	-0.960	-0.959	-0.959
30	-0.958	-0.957	-0.956	-0.955	-0.954	-0.952	-0.951	-0.950	-0.947	-0.945
40	-0.942	-0.939	-0.936	-0.931	-0.926	-0.919	-0.910	-0.897	-0.877	-0.840
50	-0.732	-0.610	-0.285	-0.083	-0.107	-0.276	-0.468	-0.624	-0.781	-0.861
60	-0.876	-0.818	-0.695	-0.537	-0.336	-0.148	-0.041	-0.122	-0.422	-0.627
70	-0.762	-0.832	-0.863	-0.883	-0.896	-0.906	-0.914	-0.920	-0.926	-0.931
80	-0.935	-0.939	-0.943	-0.947	-0.951	-0.955	-0.960	-0.964	-0.967	-0.974
90	-0.979	-0.985	-0.991	-0.997	-1.005	-1.013	-1.021	-1.030	-1.040	-1.051
100	-1.062	-1.075	-1.088	-1.102	-1.116	-1.131	-1.147	-1.163	-1.179	-1.195
110	-1.210	-1.224	-1.237	-1.248	-1.255	-1.257	-1.244	-1.197	-0.991	-0.754
120	-1.132	-1.229	-1.254	-1.259	-1.256	-1.250	-1.241	-1.231	-1.220	-1.208
130	-1.196	-1.184	-1.171	-1.159	-1.147	-1.136	-1.124	-1.113	-1.103	-1.092
140	-1.083	-1.073	-1.064	-1.055	-1.046	-1.038	-1.030	-1.023	-1.016	-1.009

Table 111

Sensitivity of Oxygen Absorption at 300 K, 180 Torr
(Percent change per degree Kelvin)

Freq. (GHz.)	0	1	2	3	4	5	6	7	8	9
10	-0.966	-0.966	-0.966	-0.965	-0.965	-0.965	-0.965	-0.964	-0.964	-0.964
20	-0.964	-0.963	-0.963	-0.962	-0.962	-0.961	-0.961	-0.960	-0.959	-0.958
30	-0.958	-0.957	-0.956	-0.955	-0.953	-0.952	-0.950	-0.949	-0.947	-0.944
40	-0.942	-0.939	-0.935	-0.931	-0.925	-0.918	-0.908	-0.895	-0.874	-0.836
50	-0.637	-0.382	-0.117	-0.265	-0.073	-0.246	-0.522	-0.540	-0.888	-0.893
60	-0.991	-0.829	-0.761	-0.465	-0.259	-0.077	-0.126	-0.191	-0.099	-0.423
70	-0.749	-0.827	-0.860	-0.880	-0.894	-0.904	-0.912	-0.919	-0.925	-0.930
80	-0.934	-0.938	-0.942	-0.947	-0.951	-0.955	-0.959	-0.963	-0.968	-0.973
90	-0.978	-0.984	-0.990	-0.997	-1.004	-1.012	-1.021	-1.030	-1.040	-1.051
100	-1.062	-1.075	-1.088	-1.102	-1.117	-1.132	-1.148	-1.164	-1.181	-1.197
110	-1.213	-1.228	-1.242	-1.255	-1.265	-1.273	-1.275	-1.265	-1.172	-0.876
120	-1.243	-1.273	-1.276	-1.272	-1.265	-1.256	-1.246	-1.234	-1.222	-1.210
130	-1.198	-1.185	-1.173	-1.160	-1.148	-1.136	-1.125	-1.114	-1.103	-1.093
140	-1.083	-1.073	-1.064	-1.055	-1.047	-1.038	-1.030	-1.023	-1.016	-1.009

Table 112

Sensitivity of Oxygen Absorption at 250 K, 720 Torr
(Percent change per degree Kelvin)

Freq. (GHz.)	0	1	2	3	4	5	6	7	8	9
10	-1.157	-1.157	-1.157	-1.157	-1.157	-1.157	-1.157	-1.157	-1.157	-1.157
20	-1.156	-1.156	-1.156	-1.156	-1.155	-1.155	-1.155	-1.154	-1.154	-1.153
30	-1.153	-1.152	-1.152	-1.151	-1.151	-1.150	-1.149	-1.148	-1.147	-1.146
40	-1.145	-1.143	-1.141	-1.139	-1.136	-1.132	-1.127	-1.119	-1.108	-1.090
50	-1.060	-0.999	-0.864	-0.685	-0.554	-0.536	-0.601	-0.719	-0.836	-0.912
60	-0.919	-0.864	-0.748	-0.636	-0.554	-0.521	-0.599	-0.772	-0.944	-1.040
70	-1.083	-1.110	-1.128	-1.140	-1.149	-1.156	-1.162	-1.167	-1.172	-1.176
80	-1.181	-1.185	-1.190	-1.194	-1.199	-1.204	-1.209	-1.215	-1.220	-1.227
90	-1.233	-1.240	-1.248	-1.256	-1.265	-1.274	-1.284	-1.295	-1.306	-1.317
100	-1.330	-1.343	-1.360	-1.370	-1.384	-1.398	-1.412	-1.425	-1.438	-1.449
110	-1.458	-1.465	-1.467	-1.462	-1.446	-1.410	-1.335	-1.186	-0.944	-0.851
120	-1.071	-1.273	-1.380	-1.434	-1.460	-1.472	-1.477	-1.476	-1.472	-1.467
130	-1.460	-1.452	-1.444	-1.435	-1.426	-1.417	-1.408	-1.399	-1.391	-1.382
140	-1.374	-1.366	-1.359	-1.351	-1.344	-1.337	-1.331	-1.324	-1.318	-1.312

Table 113

Sensitivity of Oxygen Absorption at 250 K, 360 Torr
(Percent change per degree Kelvin)

Freq. (GHz.)	0	1	2	3	4	5	6	7	8	9
10	-1.159	-1.158	-1.158	-1.158	-1.158	-1.158	-1.158	-1.157	-1.157	-1.157
20	-1.156	-1.156	-1.156	-1.155	-1.155	-1.155	-1.154	-1.154	-1.153	-1.153
30	-1.152	-1.151	-1.151	-1.150	-1.149	-1.148	-1.147	-1.146	-1.145	-1.143
40	-1.141	-1.139	-1.137	-1.134	-1.130	-1.125	-1.118	-1.109	-1.096	-1.074
50	-1.029	-0.949	-0.704	-0.385	-0.229	-0.320	-0.510	-0.704	-0.883	-0.991
60	-1.002	-0.937	-0.777	-0.598	-0.382	-0.222	-0.259	-0.531	-0.847	-0.995
70	-1.056	-1.092	-1.113	-1.127	-1.137	-1.145	-1.152	-1.159	-1.164	-1.169
80	-1.174	-1.179	-1.184	-1.189	-1.195	-1.200	-1.205	-1.211	-1.217	-1.224
90	-1.231	-1.238	-1.246	-1.255	-1.264	-1.273	-1.284	-1.294	-1.306	-1.318
100	-1.331	-1.345	-1.359	-1.373	-1.388	-1.403	-1.419	-1.434	-1.449	-1.463
110	-1.477	-1.489	-1.498	-1.505	-1.508	-1.502	-1.478	-1.402	-1.131	-0.886
120	-1.309	-1.452	-1.495	-1.509	-1.512	-1.510	-1.505	-1.498	-1.489	-1.480
130	-1.471	-1.461	-1.451	-1.441	-1.431	-1.421	-1.411	-1.402	-1.393	-1.384
140	-1.376	-1.368	-1.360	-1.352	-1.345	-1.338	-1.331	-1.325	-1.319	-1.312

Table 114

Sensitivity of Oxygen Absorption at 250 K, 180 Torr
(Percent change per degree Kelvin)

Freq. (GHz.)	0	1	2	3	4	5	6	7	8	9
10	-1.159	-1.159	-1.159	-1.158	-1.158	-1.158	-1.158	-1.157	-1.157	-1.157
20	-1.156	-1.156	-1.156	-1.155	-1.155	-1.155	-1.154	-1.154	-1.153	-1.152
30	-1.152	-1.151	-1.151	-1.150	-1.149	-1.148	-1.147	-1.146	-1.144	-1.143
40	-1.141	-1.138	-1.137	-1.132	-1.128	-1.123	-1.116	-1.106	-1.093	-1.069
50	-1.000	-0.875	-0.435	-0.038	-0.059	-0.183	-0.528	-0.619	-0.987	-1.038
60	-1.126	-0.958	-0.841	-0.533	-0.224	-0.006	-0.070	-0.200	-0.690	-0.935
70	-1.046	-1.087	-1.109	-1.123	-1.134	-1.143	-1.150	-1.156	-1.162	-1.168
80	-1.173	-1.178	-1.183	-1.188	-1.193	-1.199	-1.205	-1.210	-1.217	-1.223
90	-1.230	-1.238	-1.246	-1.254	-1.263	-1.273	-1.283	-1.294	-1.306	-1.318
100	-1.331	-1.345	-1.359	-1.374	-1.389	-1.405	-1.421	-1.436	-1.452	-1.467
110	-1.482	-1.496	-1.507	-1.517	-1.525	-1.530	-1.528	-1.506	-1.364	-1.004
120	-1.470	-1.522	-1.531	-1.531	-1.527	-1.520	-1.512	-1.503	-1.494	-1.484
130	-1.473	-1.463	-1.453	-1.442	-1.432	-1.422	-1.412	-1.403	-1.394	-1.385
140	-1.376	-1.368	-1.360	-1.352	-1.345	-1.338	-1.331	-1.325	-1.318	-1.312

Table 115

Sensitivity of Oxygen Absorption at 200 K, 720 Torr
(Percent change per degree Kelvin)

Freq. (GHz.)	0	1	2	3	4	5	6	7	8	9
10	-1.445	-1.446	-1.446	-1.446	-1.446	-1.446	-1.446	-1.446	-1.446	-1.446
20	-1.446	-1.446	-1.445	-1.445	-1.445	-1.445	-1.445	-1.444	-1.444	-1.444
30	-1.444	-1.444	-1.444	-1.443	-1.443	-1.443	-1.443	-1.443	-1.443	-1.442
40	-1.442	-1.442	-1.441	-1.440	-1.440	-1.439	-1.437	-1.434	-1.429	-1.421
50	-1.405	-1.370	-1.293	-1.151	-0.972	-0.839	-0.806	-0.873	-0.971	-1.040
60	-1.045	-0.987	-0.881	-0.805	-0.811	-0.902	-1.072	-1.245	-1.360	-1.418
70	-1.447	-1.464	-1.474	-1.482	-1.488	-1.494	-1.498	-1.503	-1.507	-1.521
80	-1.517	-1.522	-1.527	-1.533	-1.539	-1.545	-1.552	-1.559	-1.567	-1.575
90	-1.584	-1.593	-1.603	-1.613	-1.624	-1.636	-1.648	-1.661	-1.674	-1.688
100	-1.702	-1.717	-1.732	-1.747	-1.761	-1.776	-1.789	-1.802	-1.812	-1.821
110	-1.826	-1.826	-1.819	-1.802	-1.768	-1.704	-1.590	-1.394	-1.140	-1.057
120	-1.266	-1.504	-1.657	-1.744	-1.793	-1.820	-1.835	-1.842	-1.844	-1.842
130	-1.839	-1.834	-1.827	-1.820	-1.812	-1.804	-1.796	-1.788	-1.780	-1.772
140	-1.764	-1.756	-1.748	-1.741	-1.734	-1.727	-1.720	-1.713	-1.707	-1.701

Table 116

Sensitivity of Oxygen Absorption at 200 K, 360 Torr
(Percent change per degree Kelvin)

Freq. (GHz.)	0	1	2	3	4	5	6	7	8	9
10	-1.448	-1.448	-1.448	-1.447	-1.447	-1.447	-1.447	-1.446	-1.446	-1.446
20	-1.445	-1.445	-1.445	-1.444	-1.444	-1.444	-1.443	-1.443	-1.443	-1.442
30	-1.442	-1.441	-1.441	-1.440	-1.440	-1.439	-1.438	-1.438	-1.437	-1.437
40	-1.436	-1.434	-1.433	-1.431	-1.428	-1.425	-1.421	-1.416	-1.408	-1.400
50	-1.375	-1.335	-1.219	-0.965	-0.652	-0.542	-0.630	-0.829	-1.028	-1.161
60	-1.170	-1.093	-0.897	-0.715	-0.566	-0.565	-0.822	-1.136	-1.318	-1.389
70	-1.419	-1.438	-1.451	-1.461	-1.469	-1.476	-1.483	-1.489	-1.495	-1.501
80	-1.506	-1.512	-1.518	-1.525	-1.532	-1.539	-1.546	-1.554	-1.562	-1.571
90	-1.580	-1.590	-1.600	-1.611	-1.622	-1.635	-1.648	-1.661	-1.675	-1.690
100	-1.705	-1.721	-1.737	-1.754	-1.770	-1.797	-1.803	-1.819	-1.834	-1.847
110	-1.860	-1.870	-1.876	-1.880	-1.875	-1.858	-1.811	-1.685	-1.328	-1.086
120	-1.548	-1.765	-1.842	-1.872	-1.884	-1.887	-1.886	-1.881	-1.875	-1.867
130	-1.859	-1.850	-1.841	-1.831	-1.822	-1.812	-1.803	-1.794	-1.785	-1.776
140	-1.767	-1.759	-1.751	-1.743	-1.735	-1.728	-1.721	-1.714	-1.708	-1.701

Table 117

Sensitivity of Oxygen Absorption at 200 K, 180 Torr
(Percent change per degree Kelvin)

Freq. (GHz.)	0	1	2	3	4	5	6	7	8	9
10	-1.447	-1.447	-1.447	-1.447	-1.446	-1.446	-1.446	-1.446	-1.445	-1.445
20	-1.444	-1.444	-1.444	-1.443	-1.443	-1.443	-1.442	-1.442	-1.441	-1.441
30	-1.441	-1.440	-1.440	-1.439	-1.438	-1.438	-1.437	-1.436	-1.435	-1.434
40	-1.433	-1.431	-1.429	-1.427	-1.424	-1.420	-1.415	-1.409	-1.400	-1.387
50	-1.362	-1.314	-1.132	-0.676	-0.201	-0.226	-0.568	-0.733	-1.116	-1.238
60	-1.305	-1.134	-0.949	-0.650	-0.265	-0.154	-0.447	-0.981	-1.280	-1.373
70	-0.140	-1.430	-1.444	-1.454	-1.463	-1.471	-1.477	-1.484	-1.490	-1.496
80	-1.502	-1.509	-1.515	-1.522	-1.528	-1.536	-1.543	-1.551	-1.560	-1.568
90	-1.578	-1.588	-1.598	-1.609	-1.621	-1.633	-1.646	-1.660	-1.674	-1.689
100	-1.705	-1.721	-1.737	-1.754	-1.771	-1.788	-1.805	-1.822	-1.838	-1.853
110	-1.867	-1.880	-1.891	-1.900	-1.906	-1.907	-1.897	-1.856	-1.626	-1.195
120	-1.793	-1.885	-1.906	-1.911	-1.909	-1.904	-1.898	-1.890	-1.882	-1.872
130	-1.863	-1.853	-1.843	-1.833	-1.823	-1.813	-1.803	-1.794	-1.784	-1.775
140	-1.767	-1.758	-1.750	-1.742	-1.734	-1.727	-1.720	-1.713	-1.706	-1.700

Appendix C

Program Descriptions

Section A. Introduction

This appendix gives an extensive verbal description of many of the routines used in the Kalman filters of this thesis. Because of Institute regulations on thesis preparation, the listings of the programs are not included. The programs take full advantage of the 108 character line lengths allowable in PL/I and therefore do not reproduce legibly in the format allowed. It is the author's opinion that the Institute should reexamine its position on this matter and allow COM originals to be included in future theses.

This appendix will treat both the temperature and the water vapor and liquid water programs. Many of the subroutines are common to both of these programs. Routines specific to either program will be so noted. In cases where minor modifications were made to a routine between the two

versions, the temperature filter will be covered first and a subsection will note the differences between the two versions. All the routines described in this Appendix are written in PL/I with the exception of the routines PHIEPHI, SSQUARE, and MFS.

Section B. Main procedure

Name - FOO

Purpose - Compute sizes of data aggregates based on user specified inversion scheme.

Logic - The program first obtains the leftmost spot, and rightmost spot of the inversion scheme, the timing option and the printout options. On the basis of the number of spots inverted, the size of the output records produced by the program are determined. If blocked records are to be written, the blocksize is computed to be optimum for a 3330 disk track. Two output files are produced by the filter. One consists of the inversions produced by the filter, the other consists of the error covariance matrix P_j (\bullet) and the gain K_j . These files are declared with the

appropriate DCBs in a begin block. The inversion scheme options are inserted into appropriate external structures.

The routine also obtains the precomputation options and inserts them into an external structure. These options are precomputed P ; $(-)$, precomputed K ; , the time (in frames) for running the full filter before switching to the steady state gains or covariances, and the use of a precomputed file of transient gains. These options are then checked for consistency. The required size for the covariance matrix, the state transition matrix, and the plant noise matrix is then computed. If the transient gain option is used, these matrices are set to a size of 1 location since they are not needed in the balance of the program. Otherwise, the order of the filter is used for their size. All covariance matrices are stored in a compressed lower triangular form. The sizes of the various matrices are inserted into an external structure.

The program also requests the input/output options to be used in the program. The program may either read or write Regional(1) files or sequential files. If a backward filter is being run, the filter (generally) reads a direct access file from high key to low key and outputs a direct access file in the same manner. This allows non-tape datasets to be read "backwards" in a convenient manner. For production use one would (hopefully) read a tape backwards

because of the cost of this approach. A final option that is requested in the I/O section is the production of a file of gains and covariances. If a simple filter is being run, these parameters are not needed. If a non-causal filter is run, the file of covariances is required for its operation. The file also includes the gains for the purpose of producing precomputed gain matrices. The I/O options are also inserted into an external structure.

A banner giving the inversion scheme and the options is printed and the routine KALMAN is called.

Modifications - The number of parameters per footprint inverted is changed.

Section C. Main processor

Name - Kalman

Purpose - Read input data and write results. Manage general flow of control. Print user timing and output requests. Compute innovations and update vector of state. Acquire additional run time parameters. Collect performance statistics.

Logic - The routine proceeds with system initialization by requesting and reading the run size (number of frames to be processed), the observation noises, the frequency of user printout and the constant calibration offsets. It also requests the direction of processing (forward or backward) and the size of the dataset. This size is necessary if direct access files are used. If sequential files are used, it acts as a second limit on the run size. It also obtains the data reasonableness testing flags. These flags determine whether data reasonableness testing should be done, whether print output will be produced when a data point is rejected, and the sigma limit for outliers.

The procedure allocates storage for all variables such as the vector of state, covariance matrices, etc. in its declare statements. It also establishes an abnormal condition that is raised if the predicted error covariance matrix ceases to be positive definite. Raising this condition causes the routine to take a "snap-shot" of its major variables onto a file. It also completes the listing of the major options of the program and zeros the statistical gathering arrays.

The program then loops endlessly unless: 1) the end of file has been reached on the sequential input file, 2) the current key is outside the range of the specified file size,

or finally 3) the specified run size has been reached. Within this loop, the major processing occurs.

The program reads the data from the appropriate file and unpacks it into a floating point format. It then determines the frame time in seconds and compares it with the time of the last frame processed to determine the number of frames lost since the last data was processed. If the number of frames lost is greater than five, it will reset the processing state of the filter. This reset will always occur the first time through the loop. When this reset occurs, the filter sets a flag in the output record, defeats state propagation and calls routine INIT to re-initialize the filter environment. This reset behaviour is performed because it is felt that the state propagation cannot be trusted for long periods of time. If prediction is to be performed, the routine calls PREDICT to accomplish this task.

The filter then checks its direction (backward or forward). If the filter is a backward filter, the error covariance of the prior and the contents of the gain array are written to a output file. Likewise, the prior plus the various locator data, etc. are written out. If data is missing (as given by the data missing flag of the SOTA), the filter also performs output if it is a forward filter and then branches back for more data.

The routine then call CMATRIX to obtain the observation matrices and empirical corrections for the average latitude of the scan. The empirical corrections plus any constant corrections are then applied to the brightness temperatures to obtain the observation vector.

The observation vector, vector of state, and observation matrices are then combined to yield the initial innovations. These innovations will be used in data reasonableness testing. This is strictly incorrect if the Square Root Algorithm is used for the gain calculation. The data reasonableness should be checked after each data element has been assimilated, rather than at the first stage.

If the gain is to be calculated, the routine GAIN is called. Otherwise, the gain is read from a regional(1) file keyed on latitude partition. The gain is then applied to update the state with new innovations computed for each stage.

The filter then collects statistics on the errors against the NMC K27 grid (since a SOTA' tape is used for input) and outputs the results, covariance matrix, etc., if a forward filter is being run. It then loops back for more data.

Having completed the run, the routine terminates by computing the error statistics of the run and printing

them.

Modifications - The water vapor/liquid water filter maintains both a Statistical D inversion and a Kalman inversion. The Statistical D method is applied by calling routine D_MATRIX. The innovations and gains are computed with a channel/footprint loop by calling INOVATE to obtain the innovation and observation matrix and then GAIN to obtain the gain. This is a more correct use of the Square Root Algorithm.

Section E. Initialization routine

Name - INIT

Purpose - Initialize the prior and its covariance matrix. Call all initialization entry points on any routines that require such calls. Perform any other miscellaneous initialization necessary.

Logic (Temperature filter) - The procedure first initializes the prediction routine by calling PINIT. It then obtains the covariance of the initial estimate from a regional(1)

file keyed on the average latitude of the scan. The prior itself is initialized by calling the climatology routine TEMPS at the latitude of each spot. If the initialization routine has been called before, this completes the necessary tasks and it returns.

If this is the first time INIT has been called, it continues with its tasks after toggeling a flag stating that this initialization is being performed. It then initializes the observation matrix routine by calling CINIT and obtains the factors necessary in constructing the state transition matrix. These factors are a horizontal and vertical smoothing. The sum of the weight given to the level at the spot being propagated and any adjacent spots is one minus the vertical smoothing. The sum of the weight given to the levels at each of the adjacent spots is the horizontal smoothing over two. The weight of an adjacent level at an adjacent spot is thus the horizontal smoothing times the vertical smoothing over four. The state transition matrix is then constructed (if necessary) using these weights.

Logic (Water vapor/liquid water filter) - The initialization for this filter consists of reading a error covariance from a direct access file, calling INOINIT to initialize the innovations routine, DINIT to initialize the D matrix routine and PINIT to initialize the prediction routine. The

initial prior is obtained from the call to PINIT.

Section F. Propagation routine

Name - PREDICT

Purpose - Propagate state vector and error covariance matrix.

Logic (Temperature filter) - The routine first differences the state to be propagated and the last climatology. It then obtains the new climatology by calling TEMPS and adds this climatology back in. It then completes the state transition matrix and predicts the new state.

In order to complete the state transition matrix, the surface must be accounted for. To do this, the old surface elements of the state transition matrix are zeroed and the pressure of the surface found by looping through a list of pressure surface altitudes for each spot. The weight given to a slab in predicting the surface is proportional to the amount of the slab not occupied by the surface, but it must be at least the normal amount of vertical smoothing. The surface temperature at each spot is then smoothed

vertically.

After the surface has been "found" the atmospheric temperatures are smoothed vertically using the vertical smoothing factors. Following this, the horizontal smoothing is performed, and the horizontal smoothing elements for the surface are inserted into the state transition matrix.

If the filter is being used in a precomputed gain or covariance mode, this completes the propagation. If a precomputed covariance mode is in effect, the filter decides whether the current value of P_i (-) is valid. If it is not, the filter reads the square root of the precomputed covariance into the array and returns. If covariance matrix propagation is required, the matrix product $\Phi P \Phi^T$ is computed by calling PHIEPHI. The current value of the plant noise is determined by calling STATE and added to this product to give the new covariance matrix. The routine then returns.

The initialization for this routine consists of calling the state routine initialization entry point SINIT and obtaining a climatology at the initial processing point by calling TEMPS. An offset table required by PHIEPHI is also constructed.

Logic (Water vapor/liquid water filter) - This routine does a simple implementation of the prediction. If necessary, it

obtains a state transition matrix and plant noise from two regional(1) datasets. It then differences the state and the old climatology and then computes the product ΦX . The covariance update (if necessary) is again performed by calling PHIEPHI and adding the plant noise.

Initialization simply gets the current climatology and constructs the offset table.

Section G. State routine (Temperature filter only)

Name - STATE

Purpose - Return the currently valid plant noise.

Logic - The routine checks the current latitude against the range of validity of the current plant noise matrix. If a new plant noise is required, it is read from a regional(1)

file.

Section H. Special matrix routine 1

Name - PHIEPHI

Purpose - Compute the symmetric matrix $\Phi P \Phi^T$ for symmetric P.

Logic - This routine first computes the product ΦP into a scratch area. Since Φ is often sparse, it does a LTER instruction to determine if the product $\Phi_{ij} P_{jk}$ should be computed. All temporary products and sums are held in floating point registers. The multiply loops are driven by BXLE instructions. The offset table is used to eliminate the constant computation of $(I*I-I)/2$ in accessing P_{ij} .

Once ΦP is computed, the temporary scratch matrix is post-multiplied by Φ^T . Again, multiplies by zero are

bypassed.

Section I. Observation matrix routine (Temperature filter only)

Name - CMATRIX

Purpose - Return the discrete weighting functions, elements, and the empirical corrections.

Logic - The routine first decides if its current set of discrete weighting functions are correct for the latitude. If not, it reads an new set from two regional(1) files. Since the weighting function array for a latitude band is larger than a 3330 track, the array is overlaid with two based variable aggregates and the two parts of the array separately. The routine then determines the correct knot of the empirical correction spline and generates the empirical corrections.

It then constructs the discrete weighting functions and the $\frac{\partial}{\partial T_i} T_B$ elements for each channel/spot. If the elevation "map" height is greater than one, it searches the heights for which the weighting functions were computed to

determine the interpolation weights in altitude. Having determined these weights, it bi-laterally interpolates the weighting functions in altitude and reflectivity. The $\frac{\partial}{\partial T_i} T_B$ elements are the same as the discrete weighting functions for this case.

If the surface elevation "map" shows either sea level land or an altitude greater than three km, the weighting functions are simply interpolated in reflectivity.

For an ocean surface, the reflectivity of the surface is determined by the current estimate of the surface temperature and the 1000 mb temperature. The weighting functions are then again interpolated in reflectivity. The $\frac{\partial}{\partial T_s} T_B$ element for the surface is derived as described in the section of the observation matrices in Chapter IV. An additional correction is made to the empirical corrections for the reflected big bang space background.

Initialization consists of reading the empirical correction splines and the surface reflectivity file.

Section J. Statistical D routine (Water vapor/liquid water filter)

Name - D_MATRIX

Purpose - Generate estimates of liquid water and water vapor columns using the Statistical D method.

Logic - A simple matrix multiply implementation of the Statistical D method is used.

Initialization consists of reading the D matrix constants.

Section K. Innovation routine (Water vapor/liquid water filter)

Name - INOVATE

Purpose - Solve the forward equation of radiative transfer, produce sensitivities of the brightness temperature to a change in liquid water and water vapor columns.

Logic - The routine derives two indices based on the atmospheric temperature, liquid water and water vapor columns. It then checks the indices of the two spline coefficient arrays in its in-core buffers. If necessary, it brings a new set of coefficients into one or both buffers

and sets a pointer for a based overlay for the spline coefficients. One set of coefficients corresponds to a temperature above the atmospheric temperature, the other set corresponds to a temperature below the atmospheric temperature. Since the coefficients span four knots in water vapor and liquid water columns, the local region within the spline coefficients is determined. Coefficients for the region of interest are found by interpolating the two sets of spline coefficients in temperature.

Values for the upward brightness temperature, the downward brightness temperature times the extinction upwards and the extinction upwards and their derivatives are then evaluated by calling the IMSL routine DBCEVU. The sea surface reflectivity is then evaluated using a spline in the sea surface temperature. The expected brightness temperature and its partials are then evaluated by combining the various integrals, the surface reflectivity, and the surface temperature. The predicted brightness temperature is then subtracted from the observed brightness temperature to obtain the innovation.

Initiation consists of reading the reflectivity

splines.

Section L. Gain calculation routine

Name - GAIN

Purpose - Compute the Kalman gain using the Square Root Covariance I algorithm.

Logic - This routine follows the algorithm (including the notation) of Kaminski et al. (1971) and Chapter III. It first decomposes the covariance using the SLMATH routine MFS if necessary. It then computes the gain. At the point where $FF^T + N$ is computed, it has the choice of aborting further calculation if data reasonableness testing is in effect. The covariance matrix is reformed (if required) from its square root by calling SSQUARE.

Section M. Cholesky decomposition routine

Name - MFS

Purpose - Perform a Cholesky decomposition of a positive definite symmetric matrix.

Logic - This routine performs a Cholesky decomposition using the logic of the SLMATH routine MFS. It has been hand "compiled" and highly optimized. The square root code is expanded in-line, but the routine requires the square root module for the value of certain "magic constants".

Section M. Special matrix routine 2

Name - SSQUARE

Purpose - Multiply a square matrix times its transpose to yield a symmetric matrix.

Logic - The routine treats the square matrix as a vector. The address of its elements is determined by the values of the registers used in the multiplication loop BXLEs. The BXLEs run with increment four to step through the matrix in an appropriate fashion. The accumulation of products is into a floating point register.

References

- Athans, M., C. B. Chang, 1976: Adaptive estimation and Parameter identification using multiple model estimation algorithm, Massachusetts Institute of Technology, Lincoln Laboratory Technical note 1976-28.
- Fitzgerald R. J., 1971: Divergence of the Kalman filter, IEEE Trans. Auto. Control, AC-16, pp 736 - 747
- Fleming H. E., W. L. Smith, 1972: Inversion techniques for remote sensing of atmospheric temperature profiles, Proceedings of the Fifth Symposium on Temperature, Instrument Society of America, Pittsburgh, Pa., pp 2239 - 2250
- Fritz S., D. Q. Wark, H. E. Fleming, W. L. Smith, H. Jacobowitz, D. T. Hilleary, J. C. Alishouse, 1972: Temperature Sounding From Satellites, U. S. Dept. of Commerce, NOAA Rep. NESS-59.

Gandin, L. S., 1963: Objective analysis of meteorological fields, U. S. Department of Commerce [translated from the Russian by Israel Program for Scientific Translations].

Gaut, N. E., 1967: Studies of Atmospheric water vapor by means of passive microwave techniques, Ph.D. thesis, Department of Meteorology, Massachusetts Institute of Technology.

Gelb A. ed., 1974: Applied Optimal Estimation, M.I.T. Press, Cambridge, Ma.

Grody N. C., P. P. Pellegrino, 1977: Synoptic scale studies using the Nimbus 6 scanning microwave radiometer, J. Appl. Meteor., 16, pp 816 - 826

Jazwinski A. H., 1970: Stochastic Processes and Filtering Theory, Academic Press, N.Y. N.Y.

Kalman R. E., 1960: A new approach to linear filtering and prediction problems, Trans. ASME, 88D, pp 35 - 70

Kaminski P. G., A. E. Bryson, S. F. Schmidt, 1971: Discrete square root filtering: A survey of current techniques, IEEE Trans. Auto. Control, AC-16, pp 727 - 736

Kaplan, L. D., 1959: Inference of atmospheric structure from remote radiation measurements, J. Opt. Soc. Am, 49, 10, pp. 1004 - 1007.

Ledsham W. H., D. H. Staelin, 1978: An extended Kalman-Bucy atmospheric temperature profile retrieval with a passive microwave sounder, J. Appl. Meteor. in press.

Lenoir W. B., 1965: Remote sounding of the upper atmosphere by microwave measurements, Ph.D. thesis, Massachusetts Institute of Technology, Dept. of Electrical Engineering.

_____, 1968: Microwave spectrum of molecular oxygen in the mesosphere, J. Geophys. Res., 73, 1, pp 361-376.

Leondes C. F. ed., 1970: Theory and Applications of Kalman Filtering, NATO Advisory Group for Aerospace Research and Development, AD-704306

Liebe H. J., W. M. Welch, 1973: Molecular attenuation and phase dispersion between 40 and 140 GHz. for path models from different altitudes, U.S. Dept of Commerce, Office of Telecommunications Rep. 73-10.

_____, 1975: Studies of oxygen and water vapor microwave spectra under simulated atmospheric conditions, U.S. Commerce Dept., Office of Telecommunications Rep. 75-65.

_____, G. G. Gimmestad, J. D. Hopponen, 1977: Atmospheric oxygen microwave spectrum, experiment versus theory, IEEE Trans. Antennas Propagat., AP-25, 3, pp 327-335.

Meeks M. L., A. E. Lilley, 1963: The microwave spectrum of oxygen in the earth's atmosphere, J. Geophys. Res., 68, pp 1683 - 1703.

Mehra R. K., 1970: On the identification of Variances and Adaptive Kalman Filtering, IEEE Trans. Auto. Control, AC-15, pp 175-184.

_____, 1971: On-Line Identification of Linear
Dynamic Systems with Applications to Kalman
Filtering, IEEE Trans. Auto. Control, AC-16,
pp 12-21

Poon R. L. K., 1974: Atmospheric opacity near half
centimeter wavelength, Ph.D. thesis, Massachusetts
Institute of Technology, Dept. of Electrical
Engineering

_____, 1976: A power-law fit to oxygen
absorption at 60 GHz. and its application to remote
sensing of atmospheric temperature, Radio Sci.,
in press.

Reifenstein E. C., N. E. Gaut, 1971: Interaction model of
microwave energy and atmospheric variables,
NASA contractor report NASA CR-61348.

Rosenkranz, P. W., 1971: Radiometric sensing of atmospheric
water and temperature, Ph.D. thesis, Department of
Electrical Engineering, Massachusetts Institute of
Technology.

_____, F. T. Barath, J. C. Blinn, E. J. Johnston,
W. B. Lenoir, D. H. Staelin, J. W. Waters, 1972:
Microwave radiometer measurements of atmospheric
temperature and water from an aircraft, J. Geophys.
Res., 77, pp 5833 - 5844

_____, 1975: Shape of the 5 mm Oxygen Band in the
Atmosphere, IEEE Trans. Antennas Propagat.,
AP-23, pp 498 - 506.

Schmidt S. F., 1970: Computational techniques in Kalman
filtering, in Theory and Applications of Kalman
Filtering, NATO Advisory Group for Aerospace
Research and Development, AD-704306.

Schweppe F. C., 1973: Uncertain Dynamic Systems, Prentice
Hall, Englewood N. J.

Smith, W. L., and H. M. Woolf, 1976: The use of eigenvectors
of statistical covariance matrices for interpreting
satellite sounding radiometer observations, J. Atmos.
Sci., 33, 7, pp 1127 - 1140.

Staelin D. H., 1966: Measurements and interpretation of the microwave spectrum of the terrestrial atmosphere near 1-centimeter wavelength, J. Geophys. Res., 71, pp 2875 - 2881.

_____, 1969: Passive remote sensing at microwave wavelengths, Proc IEEE, 57, pp 427 - 439

_____, A. H. Barrett, P. W. Rosenkranz, F. T. Barath, E. J. Johnston, J. W. Waters, A. Wouters, W. B. Lenoir, 1975: The scanning microwave spectrometer (SCAMS) experiment, The Nimbus 6 Users Guide, Goddard Space Flight Center, Greenbelt Md., pp 59 - 86

_____, P. W. Rosenkranz, F. T. Barath, E. J. Johnston, J. W. Waters, 1977: Microwave spectroscopic imagery of the earth, Science, 197, pp 991 - 993

Valley S. L. ed., 1965: Handbook of Geophysics and Space Environments, Air Force Cambridge Research Laboratories, Bedford Ma.

Van DeHulst H. C., 1957: Light Scattering by Small Particles, Wiley, New York.

Waters J. W., K. F. Kunzi, R. L. Pettyjohn, R. K. L. Poon,
D. H. Staelin, 1975: Remote sensing of atmospheric
temperature profiles with the Nimbus 5 microwave
radiometer, J. Atmos. Sci., 32, pp 1953 - 1969

Wilheit T.T., 1970: Studies of microwave emission and
absorption by atmospheric oxygen, Ph.D. thesis,
Massachusetts Institute of Technology, Dept.
of Physics.

_____, A. H. Barrett, 1970: Microwave spectrum of molecular
oxygen, Phys. Rev. A, 1, pp 213-215.

Biographical Note

The author was born on March 8, 1948 in New York City, New York. He attended elementary and high school in Bergenfield, New Jersey, graduating from Bergenfield High School in 1966. He entered Stevens Institute of Technology and graduated with a Bachelor of Engineering degree with honors in 1970. During his junior and senior years, he was employed as a statistician/programmer by the Laboratory of Psychological Studies, Stevens Institute of Technology, engaged in the implementation and analysis of psychological tests. From 1970 thru 1973, he was employed as a member of the technical staff of Bell Telephone Laboratories, who very generously supported his Masters program at the Massachusetts Institute of Technology during 1970 and 1971. His responsibility at Bell Telephone Laboratories was the design and analysis of a sample survey of data transmission levels on interstate private lines. In 1973, he returned to Massachusetts Institute of Technology to join the doctoral program, receiving an Electrical Engineers degree in 1974. During the course of his doctoral studies he has been supported by a research assistantship in the Research Laboratory of Electronics.

He is a co-author of "Microwave Sensing of Atmospheric

Temperature and Humidity from Satellites" presented at the meeting of COSPAR in 1975 which also appears in Space Research, XVI, 82, 1976, "An Extended Kalman-Bucy Filter for the Retrieval of Temperature Profiles and Liquid and Water Vapor Columns from Passive Microwave Sounders" presented at the National Radio Science meeting January 9, 1978 in Boulder Colorado, "An Extended Kalman-Bucy Filter for Atmospheric Temperature Profile Retrieval with a Passive Microwave Sounder" scheduled to appear in the July 1978 issue of the Journal of Applied Meteorology, and "Temperature Profile Retrievals with Extended Kalman-Bucy Filters" to be presented at the meeting of COSPAR at Innsbruck Austria, June 2, 1978. He is a member of the American Meteorological Society, the Institute of Electrical and Electronic Engineers, Tau Beta Pi, and Sigma Xi.